DELFT UNIVERSITY OF TECHNOLOGY

Offshore Wind Power Connected to the Dutch Transmission System by VSC-HVDC Networks: Modeling and Stability Analysis

Mario V. Ndreko

Master of Science Thesis Sustainable Energy Technology

October 2012

FACULTY OF ELECTRICAL ENGINEERING, MATHEMATICS AND COMPUTER SCIENCE

Thesis Committee:

Prof. Ir. Mart A. M. M. Van der Meijden:	*TU Delft, chair*
Dr. Ir. P. Bauer:	*TU Delft, external member*
Dr. Ir. M. Gibescu:	*TU Delft, thesis supervisor*
Ir. Jorrit A. Bos:	*TenneT TSO B.V, daily supervisor*
Ir. Arjen A. Van der Meer:	*TU Delft, daily supervisor*

Acknowledgements

I would like to express my special gratitude to Dr. Madeleine Gibescu who gave me the opportunity to work on such an interesting and challenging topic. Exceptionally, I would like to thank Jorrit Bos and Kees Jansen who gave me the chance to join TenneT TSO B.V for my MSc thesis project. I would like to thank Jorrit for the patience he showed on problems related to PSSE. I learnt a lot from him and I am grateful for that.

I would also like to thank all the grid strategists of TenneT for being always helpful and friendly during my stay. I would like to thank Johan Schuld for the guidance he gave me concerning the Fortran modeling in PSSE and for always being a good teacher.

The project is made under the sincere guidance of Arjen A. Van der Meer, my daily supervisor in TU Delft. I would like to thank him for his interest in the success of this thesis. He has been always open and committed to give me the right guidance for the success of the MSc project. I would also like to thank Professor Mart A. M. M. Van der Meijden and Dr. P.Bauer for being the reviewers of my thesis.

I would like to thank my parents for the support they gave me and Katerina for always making me look at the bright side of life.

Summary

Wind power generation is predicted to increase massively within the next years. In this direction, offshore wind power is anticipated to play an important role in the future renewable energy share, especially in the North Sea countries. These trends have posed new challenges for transmission system operators to supply consumers with the required quality of service. Transmission system operators are responsible to ensure the adequate security of power system operation which implies system stability and satisfactory damping levels.

High voltage direct current (HVDC) transmission system technology is the only technically feasible power transmission system solution for the connection of large offshore wind farms which are located far from the shore. Additionally, the plans for the construction of a multi-terminal dc offshore network in the North Sea region would advance the integration of offshore wind power and would further improve the European electricity markets. The VSC-based HVDC transmission is considered a mature technical solution for the development of multi-terminal dc networks.

The main focus of the present thesis is the interaction of the Dutch interconnected power system with voltage source converter (VSC) based HVDC transmission systems which are facilitated for the integration of large amount of offshore wind power in the Netherlands. Special attention is given in the transient stability of critical generators in the Dutch power system in situations with large amount of onshore and offshore wind penetration. Individual and MTdc connection of offshore wind parks have been investigated both facilitated by VSC-based HVDC.

A generic modeling framework for VSC-based HVDC transmission system which is compatible with the Dutch power system dynamic model of TenneT in PSSE software package is developed to carry out transient stability analysis. An averaged model of the VSC converter along with the dc cable network model is used for transient stability simulations of meshed ac-dc networks. The interaction between the Dutch power system and different VSC-based HVDC transmission systems is investigated under ac side three phase faults.

In addition, different dc network power management strategies based on closed loop dc voltage control and dc droop characteristics are proposed to ensure smooth system operation and proper power sharing among the grid-side converter stations. The three basic power market dispatch schemes were studied and the basic differences in terms of dc voltage performance were discussed.

A power oscillation damping (POD) controller that operates at the grid-side converter is proposed in order to introduce damping of electromechanical oscillations in the ac power system. The POD controller operates at the active power control loop of the GSVSC and performs active power modulation. It was shown for a multi-machine test system that it is possible by the proposed control strategy to introduce damping of power oscillations in the system that the grid-side converter operates.

The 2010 dynamic model of TenneT has been used to represent the Dutch high voltage transmission system. Grid reinforcements which are planned for the years 2025-2030

were introduced. Additionally, certain assumptions have been made in terms of conventional generation and unit commitment. Having applied all the necessary changes, it has been achieved to build a 2025-2030 grid situation dynamic model.

Seven interconnection points were considered within the former UCTE system for the connection of large amount of offshore wind power (three in the Netherlands, three in Germany and one in Belgium) according to the NSTG project. Three types of VSC-based HVDC transmission system configurations were studied. Namely the individual connection, the multi-terminal dc network connection per country and the transnational multi-terminal dc network connection which extends from Germany via the Netherlands to Belgium. A total 5200MW offshore wind power and 4700MW onshore wind power is introduced into the power flow of the Dutch power system. Furthermore, for the German part of the UCTE network, 7500MW offshore wind power is considered. Three snapshots of the Dutch power system are taken into consideration reflecting situations with different conventional generation, load and power exchange.

From the simulation results it was deduced that the specific amount of wind power interconnected to the Dutch power system did not create transiently unstable situations. With regard to the performance of the grid-side converter stations in the three types of HVDC transmission system configuration, it was found that the main difference in the dynamic response is the active power overshoot of particular grid-side converters. All grid-side converters have illustrated capability to support the ac voltage with reactive power and contribute limited short circuit current in all three HVDC configurations. Additionally, the connection of the converter stations in the existing 380kV substations of the Dutch power system did not introduce considerably negative interaction between the generators and the converters.

Table of Contents

List of Acronyms

ac	Alternative current
AVR	Automatic Voltage Regulator
BSL	Borssele
BVW	Beverwijk
dc	Direct current
EEM	Eemshaven
FRT	Fault Ride Through
GSVSC	Grid side voltage source converter
GTO	Gate Turn off thyristor
HVDC	High Voltage Direct Current
IGBT	Insulated Gate Bipolar Transistor
MTdc	Multi-terminal Direct Current
NSTG	North Sea Transnational Grid
PCC	Point of Common Coupling
PI	Proportional Integral controller
PLL	Phase Lock Loop
POD	Power Oscillation damper
PSS	Power System Stabilizer
PWM	Pulse Width Modulation
TSO	Transmission system Operator
UCTE	Union for Coordination of Transmission of Electricity
VMM	Voltage Margin Method
VSC	Voltage Source Converter
WP	Wind Park
WPVSC	Wind Park voltage source converter
XLPE	Cross Linked Polyethylene

List of symbols

m_a	Modulation index of the converter module
$(V_{AN})_1$	AC voltage fundamental frequency component with respect to point N
$(V_{LL})_1$	voltage source converter fundamental component of the line-to-line RMS voltage
$\tilde{u}_c$	The phasor of the converter ac terminal voltage
$\tilde{u}_s$	The phasor of the system voltage
$\tilde{u}_f$	The phasor of the voltage across the filter capacitor
$\tilde{i}_{tr}$	The phasor of the transformer
$\tilde{i}_{pr}$	The phasor of the phase reactor current
X_{pr}	Phase reactor reactance installed at the converter station
X_{tr}	Transformer reactance installed at the converter station
R_{pr}	Resistance of the equivalent model of the converter station phase reactor
R_{tr}	Resistance of the equivalent model of the converter station transformer
R_{dc}	Resistance of the π-equivalent model of HVDC cable
L_{dc}	Inductance of the π-equivalent model of HVDC cable
C_{dc}	Capacitor of the π-equivalent model of HVDC cable
I_{dcj}	Dc current injection at terminal j of the HVDC cable
I_{ij}	Dc current flow between the branch defined by nodes i and j
U_{dci}	Direct voltage at node i
M	Incident matrix
$\tilde{U}_{pcc}$	Phasor of the converter voltage at PCC
u_s^d	d-axis component of the system voltage
u_c^d	d-axis component of the converter voltage
i_{pr}^q	q-axis component of the phase reactor current
i_{pr}^d	d-axis component of the phase reactor current
i_d	d-axis component of the current measured at PCC
P	Active power of the converter
Q	Reactive power of the converter
k_p	Proportional gain of the PI controller
k_i	Integral gain of the PI controller
T_{dc}	Time constant associated with the dc network
T_d	Time constant associated with the converters modulator
Y_{dc}	Dc network admittance matrix
J	Jacobian matrix
$V_{tri,peak}$	Peak of the carrier signal for the modulation of the IGBTs

$V_{control,peak}$	Peak of the sinusoidal signal for the modulation of the IGBTs
i_d^{upper}	Upper limit of the one-stage VMM controller
i_d^{lower}	Lower limit of the one-stage VMM controller
i_d^{upper1}	Upper limit of the two-stage VMM controller
i_d^{lower1}	Lower limit of the two-stage VMM controller
i_d^{upper2}	Upper limit of the two-stage VMM controller
i_d^{lower2}	Lower limit of the two-stage VMM controller

List of Figures

List of tables

Σα βγεις στον πηγαιμό για την Ιθάκη,
να εύχεσαι νά ναι μακρύς ο δρόμος,
γεμάτος περιπέτειες, γεμάτος γνώσεις.

Τους Λαιστρυγόνας και τους Κύκλωπας,
τον θυμωμένο Ποσειδώνα μη φοβάσαι,
τέτοια στον δρόμο σου ποτέ σου δεν θα βρεις,
αν μέν' η σκέψις σου υψηλή, αν εκλεκτή
συγκίνησις το πνεύμα και το σώμα σου αγγίζει.
Τους Λαιστρυγόνας και τους Κύκλωπας,
τον άγριο Ποσειδώνα δεν θα συναντήσεις,
αν δεν τους κουβανείς μες στην ψυχή σου,
αν η ψυχή σου δεν τους στήνει εμπρός σου.

...Κι αν πτωχική την βρεις, η Ιθάκη δεν σε γέλασε.
Έτσι σοφός που έγινες, με τόση πείρα,
ήδη θα το κατάλαβες η Ιθάκες τι σημαίνουν.

Κ.Π. Καβαφης

Chapter1: Introduction

1.1 Problem Background

The targets of Europe are clearly ambitious for renewable energy exploitation. Sustainable energy is in the main agenda of European Union policies. By 2020, 20% of gross final energy consumption should be met by utilization of renewable energy resources. Towards this direction, offshore wind is anticipated to play a big role, being the strategic, domestic and largely untapped resource for delivering the agreed targets [**1**].

1.1.1 Large scale offshore wind energy development

Offshore wind will secure the European countries with indigenous energy supply reducing energy import dependence. An installed capacity of 40 GW wind power would produce 140 TWh, representing a substitution of 13 Mtoe (tonnes of Oil equivalent) of fossil fuels. A fully developed European Offshore wind industry would be able to deliver a capacity of several hundred GW to supply the future energy demand. More specifically, with only less than 5% of the total North Sea surface it is possible to supply roughly one-quarter of Europe's current energy needs [**2**].

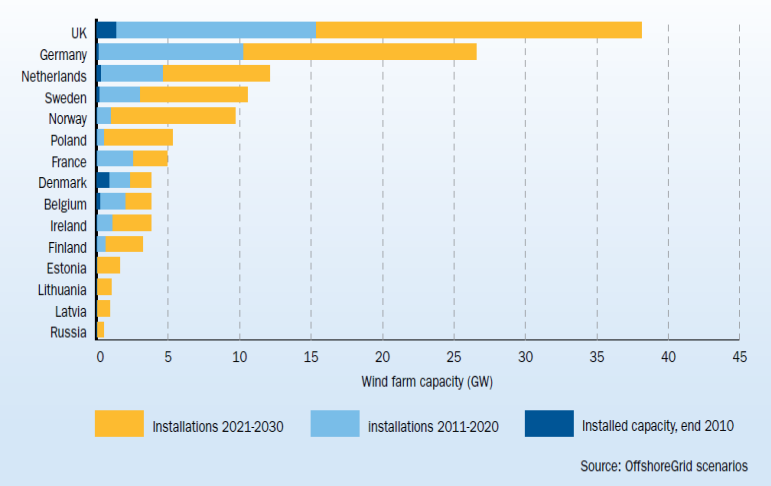

Figure 1.1: Predicted installed offshore wind capacity per country for 2020/30 scenario **[**2**]**

Globally, offshore wind power increased more than fivefold between 2000 and 2010. Countries like Denmark, Sweden, UK, Netherlands and Ireland have already in operation offshore wind power plants. For the future an installed capacity of 40GW is expected until 2020 which can reach 150GW by 2025-2030, as it is illustrated in Figure

1.1. Thus the number of installed offshore wind farms is predicted to increase within the forthcoming decades, particularly in North and Baltic Sea.

In addition, wind power penetration to the national networks will achieve levels similar to conventional power generation [**3**]. Hence, it becomes clear that the large scale integration of offshore wind power triggers challenges throughout the process of generation and transport of bulk amount of power from the offshore wind farm sites to the onshore grid feed-in points [**4**].

1.1.2 The motivation and advantage for the development of Multi-terminal HVDC offshore networks in the North Sea

The first offshore wind farms were located close to shore and had been limited in capacity. On the other hand, future offshore wind farms projects will grow large in size and will be installed far away in locations with high wind potential at distances of more than 100km from shore. In these situations, it has been suggested that the most convenient power transmission system is the high voltage direct current (HVDC) technology [**3**].

More specifically, looking at the North Sea, suggestions have been made for the construction of a whole new offshore dc network also known as North Sea Transnational Grid (NSTG) or even as "Super grid" [**5**]. This network will facilitate power transfer from far and large in capacity offshore wind farms to onshore interconnection points. More specifically, the objective of the NSTG research project [**5**] is to investigate the most efficient technical solution for the development of high capacity offshore networks in the North Sea for 2025-2030. Figure 1.2 introduces a suggestion made from EWEA for a construction of such an offshore network.

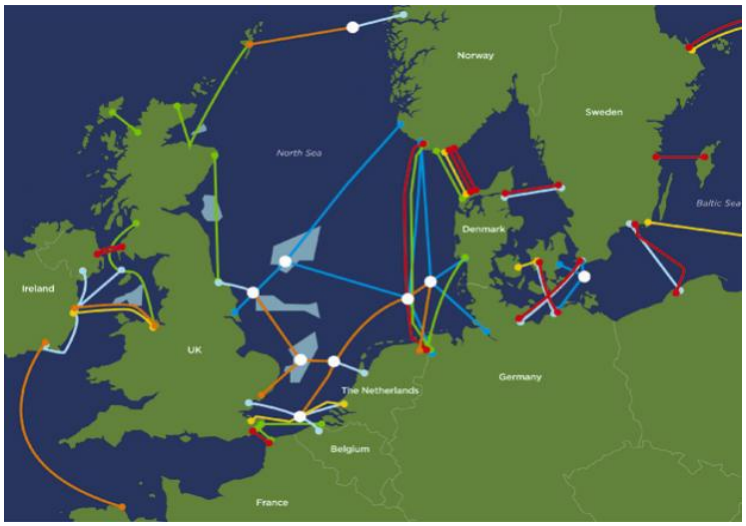

Figure 1.2: North Sea Transnational Network (NSTG), proposal according to EWEA **[**1**]**

The construction of the offshore dc network yields numerous advantages. These evolve around two main pillars. The first includes advantages related to the integration of renewable energy. The offshore network in the North Sea will improve the facilitation of offshore wind power and other marine technologies (wave and tidal energy converters) which are located far from shore. The expansion of the dc network in the

countries around the North Sea will enable the spatial smoothing of total generated wind power improving thus its inherent variability [**1**]. The second pillar of benefits, evolve around the development and evolution of the energy market in the North Sea countries. The construction of more interconnections between countries will further improve the trades and enhance the competition [**2**].

1.2 Research objectives

The focus in the present project will be the power system of Netherlands and the interaction between offshore VSC-based MTdc networks with the Dutch Power system from power system stability point of view. The transient stability of selected generators in the Dutch power system will be investigated in future scenarios with large amount of offshore wind penetration transported onshore via VSC-based MTdc networks. The 2025-2030 version of the network is considered. The main goal is to investigate how the rotor stability of critical generators in the Dutch Power system can be affected by the operation of offshore MTdc networks.

1.3 Research approach

The research procedure has been initiated with a proper literature review about the VSC-HVDC technology and modeling of VSC-based MTdc networks. A "learning by doing" stage has been followed in order to get familiar with the modeling capabilities of Siemens PTI PSSE package which is the simulation tool of this project [**6**].

The next step was to get acquainted with the 2010 dynamic model of TenneT which represents the high voltage Dutch transmission system in PSSE. In addition, dynamic models of modular MTdc networks that facilitate VSC-HVDC technology have been developed. The development of these models started within a previous MSc project at TU Delft in [**7**]. These models have been further upgraded in the present project.

Direct voltage controllers have been introduced in the models that facilitate market power dispatch schemes between GSVSCs that operate in MTdc networks. C. Ismunandur in [**8**] has given a precise description of the controllers facilitated to achieve the market power dispatch schemes. Power oscillation damper (POD) controllers have been designed in order to introduce damping of electromechanical oscillations by active power modulation of the GSVSCs. Time domain simulations with selected test systems have been performed with the intention to validate the proposed controllers.

The final stage included the upgrade of the 2010 Dutch transmission system model in PSSE to a 2025-2030 network situation. Furthermore, in order to investigate the rotor angle stability of selected generators, three snapshots have been chosen which represent steady state operating points that are interesting from transient stability point of view. In addition, three topologies of the VSC-based offshore HVDC transmission systems have been selected for investigation and analysis. L. Bergfjord in [**9**] has investigated and evaluated various MTdc networks topologies and capacity choices in the North Sea. Time-domain simulations have been executed and analysis has been performed.

1.4 Expected results

The Dutch Power system is a heavily interconnected network within former UCTE system which up to date has been highly stable. There are no weakly damped power oscillations of generator units. The rotor angle stability of all generators and the voltage and frequency stability are normally maintained without problems.

However, for the 2025-2030 network situation a large amount of offshore and onshore wind penetration is expected. Studies have already been performed that investigates the effects of interconnecting large amounts of offshore wind to the Dutch power system [**10**] [**11**]. However they utilize high voltage ac transmission technology for the connection of offshore wind farms and do not take into accounts the interconnection of large amount of offshore wind power via VSC-based transmission systems.

Especially the substitution of large amount of conventional generation with offshore wind power connected via VSC-HVDC transmission system would introduce low equivalent system inertia. For that reason the loss of a significant amount of generation as a result of disturbances could trigger power oscillations at critical generators which may be weakly damped or even unstable. With regard to the performance of the GSVSCs it is expected that they can demonstrate fault ride through (FRT) capability, ac voltage support and ability to contribute to the short circuit current.

1.5 Thesis contribution

The contribution of the present thesis is to quantify dynamic interaction of the interconnected Dutch power system meshed with transnational MTdc networks which may extend between North Sea countries in a future scenario that includes high penetration of wind energy.

The present thesis could be used as input for studies related to investigation and design of the grid code requirements for connection of VSC-based HVDC transmission systems to the west European power system. More specifically, the thesis shows the behaviour during onshore system disturbances of the grid side converters that operate either in radial or MTdc network configuration. Additionally, the thesis illustrates how converters that operate in various HVDC configurations can contribute to the onshore ac power system stability. Recommendations have been given for the design of specific controllers that introduce damping of electromechanical oscillations in the ac power system.

1.6 Thesis Outline

The report is organized in 7 chapters. Chapter 2 gives an overview of the HVDC technology up-to-date. Chapter 3 introduces the generic models of MTdc networks and simplification proposals for power system stability studies implemented in the PSSE software. Chapter 4 describes the market power dispatch schemes and proposes control strategies to implement them. Chapter 5 investigates the possibility of introducing damping of power oscillations in critical generators by application of POD that operates in the GSVSC stations. In chapter 6 the interaction of the Dutch power system with a VSC-based MTdc transnational network is investigated. Final conclusions are drawn in chapter 7.

Chapter 2: HVDC transmission system technology overview and operational aspects

2.1 HVDC technology overview for transmission systems

High voltage direct current (HVDC) transmission has emerged as an attractive option for long distance interconnection of asynchronous systems. Applications of point-to-point interconnections using HVDC technology are currently in operation in China, India, Canada and Europe [**12**].

2.1.1 Classic HVDC technology

A conventional technology for HVDC has been based on the line-commutated converters (LCC). The LCC-HVDC technology is mainly facilitated today for long distance bulk point-to-point connection including applications where only a submarine cable can be used. LCC-HVDC is well established technology with the largest project being the Itaipu system in Brazil at 6300MW power level [**12**]. Even though there is a great number of applications in different countries this technology has showed significant weakness as it will be discussed shortly.

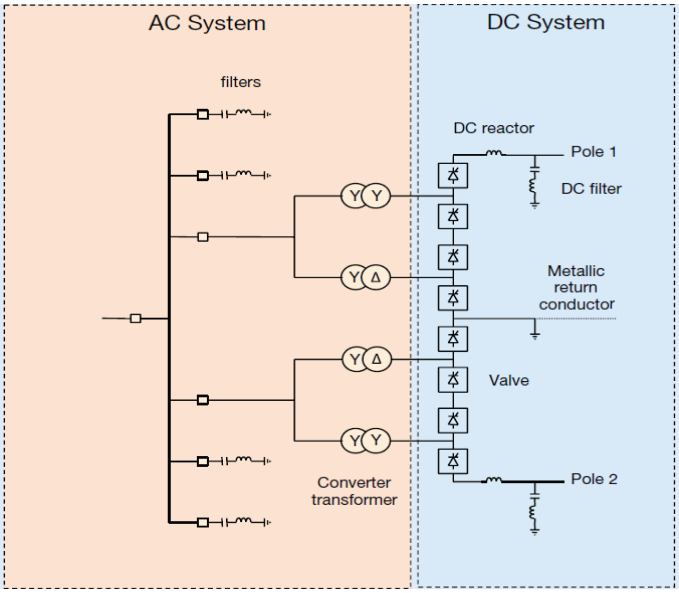

Figure 2.1: LCC-HVDC converter [**13**]

More specifically, the commutation of the converter valve is closely related to the stiffness of the ac voltage supply. For that reason the converter cannot operate properly when ac system impedance is high or system inertia is low. The reason is that the LCC cannot create ac voltage itself. It is always necessary for the operation of the LCC that the system it connects to provide the necessary voltage reference with inertia [**3**]. Another drawback for the case of LCC-HVDC system is that reactive power

compensation is needed. Significant amount of shunt reactive power compensation and harmonic filters are required for operation. This makes the substations large, occupying a big area making LCC impractical for very compact sites (figure 2.2 illustrates a typical LCC converter station layout) [**14**].

In addition, the application of LCC is limited to one direction current flow through each converter. For that reason in order to reverse the power flow of any individual terminal the dc voltage polarity must be reversed as well. This is the main reason why LCC based HVDC technology cannot be used in applications such as multi-terminal offshore dc networks [**12**] [**14**] [**15**]. In a multi-terminal dc network which applies LCC technology, changing the polarity of the dc voltage for one dc line will change the power flows in the network.

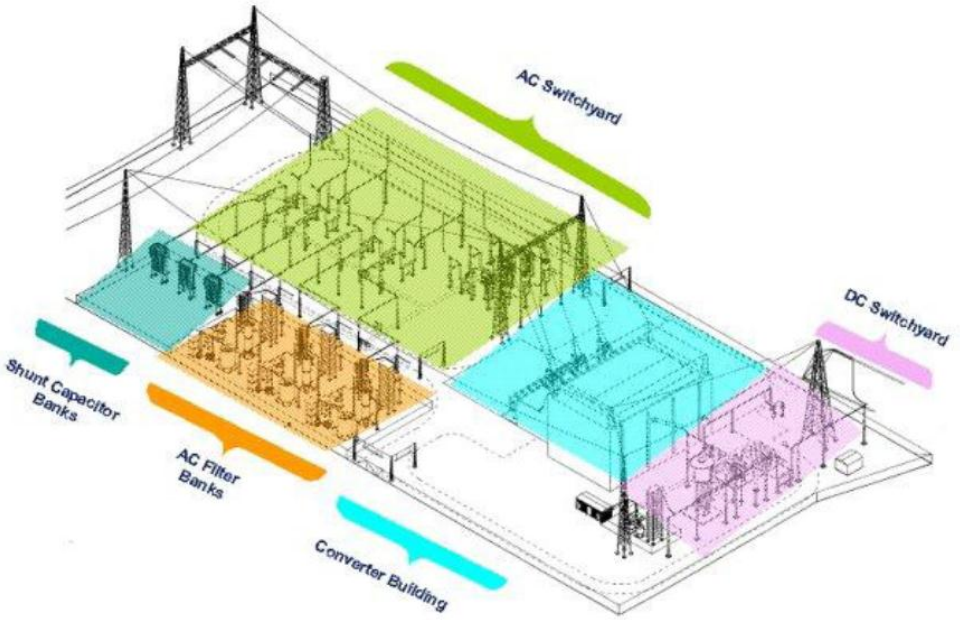

Figure 2. 2: A typical LCC converter station layout [**16**]

2.1.2 VSC-HVDC technology

The solution to the above problem is given by the utilization of the more recent version of HVDC technology known as the voltage source converter based high voltage direct current technology (VSC-HVDC). The development of VSC technology is based both on the improved performance and the increasing rating of the insulated gate bipolar transistors (IGBT). Also important role plays the controllability that IGBTs illustrate by means of capability to turn on and off and thus becoming a self commutated rather than line commutated converter. Furthermore, sinusoidal pulse width modulation technique (SPWM) gives flexibility and improves the performance of operation generating less harmonic distortion [**17**].

With the introduction of the VSC-HVDC, there is no need to change the dc voltage polarity in order to change the dc power flows, as it is the case of LCC technology. The last characteristic is very attractive for implementation of the VSC-HVDC at offshore dc networks. Furthermore, there is no need for reactive power compensation and no

need to install large filters to suppress harmonic distortion. As a result, the converter station of VSC-HVDC is more compact in comparison to the LCC technology with beneficial effects on the construction of compact and flexible offshore station [**3**]. Last but not least, with VSC-HVDC it is possible to undergo stage development of meshed ac-dc networks, with fast and cost efficient planning, construction and commissioning [**12**].

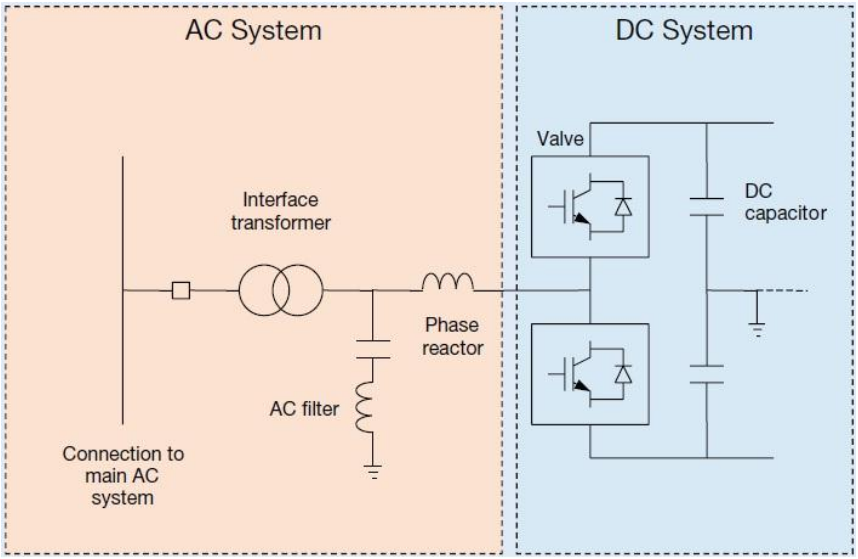

Figure 2.3: VSC-HVDC converter [**13**]

The most important technical advantage of VSC-HVDC compared to the LCC is the ability to produce its own voltage waveform independently from the ac network. VSC can produce the required sinusoidal ac voltage by proper switching of the IGBTs, even connected to a passive network. Furthermore, by utilization of suitable power synchronization control, it is possible to connect VSC-HVDC systems to high impedance weak ac systems, where the short-circuit level is low. Thus, VSC-HVDC technology has only limited requirements on the short circuit capacity of the system it connects to. On the contrary, it contributes limited short-circuit capacity to the ac system. Moreover, it can provide black start and system recovery in case of ac faults without losing pulse width modulation and commutation.

What is more, by implementing proper control scheme, such as vector control along with PWM, the VSC can adjust and control both active and reactive power independently. The latter is important for dynamic voltage support at the point of common coupling with the ac network. Also the ability to adjust active power gives inherent capability of frequency control in the synchronous area it operates.

In conclusion, the VSC-HVDC transmission system is increasingly getting more competitive in the field of transmission system technology and its applications are extended from point-to-point connection of asynchronous systems to more complex multi-terminal configurations, for the integration of large scale offshore wind power to the onshore power system network.

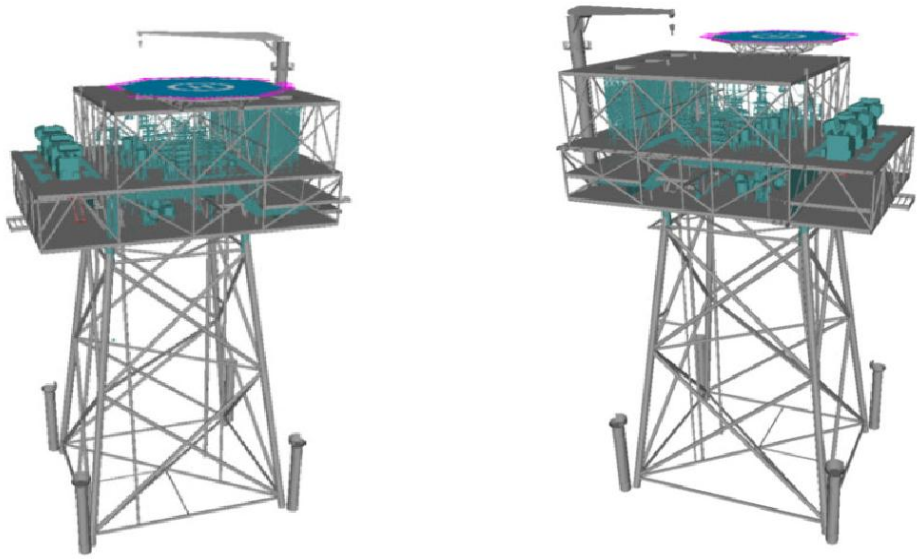

Figure 2.4: HVDC Light Offshore Platform layout [**16**]

2.1.2.1 VSC topological considerations

A classic three level VSC converter consists of three legs as illustrated in Figure 2.5. Each leg is identical to a single phase converter. There are separate controls signals for each leg. The control signals are sinusoidal waveforms with 50Hz frequency, 120^{o} shifted, as it can be seen in Figure 2.6. The sinusoidal signals are compared with a triangular high frequency carrier signal in order to create the pulses that switch on and off the IGBTs. The higher the frequency of the carrier signal, the less the harmonic distortion that appear. A typical value of the carrier frequency is in the region of 2-4kH. The amplitude of the sinusoidal signal, also known as modulation index, m_a should be in region of ($0<m_a<1$) for linear operation [**18**].

For each of the three legs, the ac voltage fundamental frequency component with respect to point N from figure 2.5 can be given as:

$$\left(v_{AN}\right)_{1,peak} = \frac{V_{control,peak}}{V_{tri,peak}}\frac{V_d}{2} = m_a\frac{V_d}{2} \tag{2.1}$$

Thus the fundamental component of the output voltage depends on the dc voltage at the input and the modulation index m_a as long as the modulation is in the linear region ($m_a<1$). From the above it is possible to calculate the fundamental component of the line-to-line RMS voltage such as:

$$\left(v_{LL}\right)_{1,peak} = \left(v_{\mathrm{AN}}\right)_1 - \left(v_{\mathrm{BN}}\right)_1 = \frac{\sqrt{3}}{\sqrt{2}}\left(v_{\mathrm{AN}}\right)_{1,peak} = \frac{\sqrt{3}}{2\sqrt{2}}\frac{V_{control,peak}}{V_{tri,peak}}V_d \approx 0.612 m_a V_d \tag{2.2}$$

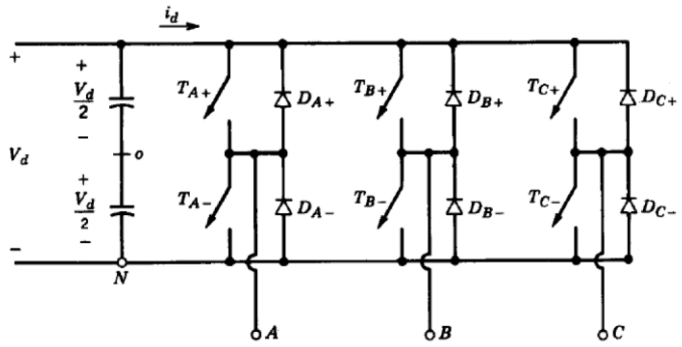

Figure 2.5: Three-phase switch-mode converter where T_c is the switching device **[**18**]**

It is important to notice that for stability studies and dynamic simulations in general, only the fundamental frequency of the voltage is of main importance. Hence, the converter can be represented as controlled in amplitude and phase voltage source with 50Hz.

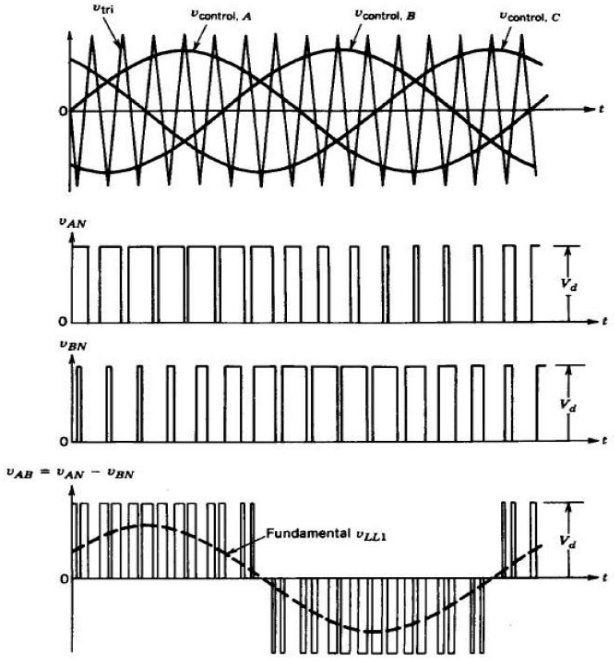

Figure 2.6: Pulse Width Modulation of a three-phase converter **[**18**]**

2.1.3 HVDC Submarines cables

HVDC submarines cables have been used since 1950s for interconnection of asynchronous systems via classic HVDC technology. Up to date there is a rapid market development especially due to the interest from offshore wind industry [**3**]. HVDC cables do not "suffer" from the charging current limitations of ac cables. Transmission distances for HVDC cables are considered high. In general their operation voltages are higher than the ac equivalent cables. The highest installed HVDC submarine cable up to date is operating at ±500kV and has a conductor cross section 3000mm^2 capable of carrying 1400MW per cable (Kii channel project crossing Japan) [**19**].

Each submarine cable consists of the conductor (or core). The main materials used for the conductor is stranded copper or aluminium (for lighter applications). HVDC cables are generally single core, but it can also be double cores allowing one bipole circuit to be laid as a single cable (application in the NorNed cable). Surrounding the core is the insulation material. The thickness of the insulation material depends on the operational voltage. A metallic sheath and a plastic outer layer protect the cable and prevent moisture ingress. Two types are widely used: the cross linked polyethylene (XLPE) and mass impregnated paper (MI) [**3**], both illustrated in Figure 2.7.

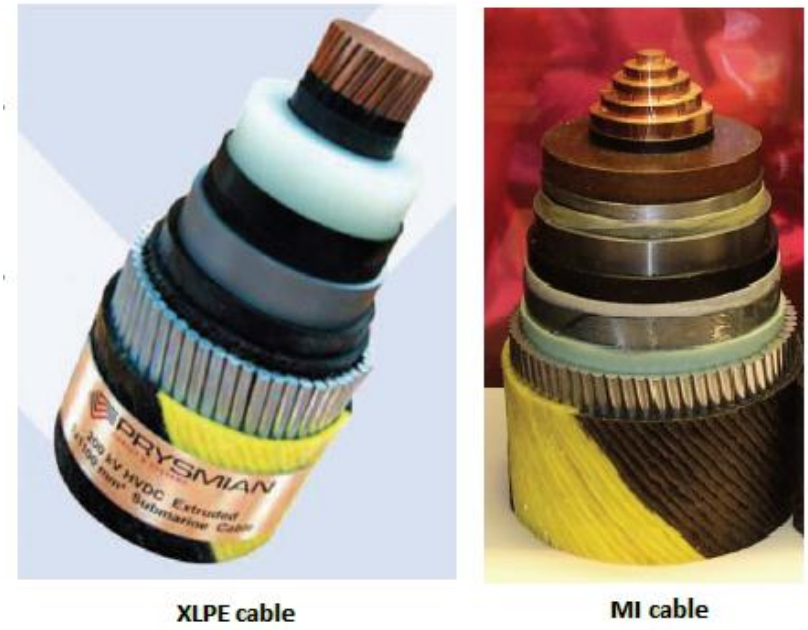

Figure 2.7: Marine Cable technology [**3**]

2.2 Meshed dc-ac network operational aspects and effects on onshore power system stability

The operation of an offshore North Sea HVDC network should be perceived as an integral part of the operation of the overall interconnected European transmission system. Consequently, good coordination of the power dispatch scheme is required between the various interconnected converters in order to ensure the security of supply. In other words, the operation of a MTdc network need to comply with the requirements of the onshore power system.

2.2.1 Operational aspects of the MTdc network

There are different modules that operate in the offshore multi-terminal dc network. A dc network will include wind park voltage source converter (WPVSC) stations that are responsible to connect each wind farm (or groups of wind farms) to the dc network. These converter stations would be located on offshore platforms. They can operate as offshore hub-stations that connect groups of wind farms to the MTdc network. The main responsibility of WPVSCs is to inject the generated power from the wind parks to the dc network. This is achieved by implementing an appropriate control strategy that keeps

the offshore wind park ac voltage amplitude constant, providing a rotating voltage reference to the wind turbines control modules [**17**].

An offshore dc network would also include a number of GSVSC stations for connection to the onshore power system. The main duty of the GSVSC stations is to dispatch power to the ac connection points. In addition, they are responsible for the control of the dc voltage in the MTdc network. The common approach described in literature in terms of the control is that all but one GSVSC station is operated in power control mode (injecting constant active power) while the last one is in direct voltage control mode [**15**] [**20**].

However it is necessary that all GSVSCs can participate in the control of the dc voltage and not only the slack GSVSC. In the last case, different control strategies are suggested for the operation of the GSVSCs [**17**] [**8**]. The most significant facilitates either a voltage margin control method (VMM) [**8**] or a dc voltage droop control method [**21**]. These controllers are responsible to control the direct voltage in the dc network and also facilitate power dispatch among the GSVSCs. Hence, the wind power that is fed into the dc network can be shared among the GSVSCs according to market scenarios while the dc voltage is kept within operational limits.

Operational challenges arise when there is need to isolate the faulty component of the dc network following dc-side faults [**22**]. Moreover, the variations of wind power can cause variations of the dc network voltage, which under specific conditions may trigger emergency or protection mechanisms. Aside from the protection and dc breaker development issues, there are primary control problems. Particularly, one of them is the autonomous sharing of power imbalance among the converters following a converter or cable outage [**23**]. As discussed above, there are committed GSVSC stations that are responsible for controlling the DC voltage. For that reason a trip of GSVSC station should be tackled with fast take over from another GSVSC station.

Therefore from operational point of view of the MTdc network there are aspects that require special attention such as the control of dc voltage and the management of dc power flows in such a multi-input/output system. All these challenges need to be investigated and addressed in a coordinated way so as the operation of the offshore dc network will not put in risk the stability of onshore power system.

2.2.2 Imposed requirements of offshore HVDC in order to ensure the security of supply

From the onshore transmission system operator (TSO) point of view, one of the major concerns is the significant loss of power in-feed (which can reach GW scale) to the onshore connection points. Moreover, the replacement of conventional generation with offshore wind power that is transported onshore through multi-terminal dc networks raise issues about the operation of GSVSCs that are connected to onshore networks. From the ac system point of view the attention is mainly placed on the operation of the GSVSC because it is the type of converter station that primary injects active and reactive power to the AC power system and secondary decouples the operation of the dc

network from the ac power system under normal and preferably faulted operating condition [**3**].

The ability of the GSVSC station to independently control active and reactive power makes it capable of providing onshore network voltage support while transmitting power. In addition, the expected large amount of power that these converters feed to the AC system in combination with replacement of conventional generation, call for functionality such as AC frequency support, voltage support, reactive power support, fault ride through capability and synthetic inertia capability [**24**] [**25**] [**26**].

Thus there is more and more the tendency to expect from these modules to emulate conventional generation behavior. In addition, the inherent ability of the GSVSC to response quickly combined with the fact that they are typically installed at non-generator buses can provide power injection control at new points within the network and can be utilized to further improve AC power system dynamic behaviour [**27**] [**28**].

It is important to mention that when a dc connection is utilized to transport power from the offshore wind farms to the onshore network, the onshore frequency variations are "invisible" to the offshore wind farm. For that reason the system inertia is lower in the case that large scale wind power is transported through dc network configurations and becomes less when conventional generation is taken away. The low inertia appeared in the onshore system may trigger unstable situations, after a disturbance occurs. For that reason in order to ensure the security of supply it is important that the GSVSCs and the MTdc network in general provides with synthetic inertia the onshore power system increasing in such a way the power system operational limits [**25**] [**29**].

Requirements such as capability to take up after a disturbance in isolated network operation, black start capability, island operation capability, reconnection after tripping, power oscillation damping capability and synthetic inertia capability at low frequency event would be some of the critical TSOs requirements.

In the present project it will be investigated how the GSVSCs can provide ac voltage support, reactive power support and participation to fault current under fault conditions. In addition, it will be illustrated how specific controllers operating at the GSVSCs can introduce damping of power oscillations to the onshore power system improving the dynamic behaviour of generators.

Chapter 3: Modular Dynamic Model of Multi-terminal DC Networks

3.1 Modular Dynamic model of MTdc network

The commonly used approach to represent power system modules in stability studies is facilitating standard equivalent time dependent phasor average models [**30**]. Standard models have been developed for the majority of power systems modules such as synchronous generators, excitations systems, governors, power system stabilizers and prime movers for hydro, steam and gas turbines. Different IEEE models of the above modules already exist in most libraries of power system software packages (such as Siemens PTI PSSE and DigSilent Power Factory). The advantage of using standard models is that data exchange between utilities and also the transition to new software is much more convenient [**30**].

However to the best of author's knowledge in the commercial software tools there are no available generic and standard dynamic models of VSC-MTdc systems that can easily be extended to every conceivable dc network topology. In PSSE for instance, there is only a four terminal (point-to-point) LCC-HVDC model, and an eight terminal system that utilizes LCC-HVDC technology limited only to a specific topology and numbers of converters [**6**]. For VSC-HVDC system, there is only a point-to-point model available (ABB, HVDC Light).

For the aforementioned reasons in this chapter a detailed proposal will be given about a generic modular dynamic model of multi-terminal VSC-HVDC network. As given in [**31**] "modularity is the practice of building complex systems from smaller subsystems that can be designed independently". More specifically for each module of the MTdc network, a relevant dynamic model has been developed. The development of the dynamic model of MTdc network into modules gives inherent flexibility and capability to further upgrade the different modules or substitute some of them with new independently from each other. In the MTdc network the main modules that can be defined and have been used are wind farm, VSC-HVDC converter stations with controllers, HVDC cables and protective systems that operate under emergency situation [**31**].

In the first part of this chapter a generic model of VSC will be given. As for the HVDC cables the π-equivalent circuit model has been adapted as the commonly used approach to model HVDC cables in stability studies [**32**] [**33**]. Moreover, it will be explained how the π-equivalent model is extended to a generic multi-terminal dc network configuration [**7**]. The model can be extended from a point-to-point connection to multi-terminal networks. In the second part of the chapter, certain simplifications of the proposed

generic model will be discussed and a simplified model will be given for development in PSSE.

To summarize, the proposed model is capable of simulating MTdc network structures with large number of converters, connected to any offshore dc network layout that can operate connected with large scale power systems [**7**]. It can easily be used in studies related to the transient stability of heavily meshed Power Systems with VSC-HVDC multi-terminal network.

3.2 Generic VSC-HVDC model for transient stability studies

The VSC-HVDC converter is connected to the ac power system via a phase reactor and a transformer. Figure 3.1 introduces the building blocks of the VSC-HVDC transmission system. The VSC module employs IGBTs (or GTOs) in order to create the three phase sinusoidal voltage waveforms. The transformer is facilitated to change the ac voltage of the converter to the appropriate ac voltage level of the connection point. The purpose of the phase reactor is to reduce high-frequency harmonic contents of the VSC current caused by the switching of the IGBTs. An ac harmonic filter is connected between the phase reactor and the transformer. The main functionality of the filter is to suppress high-frequency voltage harmonics into the ac side of the VSC [**18**].

From the dc side of the converter station there is a dc capacitor connected to the terminal of the HVDC cable. The main purpose of the dc capacitor is to smooth the dc voltage ripple in the dc side and keep in such way the direct voltage constant.

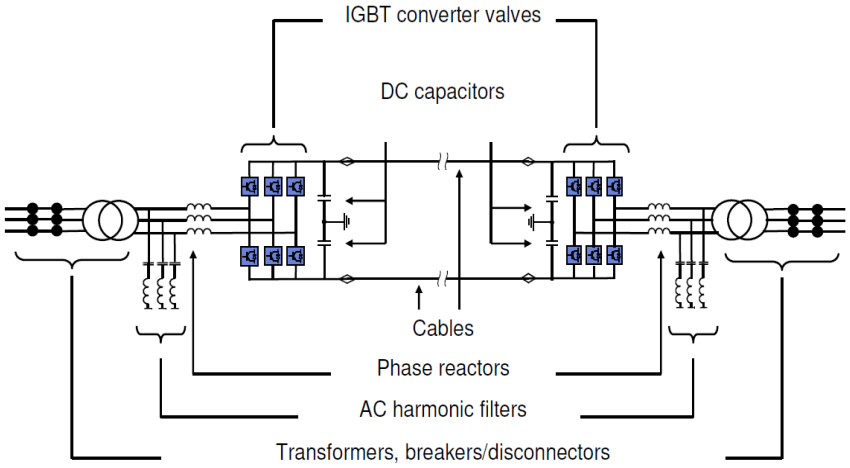

Figure 3.1: Building blocks of the VSC-HVDC transmission system

For stability studies, it is common to represent the converter module by controlled phasor average models [**34**]. Figure 3.2 introduces the equivalent ac circuit of the VSC model, where $\tilde{U}_s$ is the phasor of the system voltage and $\tilde{U}_c$ is the phasor of the converter ac terminal voltage.

In the equivalent model, X_{tr} and X_{pr} are the reactance of the transformer and the phase reactor respectively. It has been proved [**30**] that the filter shows pure capacitive behaviour at the system frequency. For that reason the filter can be represented by a

shunt capacitor as it is illustrated in Figure 3.2. In that model, $\tilde{U}_f$ is the phasor of the voltage across the capacitor and $\tilde{i}_{tr}$ and $\tilde{i}_{pr}$ is the phasor of the transformer and phase reactor current, respectively.

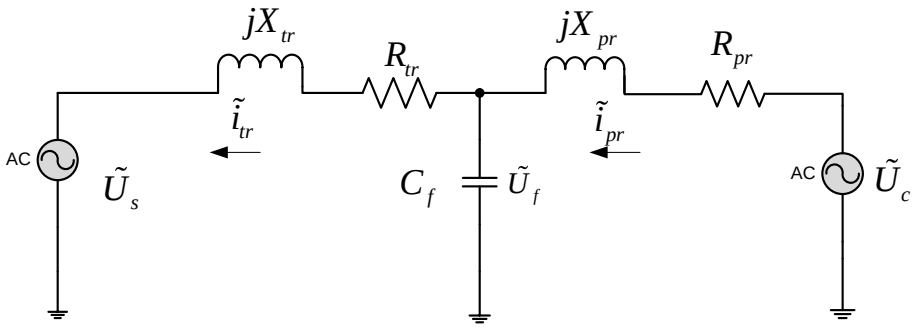

Figure 3.2: single line diagram of the AC circuit for the VSC with filter when performing inversion

From the equivalent circuit, three differential equations can be derived, one for each storage element (L and C). More specifically in the stationary reference frame for a symmetrical system, the differential equations are given as:

$$\tilde{u}_c - \tilde{u}_f = L_{pr}\frac{d}{dt}(\tilde{i}_{pr}) + R_{pr}\tilde{i}_{pr} \tag{3.1}$$

$$\tilde{u}_f - \tilde{u}_s = L_{tr}\frac{d}{dt}(\tilde{i}_{tr}) + R_{tr}\tilde{i}_{tr} \tag{3.2}$$

$$\tilde{i}_{pr} = \tilde{i}_{tr} + C_f\frac{d}{dt}(\tilde{u}_f) \tag{3.3}$$

However, in most of power system stability studies a synchronized with the system frequency, *dq* reference frame is adapted due to the advantages it gives to the calculations. Applying the relevant transformation [**35**] to (3.1) we obtain:

$$\frac{d}{dt}(i_{pr}^d e^{j\omega t}) = -\frac{R_{pr}}{L_{pr}} i_{pr}^d e^{j\omega t} + \omega i_{pr}^q e^{j\omega t} + \frac{1}{L_{pr}}\left(u_c^d - u_f^d\right)e^{j\omega t} \tag{3.4}$$

$$\frac{d}{dt}(i_{pr}^q e^{j\omega t}) = -\frac{R_{pr}}{L_{pr}} i_{pr}^q e^{j\omega t} - \omega i_{pr}^d e^{j\omega t} + \frac{1}{L_{pr}}\left(u_c^q - u_f^q\right)e^{j\omega t} \tag{3.5}$$

The angle ωt is provided by the phase lock loop (PLL). The PLL is the control system that acts on the phase difference between the reference signal and the input, such that the phase of the output is locked to the phase of the reference.

Dividing equations (3.4) and (3.5) by $e^{j\omega t}$ we obtain the differential equations of the ac circuit of the VSC in the *dq* reference frame. Equations (3.6) and (3.7) describe the current flowing through the phase reactor as a function of the voltage drop across the

reactor. The term $\omega\, i_{pr}^{q}$ that appears represents the synchronous rotation of the *dq* frame. More specifically, as it can be seen from the equations, this term introduces a cross coupling between the direct (d-axis) and quadrate (q-axis) current. The cross coupling introduces a dependence of the d-axis component of the current to the q-axis and the other way around.

$$\frac{d}{dt}(i_{pr}^{d}) = -\frac{R_{pr}}{L_{pr}} i_{pr}^{d} + \omega i_{pr}^{q} + \frac{1}{L_{pr}}\left(u_{c}^{d} - u_{f}^{d}\right) \tag{3.6}$$

$$\frac{d}{dt}(i_{pr}^{q}) = -\frac{R_{pr}}{L_{pr}} i_{pr}^{q} - \omega i_{pr}^{d} + \frac{1}{L_{pr}}\left(u_{c}^{q} - u_{f}^{q}\right) \tag{3.7}$$

Applying the same transformation to the equations (3.2) and (3.3) we finally derive the differential equations that describe the ac side of the VSC connected to an ac bus, in the *dq* rotating reference frame.

$$\frac{d}{dt}(i_{tr}^{d}) = -\frac{R_{tr}}{L_{tr}} i_{tr}^{d} + \omega i_{tr}^{q} + \frac{1}{L_{tr}}\left(u_{f}^{d} - u_{s}^{d}\right) \tag{3.8}$$

$$\frac{d}{dt}(i_{tr}^{q}) = -\frac{R_{tr}}{L_{pr}} i_{pr}^{q} - \omega i_{tr}^{d} + \frac{1}{L_{pr}}\left(u_{f}^{q} - u_{s}^{q}\right) \tag{3.9}$$

With the voltage of the filter bus given as:

$$\frac{d}{dt}(u_{f}^{d}) = -\omega\, u_{f}^{d} + \frac{1}{C_{f}}(i_{pr}^{d} - i_{tr}^{d}) \tag{3.10}$$

$$\frac{d}{dt}(u_{f}^{q}) = \omega\, u_{f}^{q} + \frac{1}{C_{f}}(i_{pr}^{q} - i_{tr}^{q}) \tag{3.11}$$

Nevertheless, many models proposed in the literature do not take into account the filter bus [**30**] [**31**] [**23**]. The use of multi-level converter technology introduces very small harmonic distortion and thus there is no need for installation of harmonic filters or if needed these filters are small and can be safely neglected for stability studies. In this situation the transformer impedance can either be included in the impedance of the phase reactor or be part of the short circuit impedance of the network at the specific bus. Hence, the equivalent circuit of the ac side of a VSC connected to an ac bus is simplified to the ac circuit illustrated in Figure 3.3. In addition, in most of situations the resistance of the phase reactor is too small and can safely be neglected as well.

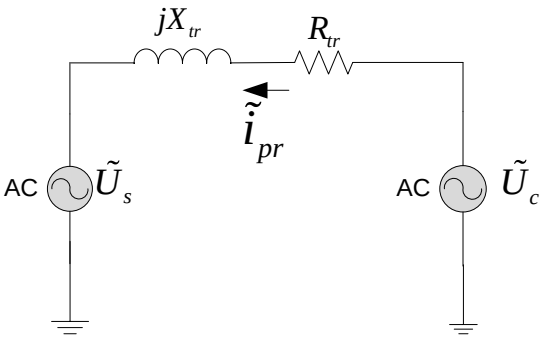

Figure 3.3: single line diagram of the AC circuit for the VSC with filter, where U_s is the network voltage while U_c the VSC voltage

The benefit of neglecting the filter in dynamic simulations relates to simplification of the differential equations by neglecting very small time constants. The time constants associated with the ac filter capacitor are in ms scale and much faster than the ac power system time constants [**34**]. Therefore, X_{pr} will be the critical parameter for the control system. Thus equations (3.6) to (3.11) reduce to equations (3.12) and (3.13):

$$\frac{d}{dt}(i_{pr}^{d}) = -\frac{R_{pr}}{L_{pr}} i_{pr}^{d} + \omega\, i_{pr}^{q} + \frac{1}{L_{pr}}\left(u_c^{d} - u_s^{d}\right) \tag{3.12}$$

$$\frac{d}{dt}(i_{pr}^{q}) = -\frac{R_{pr}}{L_{pr}} i_{pr}^{q} - \omega\, i_{pr}^{d} + \frac{1}{L_{pr}}\left(u_c^{q} - u_s^{q}\right) \tag{3.13}$$

3.3 Dynamic Model of MTdc networks cables

In this paragraph a general description of the dc link cable model used for dc network configurations will be given. The model that has been adapted for the dc cable is the π-equivalent. It consists of a capacitor which is used to model the capacitance of the cables and an inductance with resistance. In addition a description about the way that the cable models can be assembled to a generic multi-terminal dc network for every dc network topology and number of VSCs will be given. This is the main approach that has been adapted in the modeling of the HVDC cables for dynamic simulations [**32**] [**7**] [**21**].

3.3.1 DC cable equivalent model

The equivalent circuit that represents the dc cable for transient stability studies is illustrated in Figure 3.4. Applying circuit laws in time domain, the differential equations can be obtained such as introduced in (3.14) to (3.16).

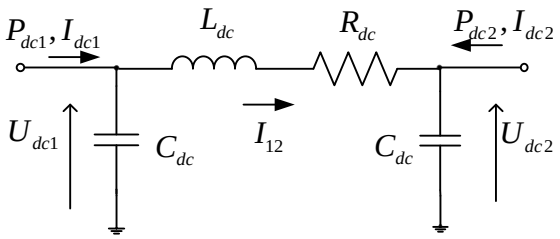

Figure 3.4: π-equivalent model for DC cables

$$C_{dc}\frac{dU_{dc1}}{dt} = I_{dc1} - I_{12} \tag{3.14}$$

$$C_{dc}\frac{dU_{dc2}}{dt} = I_{dc2} + I_{12} \tag{3.15}$$

$$L_{dc}\frac{dI_{12}}{dt} = U_{dc1} - U_{dc2} - R_{dc}I_{12} \tag{3.16}$$

Rearranging the above differential equations, it is possible to obtain the state space representation of the dc cable as showed in (3.17). It is worth mentioning that the dc capacitor of the VSC station (Figure 3.1) is included and hence modeled by the dc cable capacitance in Figure 3.4. Hence the dc cable capacitance represents the sum of VSC and the π-equivalent cable model capacitance.

$$\frac{d}{dt}\begin{bmatrix} U_{dc1} \\ U_{dc2} \\ I_{12} \end{bmatrix} = \begin{bmatrix} 0 & 0 & -\frac{1}{C_{dc}} \\ 0 & 0 & \frac{1}{C_{dc}} \\ \frac{1}{L_{dc}} & -\frac{1}{L_{dc}} & -\frac{R}{L_{dc}} \end{bmatrix}\begin{bmatrix} U_{dc1} \\ U_{dc2} \\ I_{12} \end{bmatrix} + \begin{bmatrix} \frac{1}{C_{dc}} & 0 \\ 0 & \frac{1}{C_{dc}} \\ 0 & 0 \end{bmatrix}\begin{bmatrix} I_{dc1} \\ I_{dc2} \end{bmatrix} \tag{3.17}$$

3.3.2 Generic model of MTdc network cables

In the previous paragraph it has been introduced the state space representation of simple HVDC cable. In this paragraph this method will be generalized into generic equations that describe for every possible layout of MTdc network the matrix A and B of the state space model [**7**] [**36**]. The state space model of an arbitrary MTdc network, with n number of nodes and m number of branches is given in the following generic form:

$$\frac{dx}{dt} = Ax + bu \tag{3.18}$$

Where the state vector is defined as:

$$x = \begin{bmatrix} U_{dc}^1 & U_{dc}^2 & \cdots & U_{dc}^n & I_{br}^1 & I_{br}^2 & \cdots & I_{br}^m \end{bmatrix} \tag{3.19}$$

And the input vector is:

$$u = \begin{bmatrix} I_{dc}^{1} & I_{dc}^{2} & \cdots & I_{dc}^{n} \end{bmatrix} \tag{3.20}$$

While matrix A can be written such as:

$$A = \begin{bmatrix} a_{11}^{n\times n} & a_{12}^{n\times m} \\ a_{21}^{m\times n} & a_{22}^{m\times m} \end{bmatrix} \tag{3.21}$$

Where:

$$a_{11}^{n\times n} = [0]_{n\times n} \tag{3.22}$$

$$a_{12}^{n\times m} = -diag\begin{pmatrix} \frac{1}{C_1} & \frac{1}{C_2} & \cdots & \frac{1}{C_n} \end{pmatrix}[M]^T \tag{3.23}$$

$$a_{21}^{m\times n} = diag\begin{pmatrix} \frac{1}{L_1} & \frac{1}{L_2} & \cdots & \frac{1}{L_m} \end{pmatrix}[M] \tag{3.24}$$

$$a_{22}^{m\times m} = -diag\begin{pmatrix} \frac{R_1}{L_1} & \frac{R_2}{L_2} & \cdots & \frac{R_m}{L_m} \end{pmatrix} \tag{3.25}$$

The B matrix is written as:

$$B = \begin{bmatrix} b_{11}^{n\times n} \\ b_{21}^{j\times n} \end{bmatrix} \tag{3.26}$$

Where the sub-matrices are defined as:

$$b_{1}^{n\times n} = diag\begin{pmatrix} \frac{1}{C_1} & \frac{1}{C_2} & ... & \frac{1}{C_n} \end{pmatrix} \tag{3.27}$$

$$b_{21}^{j\times n} = [0]_{j\times n} \tag{3.28}$$

M is the incident matrix which describes the topology of the dc network layout. In order to give a better understanding of the method followed to represent the dc cables in MTdc networks an example it has been given in Appendix C.

3.4 Controllers used in the VSC

Most VSC have a cascaded control structure that compromises an inner current control loop and outer controllers [**17**]. The outer controllers are facilitated to control active and reactive power flows as well as the ac and dc voltage of the VSC. The active and reactive power controllers are acting on the d and q-axis component of the VSC ac current. The same applies for ac and dc voltage controllers. The majority of control methods implemented in the VSC-HVDC system are based on vector control [**7**] [**21**] [**8**]. All the controllers are basically proportional-integral controllers (PI) [**32**] [**30**].

3.4.1 Inner Controllers

The differential equations derived in (3.12) and (3.13) describe the dynamic behavior of the current flowing though the phase reactor. In fact they describe the open loop model of the phase reactor itself (no controls are considered so far) with the converter voltage as input and the current as output. In this sense, one may think that controlling the voltage of the converter in the open loop model it is feasible to control the current flowing through the phase reactor, which as a concept is not totally wrong. However such an approach is not followed.

More specifically from figure 3.3 with the flow of current from the ac network to the converter (rectifying mode) we define the d-axis component (same applies for the q-axis) of the variable v_d such as:

$$v_d = u_s^d + \omega L i_q \tag{3.29}$$

Then equation (3.12) in the Laplace domain (s=d/dt) can be given as:

$$i_d = \frac{1}{R_{pr} + sL_{pr}}\left(v_d - u_c^d\right) \tag{3.30}$$

However the open loop system, as illustrated in equation 3.30 introduces a pole at the location $-R_{pr}/L_{pr}$. The inner resistance R_{pr} is typically very small and consequently the open loop system will have a pole close to zero, introducing integrator characteristics. Thus, it becomes clear that the open loop system of equations (3.12) and (3.13) would introduce weakly damped dynamic behavior of the VSC and is not facilitated. Figure 3.5 illustrates the block diagram representation of the open loop system.

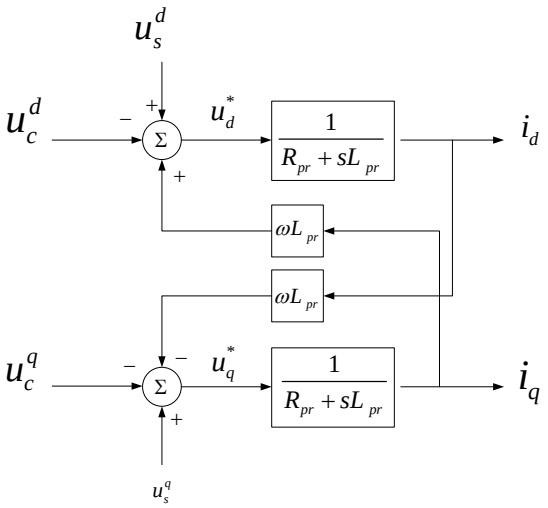

Figure 3.5: block diagram of the open loop system

In order to improve the performance of the VSC, the current loop is closed, implementing thus an inner controlled feedback. If the phase reactor current is feedback and the current error is controlled via a PI controller the system illustrates better dynamic response. It can quickly reach the reference current without undergoing oscillations and the steady state error vanishes.

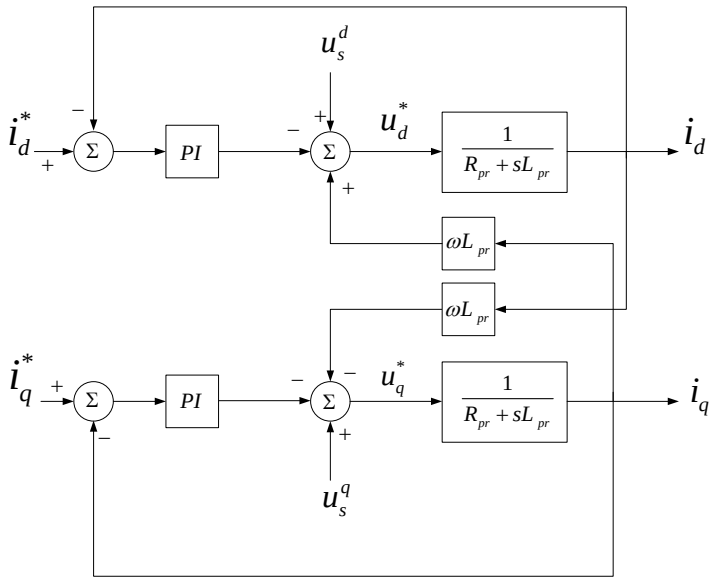

Figure 3.6: block diagram of the inner controller, closed loop system

From the above, it becomes clear that the main duty of the inner controller is to provide voltage reference values for the VSC, for any given current reference value of the outer controller. The current reference value is the output of the outer controllers which will be described in next paragraph. In Laplace domain the d and q component of the voltage reference can be expressed as:

$$u_{c,ref}^d = u_s^d + \omega L_{pr} i_{pr}^q + \left(k_{p1} + \frac{k_{i1}}{s}\right)\left(i_{pr,ref}^d - i_{pr}^d\right) \tag{3.31}$$

$$u_{c,ref}^{q} = u_{s}^{q} - \omega L_{pr} i_{pr}^{d} + \left(k_{p1} + \frac{k_{i1}}{s} \right) \left(i_{pr,ref}^{q} - i_{pr}^{q} \right) \tag{3.32}$$

In addition, the relation between the actual voltage value and the reference value of the converter can be represented by a time delay T_d. This is actually the time constant associated with the modulator of the VSC.

$$\frac{d}{dt}\left(u_{c}^{d}\right) = -\frac{1}{T_d} u_{c}^{d} + \frac{1}{T_d} u_{c,ref}^{d} \tag{3.33}$$

$$\frac{d}{dt}\left(u_{c}^{q}\right) = -\frac{1}{T_d} u_{c}^{q} + \frac{1}{T_d} u_{c,ref}^{q} \tag{3.34}$$

For application in PSSE software 3.31 and 3.32 can be written in another form. More specifically if we introduce two additional state variables, ξ_d and ξ_q such as:

$$\frac{d}{dt}\left(\xi_{d}\right) = -k_{i1} i_{pr}^{d} + k_{i1} i_{pr,ref}^{d} \tag{3.35}$$

$$\frac{d}{dt}\left(\xi_{q}\right) = -k_{i1} i_{pr}^{q} + k_{i1} i_{pr,ref}^{q} \tag{3.36}$$

and combine (3.35), (3.36) with (3.31) and (3.32) in time domain the voltage reference differential equations can be expressed by two algebraic equations (3.37) & (3.38) and two differential equations (3.35) & (3.36).

$$u_{c,ref}^{d} = u_{s}^{d} + \omega L_{pr} i_{pr}^{q} + k_{p1}\left(i_{pr,ref}^{d} - i_{pr}^{d} \right) + \xi_{d} \tag{3.37}$$

$$u_{c,ref}^{q} = u_{s}^{q} - \omega L_{pr} i_{pr}^{d} + k_{p1}\left(i_{pr,ref}^{q} - i_{pr}^{q} \right) + \xi_{q} \tag{3.38}$$

The algebraic and differential equations can be utilized in the case that the dynamic models are developed in PSSE software package. In PSSE every dynamic model is separated into modes. A mode represents a different stage in the dynamic simulation process. In the beginning the model must initialize the state variables and algebraic variables (mode 1). For every time step first the differential equations (3.35) and (3.36) are solved by calculation of the state derivatives or DSTATES (in mode 2) and then the algebraic equations (3.37) and (3.38) determine the converter voltage (in mode 3). An analytical description of the method to build dynamic models in PSSE can be found in [**6**].

3.4.2 Outer Controllers

The grid side converter station is capable of controlling active and reactive power independently. This can be achieved by implementing a proper vector control method. The basic principle behind the vector control is to align the d-axis (or the q axis respectively) of the rotating *dq* reference frame with the synchronously rotating vector of the system voltage, U_s.

Figure 3.7 introduces the phasor diagram of the VSC connected to an infinite bus with the phase reactor resistance neglected. It can be observed that in the case the synchronously rotating reference frame is aligned to the rotating voltage vector of the system, there is no q-axis component of the system voltage $\tilde{U}_s$ while the d-axis component is equal to the voltage amplitude.

$$\text{Thus, } \left|\tilde{U}_s\right| = \sqrt{\left(u_s^d\right)^2 + \left(u_s^q\right)^2} \xrightarrow{u_s^q = 0} \left|\tilde{U}_s\right| = u_s^d \tag{3.39}$$

In this situation the active power through the phase reactor can be given from:

$$P = u_s^q i_{pr}^q + u_s^d i_{pr}^d \xrightarrow{u_s^q = 0, u_s^d = U_s} P = u_s^d i_{pr}^d \tag{3.40}$$

And the reactive power, respectively:

$$Q = u_s^q i_{pr}^d - u_s^d i_{pr}^q \xrightarrow{u_s^q = 0, u_s^d = U_s} Q = -u_s^d i_{pr}^q \tag{3.41}$$

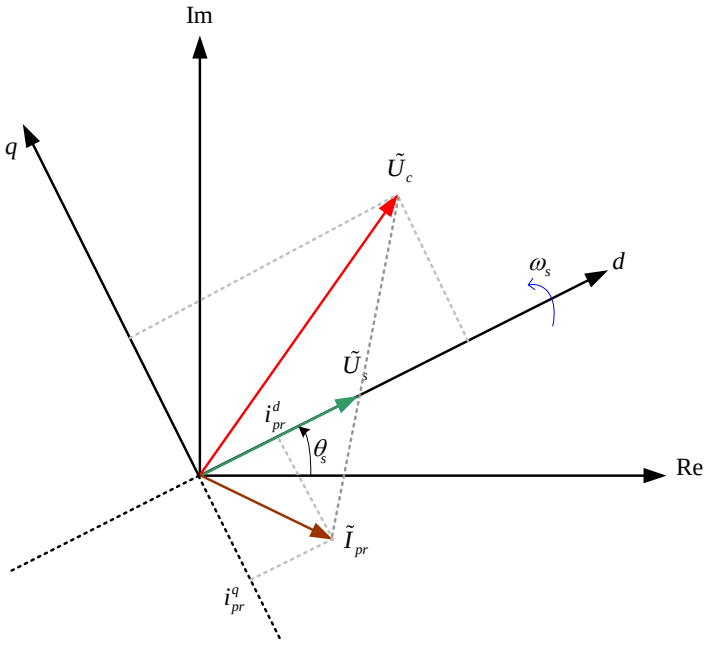

Figure 3.7: Phasor diagram for explanation of the vector control

From the above two equations it can be concluded that implementing a proper vector control it is possible to decouple the control of active and reactive power. The only constraint in this control scene is that a stiff ac bus is required to provide rotating voltage reference.

3.4.2.1 Active Power Controller

The active power controller is responsible to control the power injection of the VSC to the ac bus it connects to. Applying the vector control scheme that has been described above it is possible to decouple the control of active and reactive power. Also in the same synchronized *dq* reference frame it has been shown that active power can be given by the following equation.

$$P = \left|\tilde{U}_s\right| i_{pr}^{d} \tag{3.42}$$

Hence, from equation (3.42) it becomes clear that controlling i_{pr}^{d}, it is possible to control the active power of the VSC. Consequently, facilitating a PI controller it is possible to insert a feedback loop which will control the active power of the converter. The active power controller is given in Laplace domain as:

$$i_{pr,ref}^{d} = \frac{P_{ref}}{u_s^d} + \left(k_p + \frac{k_i}{s}\right)\left(P_{ref} - P\right) \tag{3.43}$$

The change in i_{pr}^{d} current is facilitated by the inner controller given in Figure 3.6. In that control scheme, the reference current $i_{pr,ref}^{d}$ is the output of the active power controller introducing thus another control feedback to the system.

3.4.2.2 Direct Voltage Controller

The direct voltage controller is responsible for controlling the voltage at the terminal of the dc line of the VSC. It is worth stressing out that in the MTdc network always there should be a VSC that controls the direct voltage within adequate limits [**21**]. Figure 3.8 introduces the equivalent circuit that demonstrates the way that ac and the dc part of the VSC are coupled.

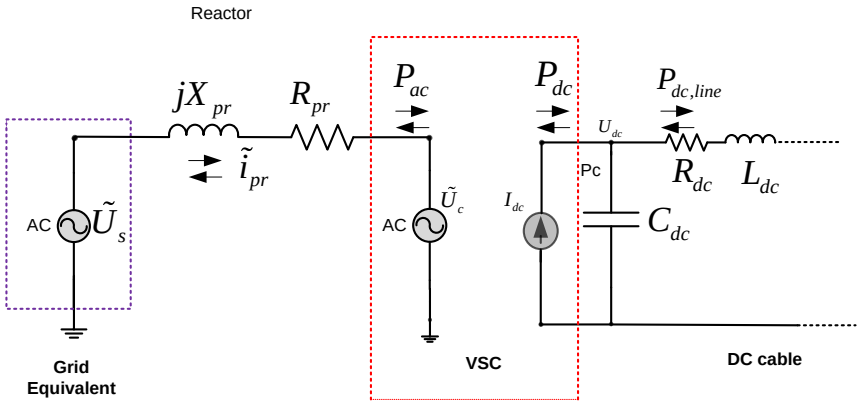

Figure 3.8: Equivalent circuit of the ac and the dc side of the VSC

The converter itself is a controlled voltage source from the ac side while from the dc side it is modeled as a controlled dc current injection [**21**]. The ac and dc side are coupled by the active power balance, while the losses are not considered in this case. In practice the converter has an active power loss in the region of 1%, but in this study it is modeled lossless [**30**]. For that reason the dc input (output) power P_{dc} equals the ac output (input) P_{ac} such as:

$$P_{ac} = P_{dc} \Rightarrow u_c^q i_{pr}^q + u_c^d i_{pr}^d = I_{dc} U_{dc} \tag{3.44}$$

In addition, the DC power balance at the terminal of the dc capacitor C_{dc} is given as:

$$P_{dc} - P_{dc,line} = P_c = \frac{dW_c}{dt} = \frac{d\left(\frac{1}{2}C_{dc}U_{dc}^2\right)}{dt} \tag{3.45}$$

If we substitute (3.44) into (3.45) we receive:

$$P_{ac} - P_{dc,line} = \frac{1}{2}C_{dc}\frac{d\left(U_{dc}^2\right)}{dt} \tag{3.46}$$

From (3.46) it can be concluded that the ac active power control is intimately linked to the direct voltage (U_{dc}). From the above it becomes clear that controlling the active power injection of the VSC at a specific ac bus, it is possible to control the power balance in the DC capacitor and thus the dc voltage at the terminal of the dc line.

In such way, another control loop is introduced in the direct axis component of the current reference such as:

$$i_{pr,ref}^{d} = i_{pr,ref\,0}^{d} + \left(k_p + \frac{k_i}{s}\right)\left(U_{dc,ref} - U_{dc}\right) \tag{3.47}$$

In this control loop the actual direct voltage at the dc terminal is compared with the reference direct voltage. The error signal is the input of the PI controller. In such a way it is possible to control the dc voltage of the VSC. The VSC normally operates either in direct voltage control mode (utilizing controller 3.47) or in active power control mode (controller 3.43).

3.4.2.3 Reactive Power Controller

Reactive power control is also a very important capability of VSC. In order to achieve decoupling of active and reactive power control the same vector control scene is used as in the case of active power control. Consequently, reactive power in the dq reference frame is given by equation 3.48.

$$Q = u_s^q i_{pr}^d - u_s^d i_{pr}^q \xrightarrow{u_s^q = 0} Q = -\left|\tilde{U}_s\right| i_{pr}^q \tag{3.48}$$

The q-axis current set point can be now calculated from the reactive power set point Q_{ref}. Therefore the reactive power controller is given as:

$$i_{pr,ref}^{q} = \frac{-Q_{ref}}{u_s^q} + \left(k_p + \frac{k_i}{s}\right)\left(Q_{ref} - Q\right) \tag{3.49}$$

For given reactive power reference set point, the reactive power controller regulates the injection of reactive power at the PCC point.

3.2.2.4 AC Voltage Controller

In the previous paragraph it has been explained how reactive power can be controlled via VSCs. However system operators require from converter stations to provide reactive power support based on the PCC AC voltage levels. In this way, VSC can support the PCC with reactive power contributing to the ac voltage stability.

$$i_{pr,ref}^{q} = i_{pr,ref\,0}^{q} + \left(k_p + \frac{k_i}{s} \right)\left(U_{s,ref} - U_s \right) \tag{3.50}$$

The main function of the ac voltage controller is to control the q-component of the current, based on ac voltage level, controlling thus reactive power injection.

3.5 Simplification of the generic models of the MTdc network for transient stability studies

The generic model introduced the differential equations that describe the VSC-HVDC system for transient stability studies. However in interconnected dc/ac systems, small time constants that the generic model facilitates reduce the calculation speed due to the small integration time steps that are required to solve the differential equations.

One way to solve this problem is by applying reduced or simplified models. The idea in deriving simplified models is to eliminate very small time constants that can be safely disregarded without changing the dynamic behavior of important states. In other words very fast dynamics are infinitely fast compared to slower phenomena, and can be neglected. The last argument can be applied in the case of the VSC based HVDC networks [**30**].

The full dynamic model of multi-terminal VSC-HVDC system includes five time constants. In the ac side, it is the time constant T_d related to the delay of the power electronic converter modulator. Normally this time constant is very small (20ms) in comparison to the time constant of the ac power system and can be neglected in stability studies. The second time constant from the ac side of the VSC refers to the phase reactor response time and more specifically to the response time of the current flowing through the phase reactor. At the dc circuit side, there is the time constant T_{dc}, which relates to the L_{dc} and C_{dc} of the cable model in figure 3.4. A typical T_{dc} is in the region of hundreds μs.

If the time constant related to the power electronic converter, T_d, is removed, the VSC voltage reference value is reached instantaneously. Removing the phase reactor from the ac circuit, the ac current would respond instantaneously to variations in the voltage between the system and the converter. However this simplification is only of theoretical interest because the phase reactor is the most important element of the VSC ac side.

In the dc side, if we neglect the dc capacitors from the π-equivalent model of figure 3.4, or the dc capacitor of the VSC station, the dynamics that appear in the dc voltage of the voltage source converter disappear. In addition, neglecting the dynamics of the dc

voltage it is impossible to study the influence of the direct voltage controllers on the active power injection of the VSC. Hence, it is not possible to study how ac side disturbances impinge on the operation of the VSCs and consequently the operation of dc network.

Removing L_{dc}, the dynamics of the dc line currents disappear. However the RC equivalent circuit for the dc cable appears to have smaller time constants than the RLC circuit and thus practically there is no benefit in reducing the necessary time step for the arithmetical solution of the differential equations. The most important difficulty in proposing standard simplified models is that the small time constants depend strongly on the parameters of the line and the controller gains which can vary significantly between different systems or nodes of the dc network.

Nevertheless as an ultimate conclusion there are two basic principles that can be adopted [**30**]. The dc capacitor is the dominant element in the dc circuit and its corresponding time constant should be taken into consideration when models are built for studying interaction between dc network and dc systems. The dynamic response of the dc voltage is related to the active power injection of the converters and this information should not be neglected from the model. In the ac side the phase reactor is the dominant element and it should be included in the models.

3.6 User written models of MTdc network for implementation in PSSE

In this project Siemens PTI PSSE simulation package has been used to model MTdc network configurations in order to investigate the interaction between the dc and ac power systems from the transient stability point of view. As it has been mentioned, in PSSE there is no available VSC based MTdc network model. For that reason the differential equations of the generic model which is given in paragraphs 3.1 and 3.2 has been utilized in order to develop dynamic models for the specific modules of the MTdc network. Standard dynamic models have been developed in [**7**] for MTdc networks which have been further upgraded with direct voltage controllers and power oscillation dampers in the present project with ultimate goal to study the interaction between large power systems meshed with VSC-HVDC networks.

More specifically, PSSE provides the option to develop user written dynamic models for transient stability studies. For any module of the power system, if the differential equations that describe the system are given, it is possible using FORTRAN programming language to develop the relevant dynamic model. After compiling the model it is possible to use it in a similar way as the other models of the PSSE library. Furthermore, in order to initialize the states of the proposed models and to coordinate the simulation, PYTHON programming language is utilized. For that purpose, a dc network power flow script has been used that is responsible to initialize the states of the dc network model [**7**]. Furthermore, PYTHON is used to coordinate and facilitate the operation of the PSSE software and execute simulations.

It has been mentioned that the MTdc network dynamic model is developed into modules. More specifically it includes the following modules:

- Grid side voltage source converter (GSVSC) model
- Wind park voltage source converter (WPVSC) model
- Aggregate offshore wind farm model
- Multi-terminal dc network model
- Dc chopper model
- Current limiter model
- A dc network load flow script

The main assumptions that have been adopted in the present project are:

- Only the fundamental frequency is taken into account. Thus it is considered that higher harmonics are not present and do not influence the dynamic behavior of the system.
- Ac Network quantities (Voltages and Currents) are represented by time-varying phasors in system per unit values.
- Generation modules (wind turbines, synchronous generators and VSCs) are modeled by time-varying current sources. This is the typical approach adapted in PSSE for dynamic simulations.

3.6.1 GSVSC model

In PSSE the dynamic models of generation units are represented by definition as controlled Norton equivalent current sources [**6**]. For that reason the voltage source equivalent model of the VSC needs to be transformed to a current source equivalent. It is important for the reader to clarify that under no circumstances the transformation means that the VSC is a current source converter. Figure 3.9 illustrates the two equivalent ac circuits.

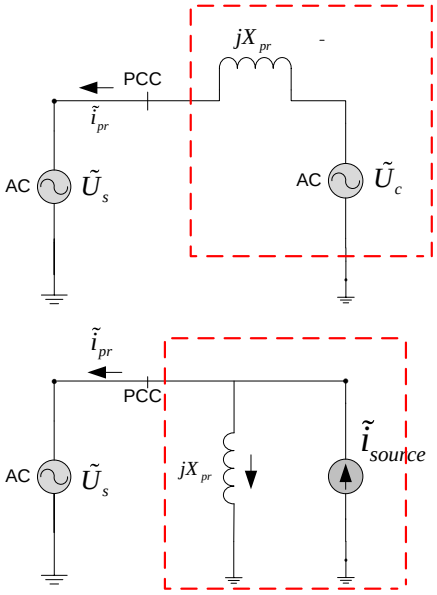

Figure 3.9: (a) VSC model represented as voltage source. (b) VSC Norton equivalent current source

In addition, the most important simplification that has been considered for developing the PSSE model of the GSVSC is that the converter instantly reaches the current reference given by the outer controllers [**7**]. This assumption can reduce the number of states and improve the cost of calculation as it neglects the time constant associated with the phase reactor, the time constant of the converter and the inner current controller.

Furthermore, with the purpose to simplify the calculations the block diagram of Figure 3.6 can be written in an equivalent block diagram as described in Figure 3.10. The inner current controller will be assumed to be a simple proportional gain. Let us now consider the transfer function G(s) from the d-axis current reference set point i_d* to the actual d-axis current i_d (same applies also in the case of i_q).

Thus G(s) is defined such as:

$$i_d = G(s) i_d^* \tag{3.51}$$

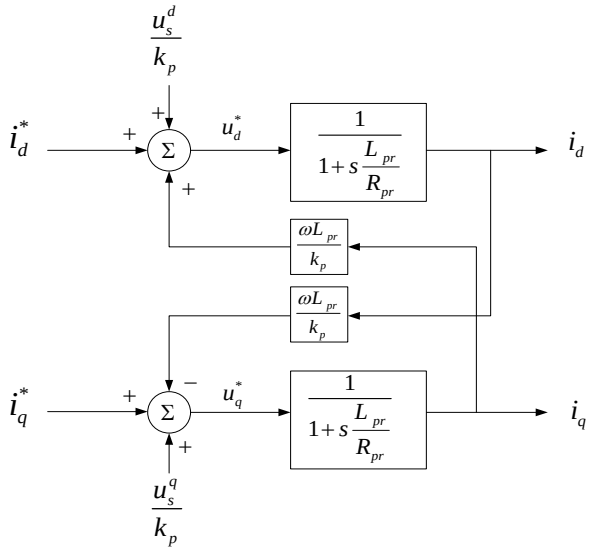

Figure 3.10: Block diagram of the reordered Inner current controller

Then in order to calculate transfer function of G(s) in the multi-input-multi-output (MIMO) system, the MIMO system is only excited by the i_d* while e_d and i_q* are considered inactive. The block diagram representation is such a situation is the one illustrated in figure 3.11

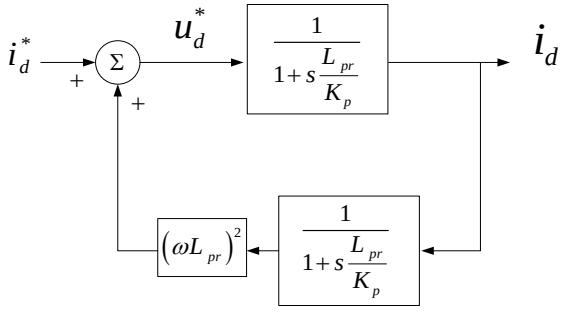

Figure 3.11: Block diagram of G(s)

The transfer function for the above block diagram in Laplace domain can be given as:

$$G(s) = \frac{1 + s\frac{L_T}{K_p}}{\left(\frac{\omega L_T}{K_p}\right)^2 + \left(1 + \frac{sL_T}{K_p}\right)^2} \approx \frac{1}{1 + \frac{sL_T}{K_p}} = \frac{1}{1 + sT_{pr}} \tag{3.52}$$

Hence G(s) has been reduced to a first order transfer function. The time constant T_{pr} is given as L_T / K_p. A typical phase reactor inductance is in the neighborhood of 0.02H for a 500MVA converter [**37**]. Looking closer at G(s) it can be concluded that the current reference can be reached infinitively fast (in comparison to ac side time constants) in the case that the proportional gain K_p of the current control loop is significantly high.

Therefore, under the assumption that a significantly high proportional gain is introduced to the inner current control loop, the direct axis (or respectively q-axis) current component can be reached almost instantly. In order to give a more quantitative illustration of the above argument, Figure 3.12 illustrates for different values of T_{pr}, the response of the i_d when step in the reference current i^*_d is introduced.

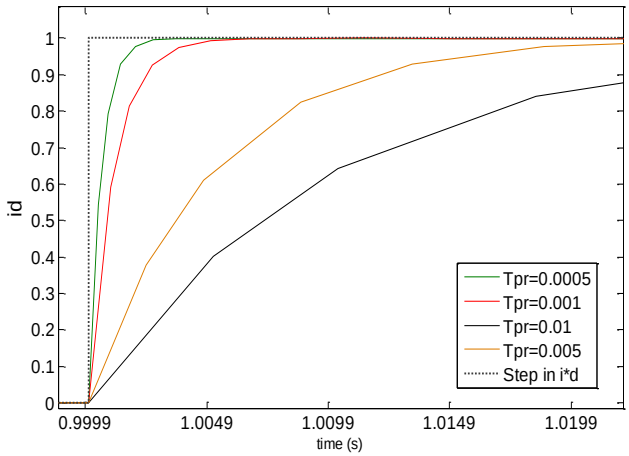

Figure 3.12: Time domain response of the reduced first order G(s) as a function of T_{pr}

A second assumption that has been taken into account for the model of the GSVSC is that the control system tracks perfectly the PCC. Thus the phase locked loop (PLL) is not modeled at all. According [**30**] PLL model introduces a small delay in the system. Nevertheless there are minor differences in the performance of the VSC with and without the PLL dynamic model and doesn't significantly impact the other state variables. For that reason it has been concluded that it is safe to neglect the dynamic model of PLL in stability studies. Under the above assumptions, the final model of the GSVSC is simplified to the one introduced in Figure 3.13.

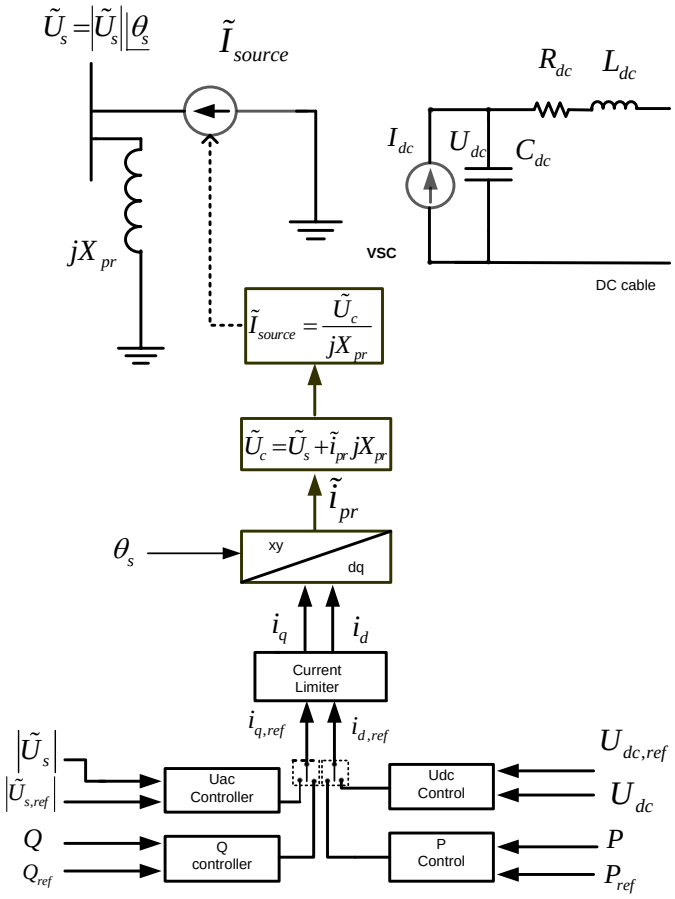

Figure 3.13: Model of the GSVSC

3.6.2 WPVSC model

The main functionality of the WPVSC is to keep constant the ac voltage of the offshore wind park by injecting in such a case all the generated power into the dc network system. Similar to the GSVSC, the WPVSC is modeled by the Norton equivalent controlled current source.

The WPVSC provides the necessary rotating synchronous voltage reference to the wind park. Vector control cannot be applied in such a case as there is no available stiff ac bus and the short circuit level is too small. For that reason the model of the WPVSC is built in the stationary reference frame. Two controllers are present in this model, the ac voltage controller and the angle controller. The ac voltage controller facilitates a PI controller which adjusts the converter ac voltage amplitude in such a way that the PCC voltage amplitude remains constant. The angle controller controls the voltage angle by utilizing a PI controller. Its functionality is to keep the voltage angle constant providing thus the 50Hz rotating voltage reference at the wind park. The model of WPVSC is illustrated in Figure 3.14.

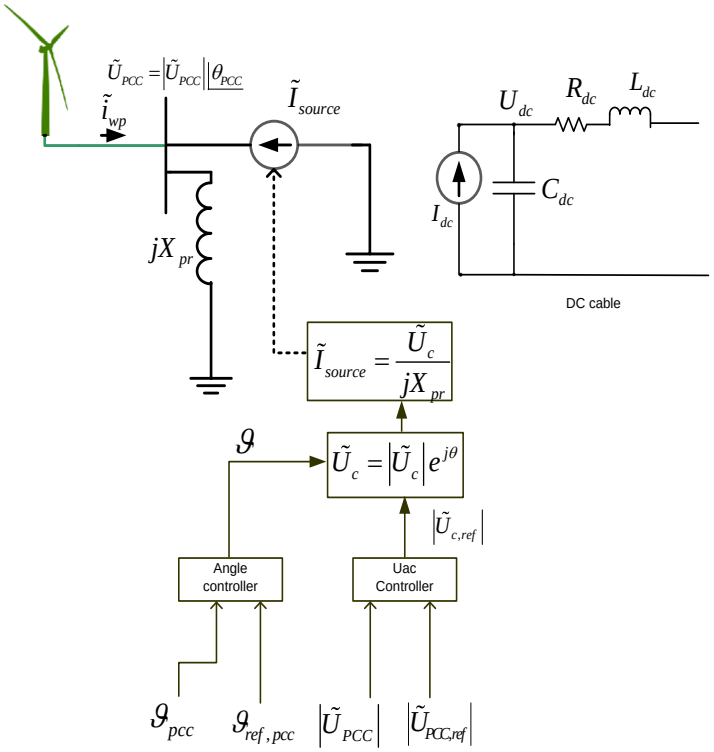

Figure 3.14: Model of the WPVSC

3.6.3 Model of the wind farms

In a future MTdc network, the WPVSC will operate as an offshore hub converter station. It will collect the generated by the offshore wind parks power per zone. For that reason in the present study the approach that has been followed to model offshore wind power plants is by an aggregate wind turbine model.

Figure 3.15 introduces a graphical representation of offshore wind farms connected to a WPVSC. As it can be seen there is an offshore ac grid that connects the wind farms to the WPVSC terminal. Thus, it becomes evident that it is possible to substitute the offshore wind farms by and aggregate wind farm model connected to the WPVSC. The aggregate wind farm is modeled by a wind turbine model. In the present study standard wind turbine models have been facilitated with standard parameters [**6**].

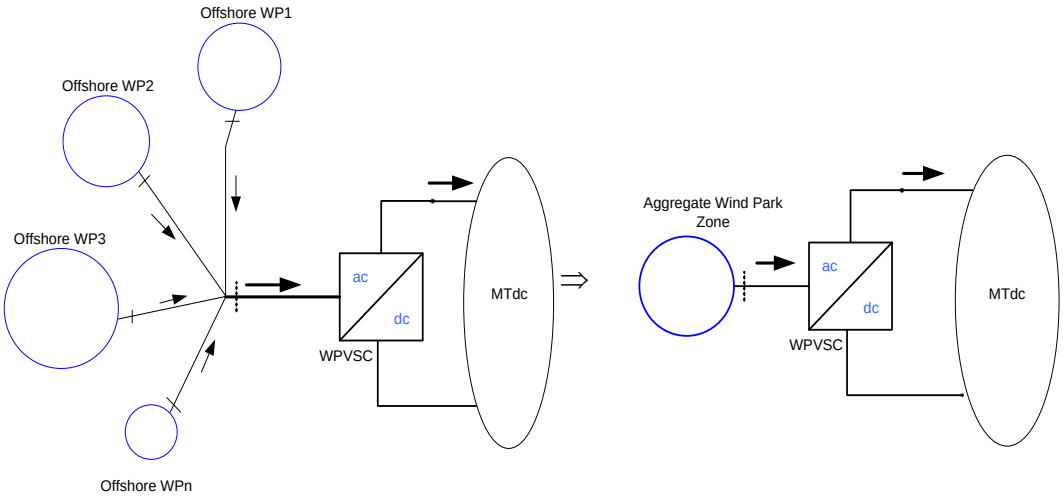

Figure 3.15: Aggregate model per wind farm zone

3.6.3 MTdc network model in PSSE

In paragraph 3.3, an explicit description has been given for the state space equations facilitated to model the HVDC cables. The advantage of this representation is that it is possible to reproduce any topology of the multi-terminal dc network configuration if the incident matrix that describes its layout is given. The input signals at the dc network state space model is the vector of dc current injections at the nodes where a VSC is present. The dc current injections are calculated from the GSVSC and WPVSC model respectively [**7**].

3.6.3.1 Description of the dc power flow for the initialization of the MTdc network model

The user written models that have been developed for the PSSE simulation tool require to be initialized correctly in order to conduct dynamic simulations. For that reason, initially an ac power flow needs to be executed in order to define the operation point of both the offshore ac wind park network and the on shore power system. For that reason a sequential ac-dc power flow has been utilized [**38**].

More specifically for the ac power flow, GSVSC is modeled as a PV bus. First, the active and reactive power of the GSVSCs is defined and then an ac power flow is run. In the case of the offshore wind park a similar ac power flow need to be executed. For the offshore network ac power flow, the WPVSC is modeled as a slack bus while the wind park is modeled as PV bus. Thus for any given wind power injection, the WPVSC operates as a sink of power. So it becomes clear that when an ac power flow is run in PSSE, both GSVSC and WPVSC set their active and reactive power set points respectively.

Even though PSSE is capable to execute ac power flows, there is not a direct way to run the dc power flow in the MTdc network model directly from PSSE, at least with the modular way the models have been built in this project. Correct initialization of the dc network is indispensable because the states of the dc network dynamic model (which

represent dc node voltages and branch currents) need to be initialized in coordination with the power feed to the dc network by both GSVSC and WPVSC.

Subsequently, in order to solve this obstacle an external dc power flow script developed in PYTHON is used. With PYTHON it is possible to access the variables of PSSE associated with the ac power injection of VSCs at specific ac buses. These active power values are VSC set points introduced in the ac power flow.

In the dc power flow always one dc bus is considered as slack bus (with defined dc voltage) being responsible for the losses while N-1 buses are constant power nodes. As soon as the dc power flow has converged, the calculated voltages and currents constitute the initial states in the state space model of the dc network (equation 3.19). Figure 3.16 gives an overview of the MTdc network model and the relevant power flow.

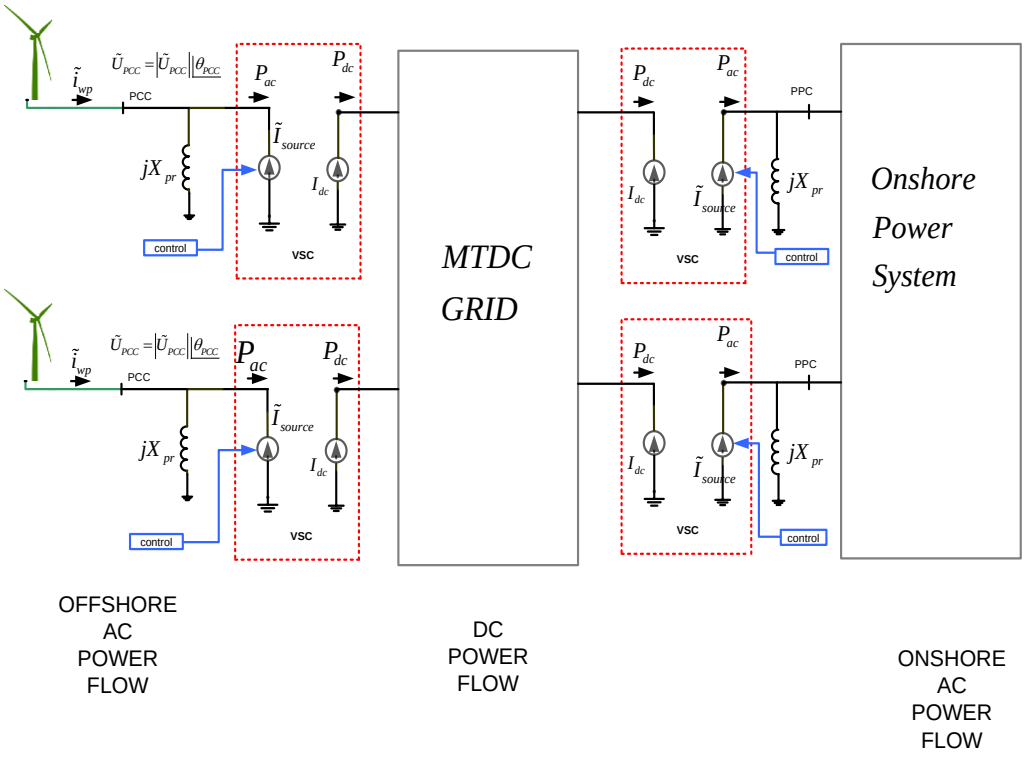

Figure 3.16: AC and DC power flows in the DC network

In addition, the defined from DC power flow initial steady state operation point need to be introduced as initial condition of the dc network model. For that reason the initial states are introduced as dynamic model file (*dyr* file) in the PSSE. Thus once the dc power flow is converged, the *dyr* file is created which can be used to correctly initialize the dc network dynamic model.

The same applies for the case of the GSVSC and WPVSC models. The results from the dc power flow are used to initialize the operation point of the used controllers. Similar to the way used in the dc model, the initial states of the VSCs are introduced to PSSE via the dyr file. Once the system is correctly initialized, it is then possible to run dynamic simulations of the VSC-HVDC multi-terminal dc network system.

3.6.3.2 Dc power flow equations

In steady state the dc grid power flow is dictated by the line resistances and the dc voltage magnitude differences between the dc buses [**7**] [**38**]. The nodal voltages and the current injections for each node of the MTdc network are given in the form of vectors such as:

$$U_{dc} = \begin{bmatrix} U_{dc}^{1} & U_{dc}^{2} & \cdots & U_{dc}^{N} \end{bmatrix} \tag{3.53}$$

$$I_{dc} = \begin{bmatrix} I_{dc}^{1} & I_{dc}^{2} & \cdots & I_{dc}^{N} \end{bmatrix} \tag{3.54}$$

Given the dc cable resistances and the incidence matrix it is possible to calculate the dc network admittance matrix Y_{dc}. More specifically the admittance matrix is given as:

$$Y_{dc}^{N\times N} = M \begin{bmatrix} \frac{1}{R_1} & 0 & 0 & 0 \\ 0 & \frac{1}{R_1} & 0 & 0 \\ 0 & 0 & \ddots & 0 \\ 0 & 0 & 0 & \frac{1}{R_N} \end{bmatrix} M^{T} \tag{3.55}$$

The dc current injections are unknown prior to the dc power flow solution. On the other hand, dc power injections are known as a result of ac power flow for all buses except the dc slack bus. As for the dc voltages only the dc slack bus voltage is known whereas all the other nodes voltages are defined by the dc power flow solution.

The vector of the unknowns can be written as:

$$X = \begin{bmatrix} U_{dc}^{1} \\ \vdots \\ U_{dc}^{N-1} \\ P_{dc,slack} \end{bmatrix} \tag{3.56}$$

It can be seen that in the vector of the unknown variables, the dc slack bus is considered the last grid side converter in the dc network. Last the non-linear algebraic equation to be solved is given as:

$$F(U_{dc}) = Y_{dc}^{N\times N} U_{dc} - \begin{bmatrix} \frac{P_{dc}^1}{u_{dc1}} & & & \\ & \frac{P_{dc}^1}{u_{dc1}} & & \\ & & \ddots & \\ & & & \frac{P_{dc}^1}{u_{dc1}} \end{bmatrix} = 0 \quad (3.57)$$

In order to solve the system of non-linear algebraic equations Newton Raphson arithmetical method has been used. Where the Jacobian matrix is defined as:

$$J = \frac{\partial F}{\partial U_{dc}} = Y_{dc}^{N\times N} + \begin{bmatrix} \frac{P_{dc}^1}{(u_{dc1})^2} & & & \\ & \frac{P_{dc}^2}{(u_{dc1})^2} & & \\ & & \ddots & \\ & & & \frac{P_{dc}^1}{(u_{dc1})^N} \end{bmatrix} \quad (3.59)$$

And the DC voltages are given for every iteration as

$$U_{dc}^{k+1} = U_{dc}^{k} - J^{-1} F\left(U_{dc}^{k}\right) \quad (3.58)$$

3.6.4 Model of the dc chopper

The dc chopper is a controlled aggregate resistor connected to the dc node of each converter station in parallel with the dc capacitor. The switches are facilitated by power electronic components (IGBTs ot GTOs). The main functionality of the dc chopper is to dissipate power in emergency conditions in order to limit the increase in the direct voltage.

An emergency condition is experienced during disturbances at the ac side of the GSVSCs. When an ac fault occurs in the ac side, the active power that cannot flow to shore will create a direct voltage increase. This happens as a result of power surplus which is instantly stored at the dc capacitors. In that way, the dc chopper will dissipate the power that cannot flow to the ac network keeping thus the dc voltage at the capacitor at acceptable operational levels.

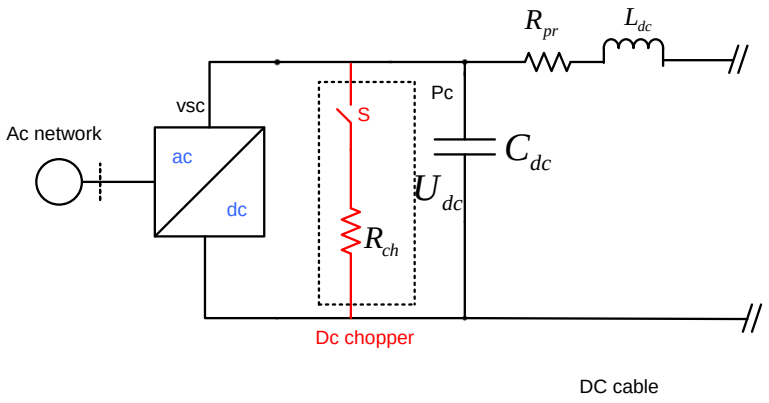

Figure 3.17: DC chopper connected at the dc terminal of the VSC station

3.6.5 Model of the current limiter

The ac current of the VSCs need to be limited at the maximum acceptable value in order to protect the switching devices. Three strategies can be followed for the limitation of the VSC current. The first gives priority to the d-axis component of the current and thus priority to active power. The second gives priority to the q-axis component of the current and thus to reactive power and last gives equal priority. Figure 3.18 introduce the three strategies facilitated to limit the VSC ac current. The role of the current limiters to the participation of the VSC at fault current and to reactive power support will be discussed in chapter 6.

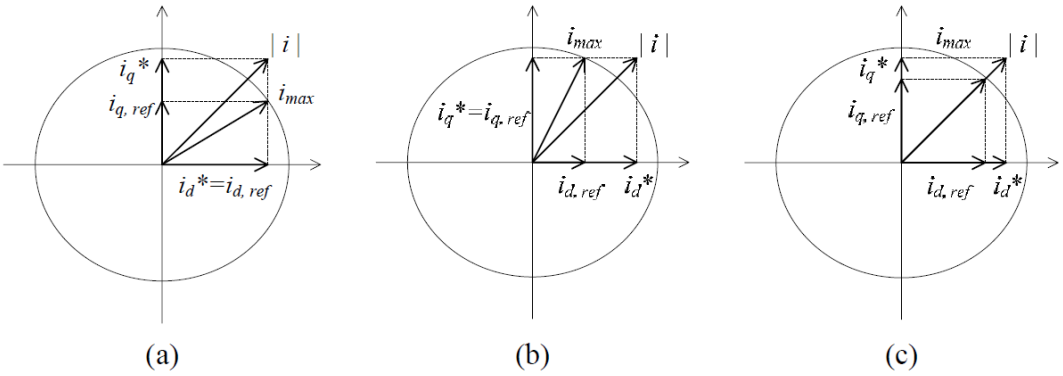

Figure 3.18: Current limiting strategies **[**8**]**

Chapter 4: Control of Direct Voltage and dc Power Dispatch Management in MTdc Network

4.1 Introduction

The control of the direct voltage is essential for the operation of the future multi-terminal VSC-Based HVDC network. The voltage is directly related to the power balance at the dc capacitor side of the converter station. A high overvoltage may activate protection mechanics (such as the dc chopper resistors). On the other hand, voltage drops may trigger non-linear PWM modulation of the converter station. For the above reasons, the voltage should be always maintained within rigid operational limits ensuring the smooth operation of the MTdc network [**39**].

The control of the direct voltage can be assigned either to one converter station or a group of converters. In large scale networks more than one converter need to be in dc voltage control mode participating in the control of the voltage. The main reason is the limited capacity of the converter stations and the possibility of loss of a converter as a result of a disturbance [**36**].

4.2 Market dispatch schemes

Next to the direct voltage control, the converter stations should be capable of performing power market dispatch schemes. Namely, there are three dispatch schemes that can be facilitated [**8**] [**40**]. The *fixed power sharing*, the *priority power sharing* and the *proportional power sharing*.

In the *fixed power sharing* one or more converters receive a fixed amount of power while the other converters balance the wind park variability. *In priority power sharing* one converter station has priority in getting first the generated wind power while the other converters receive the excess power. Last, in *proportional power sharing* all the grid side converters share the generated wind power in predefined portions [**8**] [**36**].

4.3 Dc voltage control strategies

There are two main direct voltage control strategies that can be applied in MTdc networks, the direct voltage droop method and the voltage margin method. The direct voltage droop control method has illustrated capability of performing proportional power sharing [**36**]. Furthermore, it has revealed acceptable operation during disturbances in the onshore grid [**21**] [**8**]. For that reason the droop control method has been suggested as the best choice for performing proportional power sharing and will be facilitated in the present project.

The dependence of the droop method on the network topology [**17**] combined with the difficulty to perform fixed and proportional power sharing [**8**] has led to the development of the second control strategy, the voltage margin method (VMM) [**8**]

[**36**]. The performance of both the droop and VMM direct voltage control strategy will be investigated in the present chapter.

4.3.1 Direct Voltage Droop controller

The direct voltage droop control strategy facilitates a proportional controller which represents a droop characteristic. The droop characteristic introduces a unique linear relation between the direct voltage and the d-axis component of the converter ac current. In this way the variations of the dc voltage are related to variations of d-axis current and hence variations of active power of the converter station according to equation 3.43.

Therefore, when an overvoltage (or voltage drop) appears at the dc side of the converter, the droop controller will adjust accordingly the active power delivered by the converter in order to maintain the dc voltage at normal levels. This direct relation of the converter active power to the dc voltage makes the droop controller incapable of executing fixed power sharing [**8**].

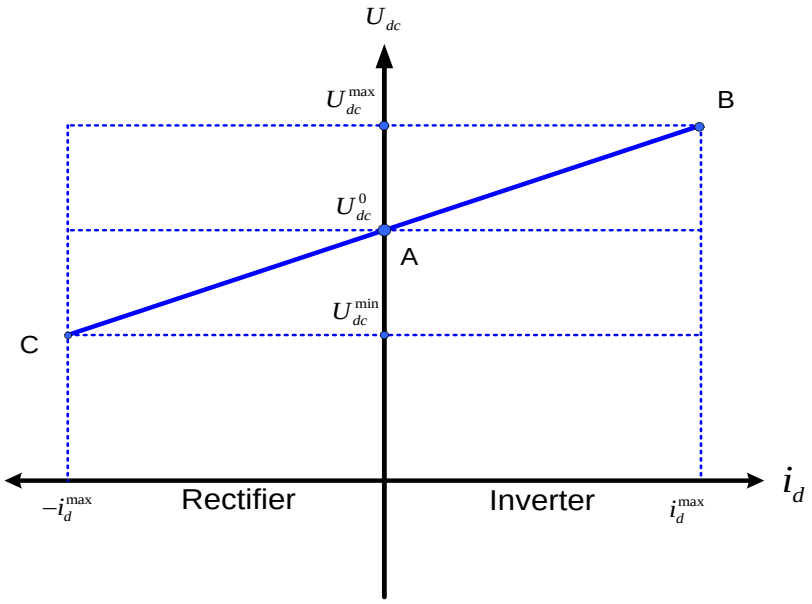

Figure 4. 1: Typical droop characteristic of the DC voltage controller

Figure 4.1 introduces a typical droop line characteristic. The positive reference for the current and thus for active power, is taken in inversion operation. As can be seen, when the direct voltage at the capacitor of the converter station is equal to U_{dc}^{0} there is no active power injection and the converter station is operating at point A. As soon as the dc voltage starts increasing, the droop controller will increase the d-axis component of the current following the droop line. As a result of increase in the d-axis component of the current, the active power injection to the ac network will increase as well. The increased active power will bring balance to the dc capacitor. The dc voltage will move to a higher value and the operational point will shift from point A to a point between A and B on the droop line which is exclusively defined by the controller droop characteristic. More specifically, the linear equation between the dc voltage and the d-

axis component of the current is given by equation 4.1. The slope of the droop characteristic is defined as the inverse of the proportional gain.

$$U_{dc} = \frac{1}{k_p} i_d + U_{dc}^{ref} \tag{4.1}$$

In addition, when the dc voltage reduces below U_{dc}^{0} the converter will perform rectifying and power will flow from the ac network to the dc grid. The dc voltage will reduce and the operational point will shift to the left part of the droop characteristic.

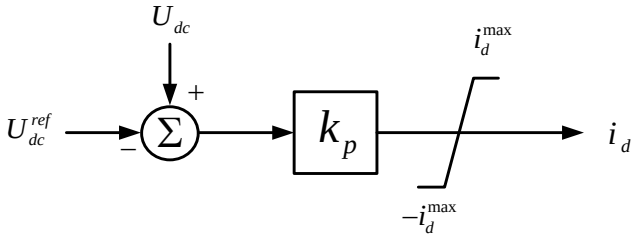

Figure 4. 2: Block diagram of the DC voltage controller that implements Droop control strategy for the control of DC voltage

4.3.2 One-stage Voltage Margin Method controller

The VMM control strategy facilitates the dc voltage controller that has been described in paragraph 3.2.1 and a current limiter. Figure 4.3 introduces a typical one-stage VMM controller. The dc voltage controller implements a proportional-integral (PI) controller which maintains the dc voltage equal to the reference value. The limiter is applied to the d-axis component of the ac current. The d-axis component of the current is related to the active power of the converter when the synchronized with the system voltage vector control scheme is applied.

A typical one stage VMM characteristic is given in figure 4.4. In the (AB) region the converter is performing inversion while in the (AC) rectifying. Throughout (BAC) line the direct voltage is maintained constant to the reference value. When the converter is operating at point A, there is no active power exchange with the ac network. As long as an increase in direct voltage occurs, the VMM controller will accordingly increase the d-axis component of current and thus increase active power injection to the AC network while the dc voltage will return to its reference value (as a result of the PI control operation). The new operation point will then shift to the right of the point A.

As soon as the upper limiter is reached the converter cannot increase the d-axis current further. At the same time the active power injected to the ac network will be kept constant at the upper limiter value and the dc voltage will ascend. In such way the one-stage VMM controller is capable of executing fixed power sharing. It is worth mentioning that as soon the upper limit is reached another converter station should be responsible to take on the control of the dc voltage within the dc network.

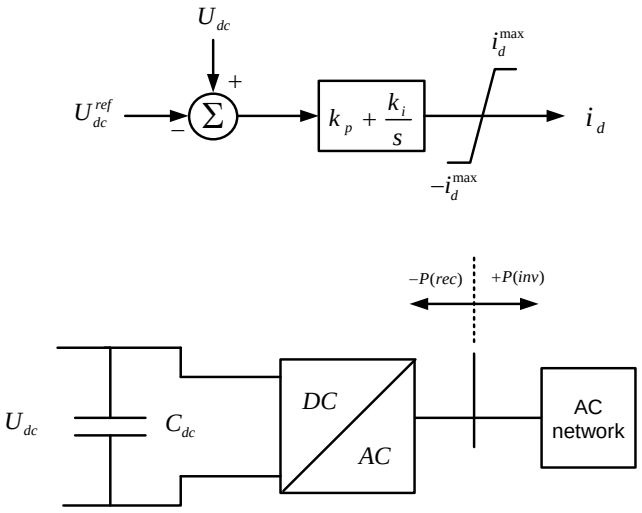

Figure 4. 3: One stage VMM controller

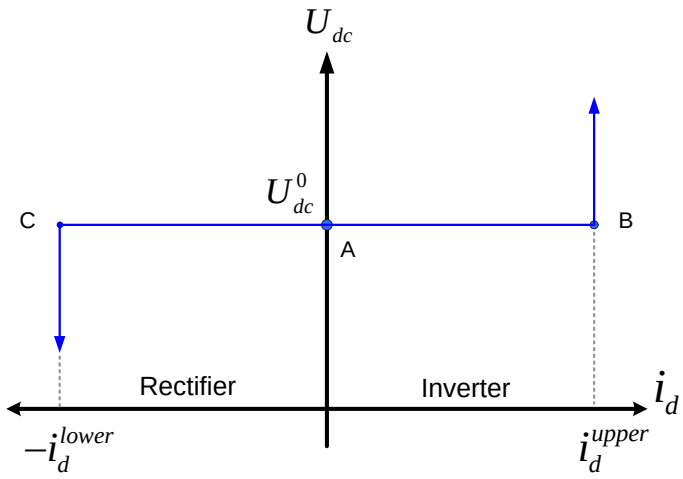

Figure 4. 4: One stage VMM characteristic

4.3.3 Two-stage Voltage Margin Method direct voltage controller

The one stage VMM is capable of executing fixed power sharing but not priority power sharing. For that reason, a two-stage VMM controller has been proposed [**8**] and has been introduced in the grid side converter model of this project. Figure 4.5 introduces the block diagram of the two-stage VMM controller which consists of two identical one-stage VMM controllers. The voltage reference of the second controller is set higher than the reference of the first. Furthermore, the upper limiter of the first controller is adjustable by the output of the second controller.

In such a scheme, the first controller controls the voltage at U_{dc}^{ref} as long as the upper limiter of controler1 (upper1) is not reached. As soon as the upper limiter is reached controller1 is not capable of controlling the direct voltage anymore and the voltage will rise. When it reaches the value of $U_{dc,ref}^{high}$ the second controller will employ the control of the dc voltage.

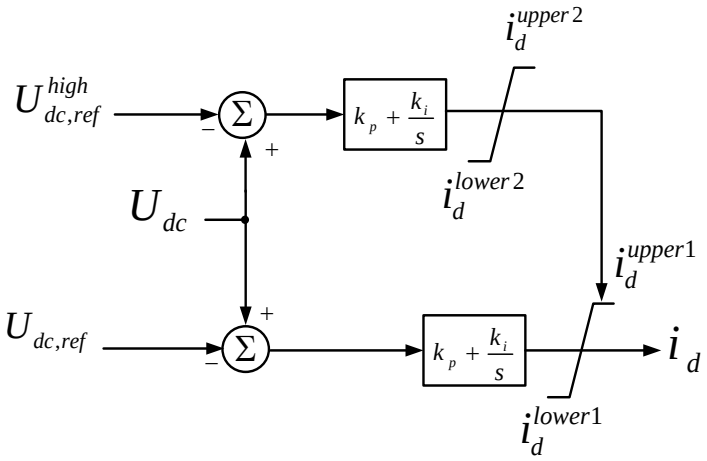

Figure 4. 5: Two stage VMM controller

From the above, it becomes apparent that there are two dc voltage references and thus two voltage levels where the voltage is kept constant. Figure 4.6 introduces a typical two-stage VMM characteristic. In the (BC) line the converter will perform inversion by keeping the dc voltage constant. In the (AB) line the converter will perform rectifying as long as the lower limit1 is not reached. In inversion mode, when the point C is reached the dc voltage will increase through (CD) line. As soon as point D is reached, the second controller will control the voltage in the (DE) line provided that the upper limit2 is not reached. With implementation of such control scheme it is possible to undergo priority power sharing among the grid side converter stations. The next paragraph will investigate this possibility by introducing the relevant simulation results.

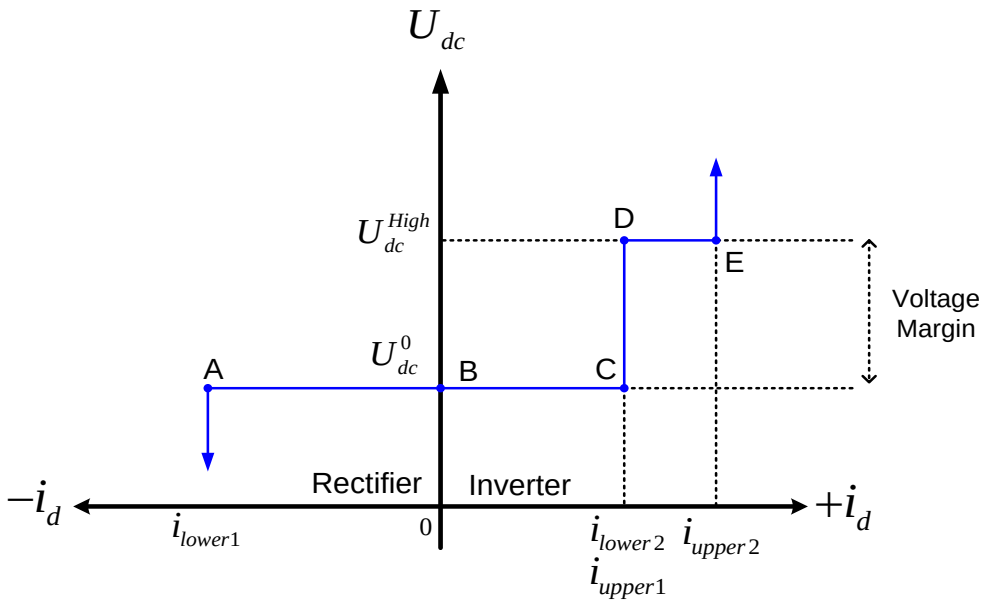

Figure 4. 6: Two stage VMM control characteristic

4.3 Simulation results

The three power dispatch schemes described above will be evaluated facilitating droop and VMM direct voltage control strategies. More specifically, the droop controller will be used for proportional power sharing among the grid side converters, while the two-stage VMM controller will be used for the fixed and priority power sharing.

4.3.1 Test system

The test system used for evaluation of the power dispatch schemes is introduced in figure 4.7. It is originated from the IEEE three-generator test system where for this project three GSVSC have been introduced at specific nodes. All the generators and converters are rated at 400MVA. The voltage levels of the generators are 13.8kV whereas the voltage levels in the ac lines 230kV. For the considered ac snapshot, G1is generating 300MW, G2 50MW and G3 250MW. The slack bus of the ac network is considered G2. The load at bus 303 is 300MW while at bus 306 and 309, 150 MW respectively. Standard 6^{th} order synchronous generators models have been used, with standard governor and excitation system [**6**]. All the parameters of the dynamic models in the test system are given in Appendix E.

For the MTdc network, a star layout is considered. Two wind farms each rated at 400MVA are connected via WPVSCs at the dc network. Both wind farms have been modeled by aggregate standard direct drive models [**6**]. The rated voltage of the dc network is considered ± 125 kV for this case study. However it is worth mentioning that the converters are modeled as mono-polar VSC for this project as it has been explained in chapter 3.

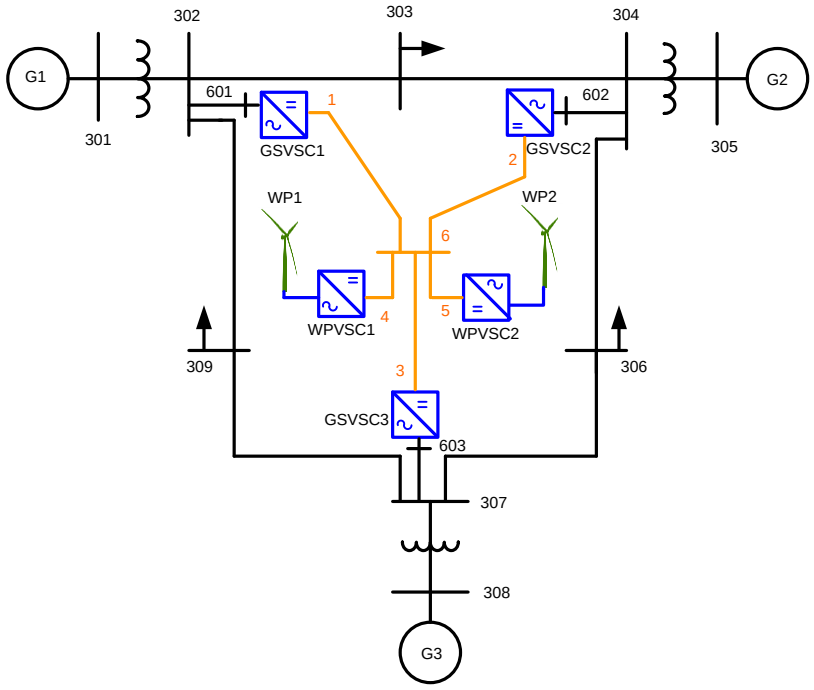

Figure 4. 7: Test system for evaluation of the Dc voltage control strategies

4.3.2 Droop - Proportional sharing

With the aim to perform proportional power sharing a droop control strategy is implemented. For each of the droop controllers, different proportional gains have been selected. The different gains introduce different droop line characteristics as depicted in figure 4.8. Table 1 illustrates the selected proportional gains, the maximum dc voltage calculated by the equation 4.1 and the share of total power per converter. It is important to notice that the maximum dc voltage for each converter should be less than the threshold value where the dc chopper is activated (1.1pu for this project).

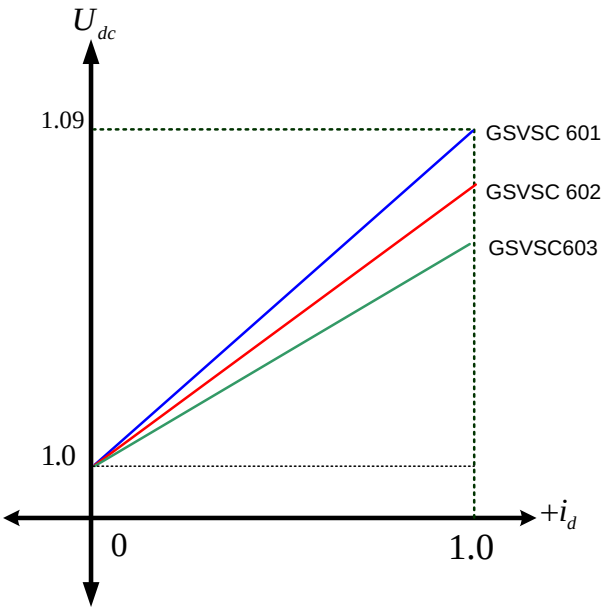

Figure 4. 8: Dc voltage droop characteristic of the GSVSCs of the test system.

Bus #	K_p	$U_{dc\ max}$	Share (%)
601	11	1.09	28
602	14	1.07	34
603	16	1.06	38

Table 1: Selected gains for proportional power sharing

Figure 4.9 introduces the simulation results for given steps in wind power. More specifically, at 1sec, WP1starts generating power. As a result of the power injection into the dc network, the dc voltage will increase in all grid side converter stations. The droop direct voltage controller facilitated at GSVSC will increase the active power injection of the converters and the dc voltage will move to a new level. Therefore the generated from the wind farm power will be shared among the grid side converters according to the predefined droop characteristics.

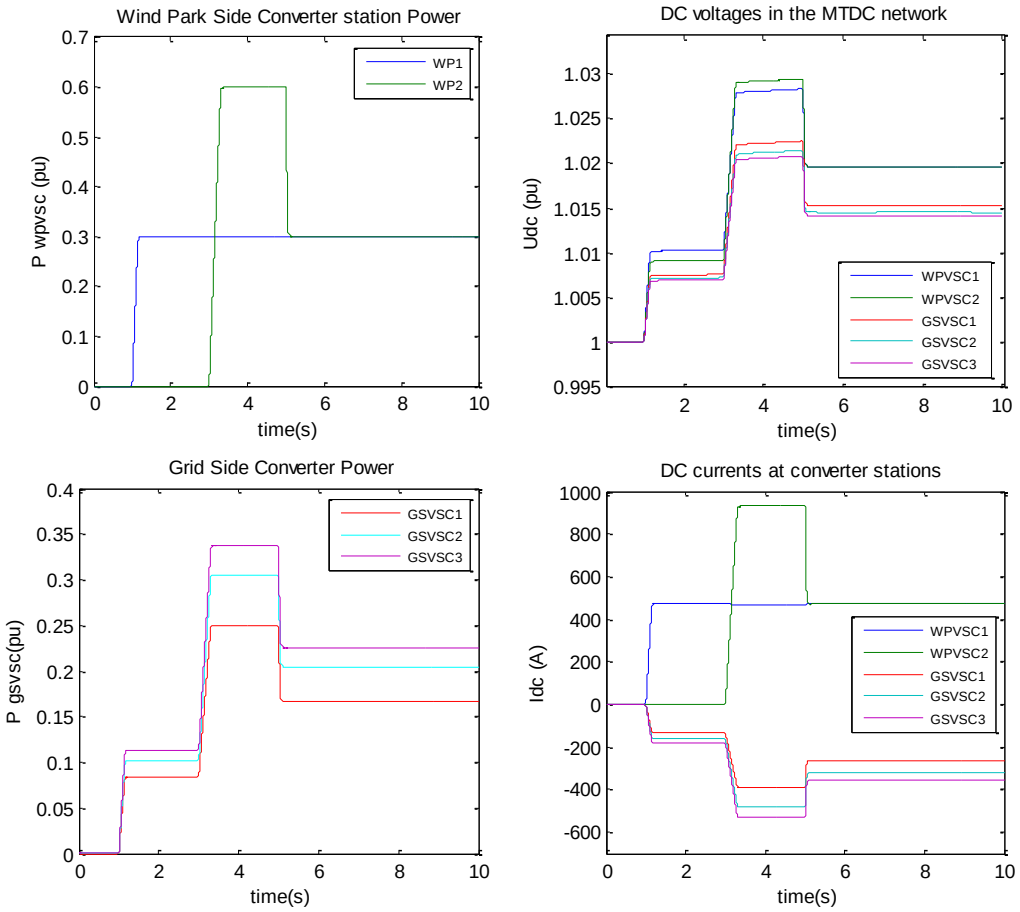

Figure 4. 9: Simulation results using Droop controller – Proportional Power sharing (S_b=400MVA)

At time 3s, there is additional generated power by WP2. The droop controllers will further increase the injected active power and consequently the direct voltage will move to higher level, as can be seen in figure 4.9. The new generated power is shared according to the droop line characteristic while the ratio is held constant. Finally, at time equal to 5s, WP2 generation will reduce. As a result the dc voltage and the GSVSCs active power will reduce according to the droop characteristic.

The ultimate conclusion for the droop control strategy is that the fast wind power variations are followed by the GSVSCs. In addition, the dc voltage is shifting from one operational level to another without any extreme dynamic response. The same applies to the dc currents as can be seen in figure 4.9. The change of operation point of the grid side converters does not create over-currents or fast dynamics in the dc network. Consequently, the droop control strategy implemented to facilitate proportional power sharing has illustrated satisfactory performance for the specific test system.

4.3.3 VMM - Fixed Power sharing

With the intention to implement fixed power sharing among the grid side converters, the two stage VMM controller has been facilitated. Figure 4.10 introduces the applied two-stage VMM characteristics that implement fixed power sharing.

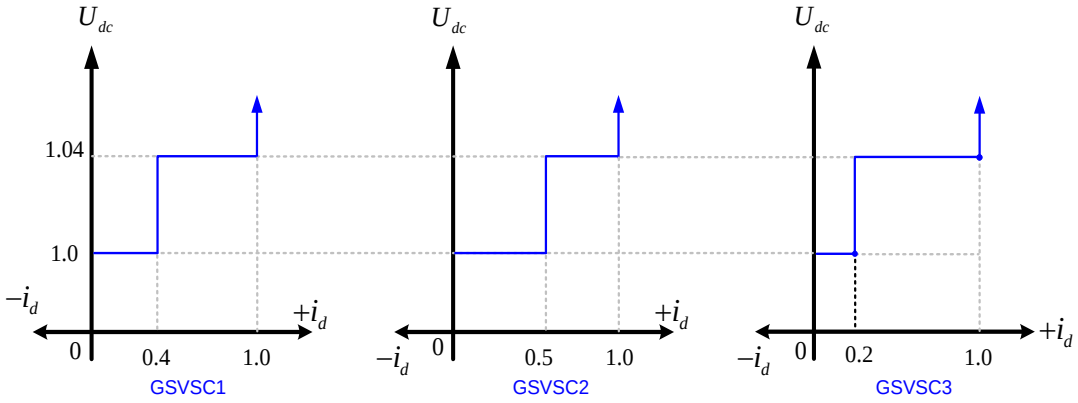

Figure 4.10: two-stage VMM characteristics implemented on the test system – Applying Fixed Power sharing

Bus #	P_{lower1}	P_{upper1}	P_{lower2}	P_{upper2}
601	0	0.4	0.4	1.0
602	0	0.5	0.5	1.0
603	0	0.2	0.2	1.0

Table 2: Implemented limits at the two-stage VMM control for fixed power sharing

As it can be seen from the VMM characteristics, all the grid side converters control the direct voltage and will receive specific amounts of power before they reach their upper limit. The first controller that reaches the upper limit is GSVSC3. When this happens, the dc voltage of GSVSC3 converter will start increasing and only GSVSC1 and GSVSC2 will be responsible to control the direct voltage in the dc network by adjusting their active power.

Figure 4.11 introduce the responses of the GSVSCs when they are implementing fixed power sharing. More specifically, at 1 s WP1 injects 0.3 p.u. This amount of power is equally shared by the three GSVSCs. At 3s WP2 will start injecting 0.6p.u in the dc network and all the GSVSCs will increase their active power. When GSVSC3 reaches its upper limit (0.2p.u) the dc voltage will be controlled only by GSVSC1 and GSVSC2, which will share the generated wind power.

At time 5s, the generated from WP2 power will reduce to 0.3p.u. As a result, the active power of GSVSC1 and GSVSC2 will follow this reduction in order to keep the dc voltage at reference value. Important to note is that when a step occurs in the power generated from wind farms, a dc voltage dynamic overshoot is created as it can be seen in figure 4.11. The higher the step in generated wind power, the higher the overshoot in the direct voltage. Hence, it is important that this overshoot that occurs as a result of the

dynamic response of the controller will not reach the threshold value that the dc chopper is activated.

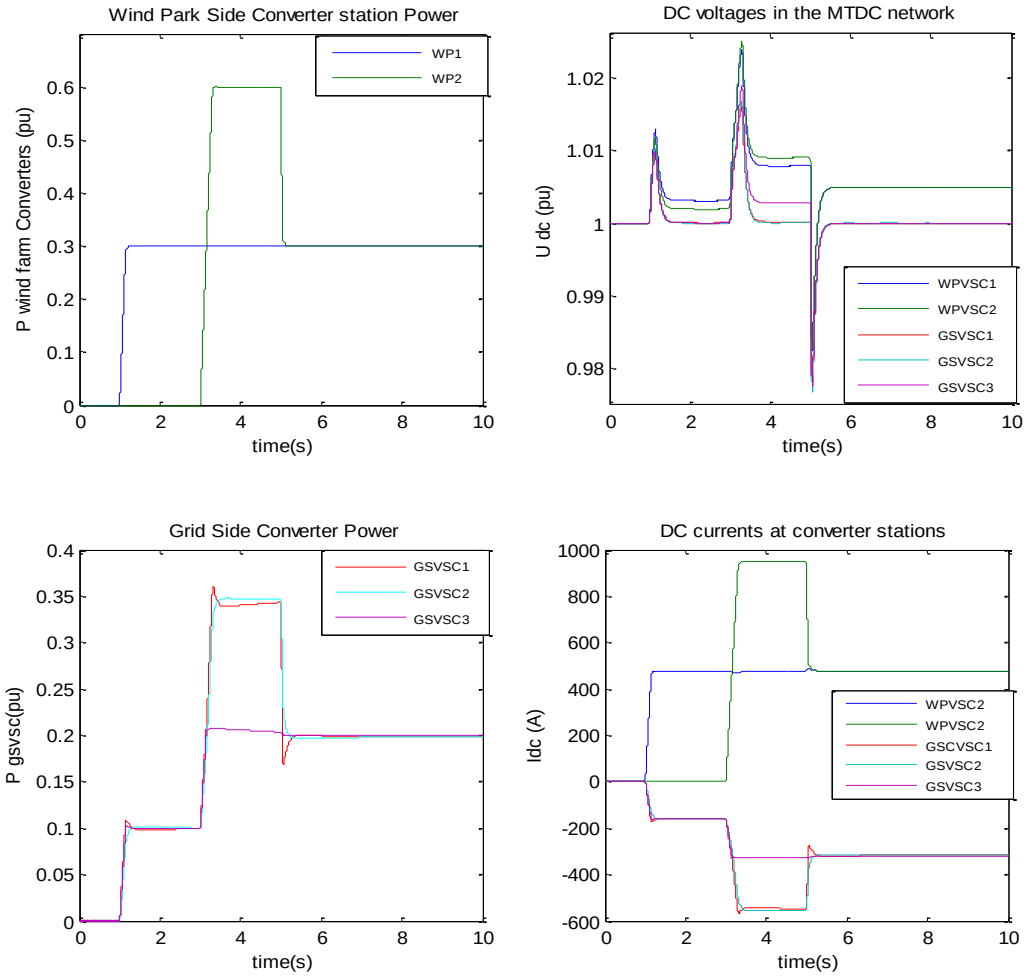

Figure 4.11: Simulation results with VMM method – Fixed power sharing (S_b=400MVA)

4.3.4 VMM - Priority Power sharing

In order to implement priority power sharing among the grid side converter stations, a two-stage VMM controller is implemented in GSVSC3 whereas GSVSC1 and GSVSC2 facilitate one-stage VMM controllers. Figure 4.12 introduces the VMM characteristics that have been used in the present project to illustrate how priority power sharing can be achieved in MTdc networks. In addition, table 3 introduces the lower and upper limits of the VMM controllers.

As it can be seen from the VMM characteristics only GSVSC2 and GSVSC3 get first the priority to share the generated wind power. They will both control the DC voltage at the lower reference value as long as their upper1 limit is not reached. Once this happen the direct voltage will increase end only GSVSC1 will be responsible to control the voltage. In such way it is given priority to GSVSC2 and GSVSC3 to first receive the generated wind power. Once the upper limit of GSVSC2 and GSVSC3 is reached and

there is excess in wind generation, then the extra power will be distributed onshore by GSVSC1.

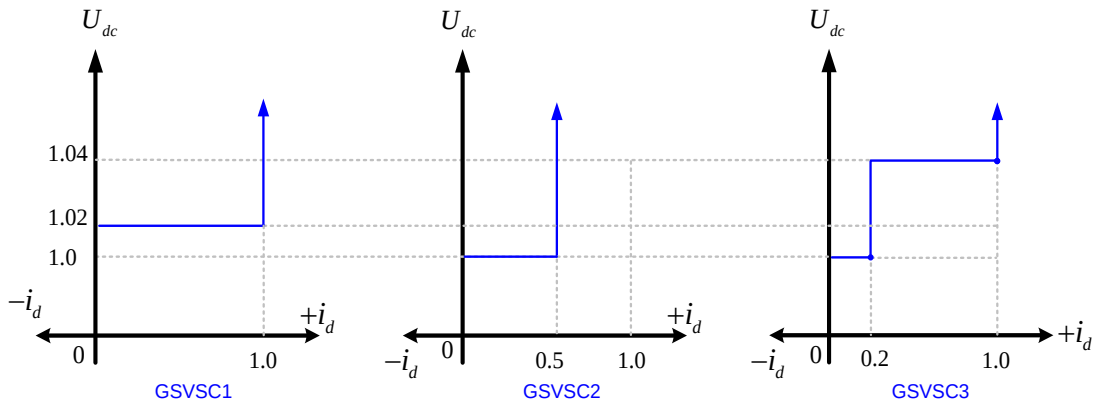

Figure 4. 12: two stage VMM characteristics implemented on the test system – Applying Priority Power sharing

Bus #	P_{lower1}	P_{upper1}	P_{lower2}	P_{upper2}
601	0	1.0	-	-
602	0	0.5	-	-
603	0	0.2	0.2	1.0

Table 3: Implemented limits at the two-stage VMM control for fixed power sharing

Figure 4.13 depicts the responses of the grid side converters in the predefined path of changes in generated wind power. More specifically, at 1s when wind farm1 starts generating power only GSVSC2 and GSVSC3 will share this amount of power. Due to the fact that the direct voltage is controlled at the lower reference value (1.0pu) GSVSC1 will not distribute power, according to the VMM characteristic.

At 3s, when there is further increase in the generated wind power, both GSVSC2 and GSVSC3 will reach their upper limit. As a result the direct voltage in the MTdc network is not controlled anymore and voltage will increase. When the voltage at the GSVSC1 station reaches 1.02p.u this converter will start distributing active power and in such way control the voltage which is now maintained constant at the high voltage reference.

It is important to mention that the disadvantage of the priority power sharing is that according to the at hand simulations, there is a large direct voltage drop when active power is reduced especially in the case that the converters with last priority are in operation. As it can be seen in figure 4.13, at 5s the generated from WP2 power is reduced. As a result dc voltage will drop and GSVSC1 will be the first that will stop to distribute power. GSVSC3 will continue to inject its maximum power while only GSVSC2 will control the dc voltage.

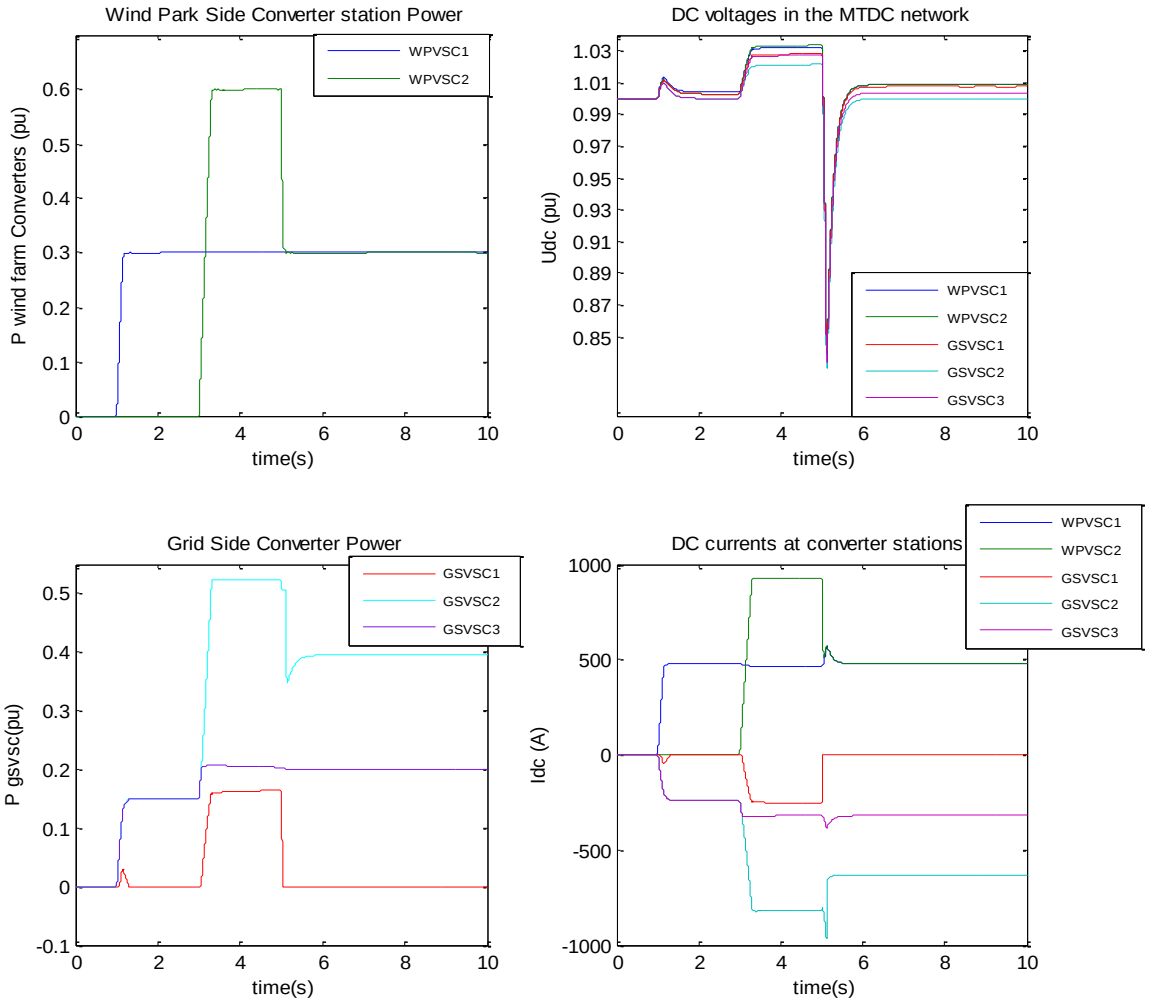

Figure 4.13: Simulation results with VMM method – Fixed power sharing (S_b=400MVA)

4.3 Conclusion

In the present chapter the three main market power dispatch schemes (proportional, fixed and priority power sharing) have been described and control methods in order to achieve them have been introduced in the dynamic model. Namely two control strategies, the droop and voltage margin method have been developed.

From the simulation results it can be concluded that the performance of droop control is satisfactory for implementation of proportional power sharing among the grid side converters for any given variation in generated wind power. The droop controller is capable of controlling the dc voltage within stiff operational limits. There are no unacceptable dynamic phenomena in the direct voltage or direct currents and the transition from one operational point to another is conducted smoothly.

For implementation of the fixed power dispatch scheme, the performance of the two-stage VMM controller is characterized as acceptable and the dynamic response of the controller is not creating serious problems in terms of the DC voltage control. The direct voltage overshoot and voltage drops when the GSVSC changes operating point need to be tackled properly in order to prevent the switching of the dc chopper. High proportional gains can decrease the overshoot but it also makes the direct voltage response slower.

Last, for the implementation of priority power sharing, simulation results revealed that there is a weakness in terms of dc voltage performance when the converter with the last priority is operating and a significant decrease in wind power occurs. The main reason for this dc voltage dynamic response is the state related to the integral part of dc voltage controller1 in the two-stage controller. More specifically, when the upper limit of controller 1 in Figure 4. 5 is reached, the state of the integral part of the controller 1 will continue to grow above the upper limit. As a result when the dc voltage returns to the region close to the lower reference value and controller1 is again in operation, the value of this state will still be high. The high value of the state related to the integral part will create an instantaneous pulse in the d-axis current and thus in the active power injection which creates a voltage drop in the dc network. The last argument can be seen in the profile of the dc currents in Figure 4.13. More specifically, as it can be seen, there is a spike in the dc current of the GSVSC1 and GSVSC2.

One solution would be to “freeze” the states related to the integral part of the dc voltage controller when the upper limiter is reached or limit the state within the operational limits of the controller. The large dc voltage drop that appears may create nonlinear phenomena in the converter’s modulation. For that reason in the case that priority power sharing is facilitated utilizing two-stage VMM special care need to be taken with reference to the dc voltage variations. A selection of high proportional gains will minimize the voltage drop because the effect of the integral part would be smaller but it would also make the direct voltage controller response more sluggish.

Chapter 5: Damping of Electromechanical Oscillations by utilization of VSC-HVDC that operate in heavily meshed ac-dc multi-terminal networks

5.1 Introduction

This chapter discusses various control strategies facilitated at GSVSCs which operate connected to a multi-terminal VSC-HVDC network in order improve onshore power system stability. More specifically the focus is placed on applied controllers which can introduce damping of inter-area oscillations of electrical power systems by active power modulation of the GSVSC station [**24**].

Three different controllers will be discussed. The first is the classic power system stabilizer controller. The second is a proportional controller with washout block and the last, a band-pass controller. All the proposed methods are based on active power modulation of the grid side converter station. Simulations with meshed ac/dc networks will be performed. A full description of the advantages and disadvantages of the proposed controllers will be given and the performance of the MTdc network will be discussed.

5.2 Methods of damping power system oscillations

Power system oscillations appear as a result of disturbances in power systems. They occur mainly as rotor oscillations of one generator or as oscillations of group of generators against another or even oscillations of a whole area against another area [**35**]. Power oscillations are related to the equivalent inertia of each system. In other words, a disturbance in one power system accelerates (or decelerates) its equivalent inertia towards the equivalent inertia of another system.

Damping of power oscillations can be achieved when extra energy is injected to the power system [**35**]. The damping energy should have the correct phase shift relative to the accelerated or decelerated systems. In principle there are two ways to damp power system oscillations as given in Figure 5. 1. The first facilitates application of powers system stabilizers that operate in conjugation with the excitation system of synchronous generators (right part of the chart). The main duty of the power system stabilizer is to increase the damping torque component of the synchronous generator under a disturbance [**35**]. The second group (left part of the chart) includes methods that operate in the transmission system such as modulation of line impedances or modulation of active (or reactive) power injection at the end of the transmission lines.

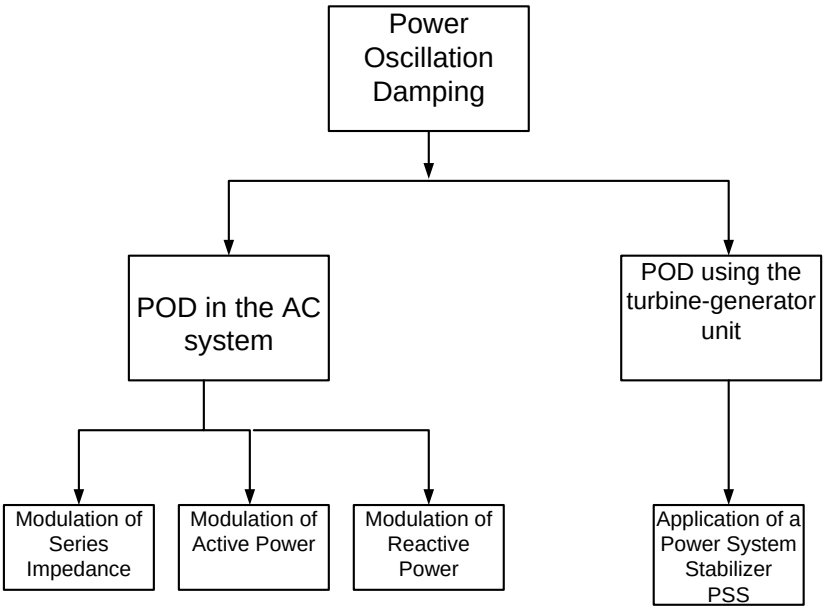

Figure 5. 1: Methods of damping power oscillations in power systems

5.3 Proposal for damping power oscillations by active power modulation of the grid side VSC terminal

Significant damping of power oscillations in power systems can be achieved when there is active power modulation at the end of transmission lines. This technique is used and has illustrated significant success in HVDC transmission systems that operate in parallel to high voltage ac transmission lines [**26**]. Particularly, there has been significant research suggesting improvement of power system stability (both transient and voltage stability) by utilization of VSC-based HVDC lines [**28**] [**41**]. The modulated active power accelerates (or decelerates) the local generators contributing a net damping effect to the power system [**26**]. In addition, generators in the remote system are only slightly affected.

In this technique, the active power of the AC transmission line is used as input signal and more specifically its time derivative. The main advantage is that active power can be measured easily. The disadvantage is that the relation between active power and frequency is non-linear. Thus if the angle exceeds 90 degrees during oscillations then the sign will change and the POD will produce a negative signal. Another approach is to use the derivative of voltage angle at a generator bus or even generator speed deviation. Nevertheless in most of the applications the derivative of active power is frequently used as an input signal [**26**].

Figure 5.2 introduces a graphical overview of a power system where synchronous generators and grid side converter stations are simultaneously operating. As it can be seen in order to improve the damping in the power system either a PSS could be utilized operating at synchronous generators' excitation system or a POD at the grid side converter stations, or even both.

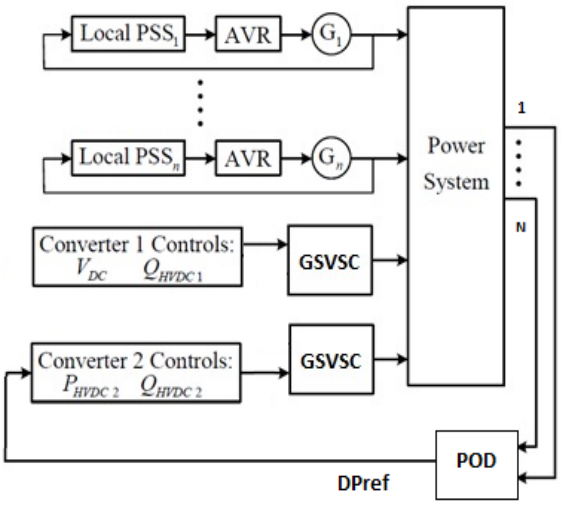

Figure 5.2: Graphical representation of full system control structure for introducing damping of electromechanical oscillations

5.3.1 PSS-type POD stabilizer for utilization in VSC-Based Multi-terminal networks

Even though there has been a lot of research that enables VSC-based HVDC lines to enhance power system stability, there is no significant research on how VSC-based multi-terminal HVDC networks can contribute damping of electromechanical oscillations [**24**]. The technique of active power modulation at the terminal of the HVDC lines [**26**] can also be facilitated to GSVSCs that operate in multi-terminal HVDC networks.

More specifically, as it has been explained in chapter 4, in VSC-based MTdc networks there should always be one or more GSVSC stations responsible for maintaining the dc voltage at operational limits. However, it is possible that one or more GSVSCs operate in active power control mode. These converters, next to their capability to transport constant active power under normal operation, they could facilitate a POD controller that modulates the active power injection of the GSVSC under fault condition. In this way, the GSVSC can suppress low frequency oscillations that appear in the AC system.

As mentioned above, GSVSCs need to be in active power control mode in order to facilitate POD controllers. The main difference of active power and dc voltage control mode is that in the dc voltage control there is no "direct" active power order to the converter station to change active power set point. Active power is changed "indirectly" based on the dc voltage level at the DC capacitor of the converter station. On the other hand, in active power control mode, the controller is capable to directly modulate the active power set point of the GSVSC. The latter is important because these converter stations can improve AC power system stability by implementation of a POD controller. Figure 5. 3 illustrates the control modes of the GSVSC whereas Figure 5. 4 introduces the classic PSS-type POD.

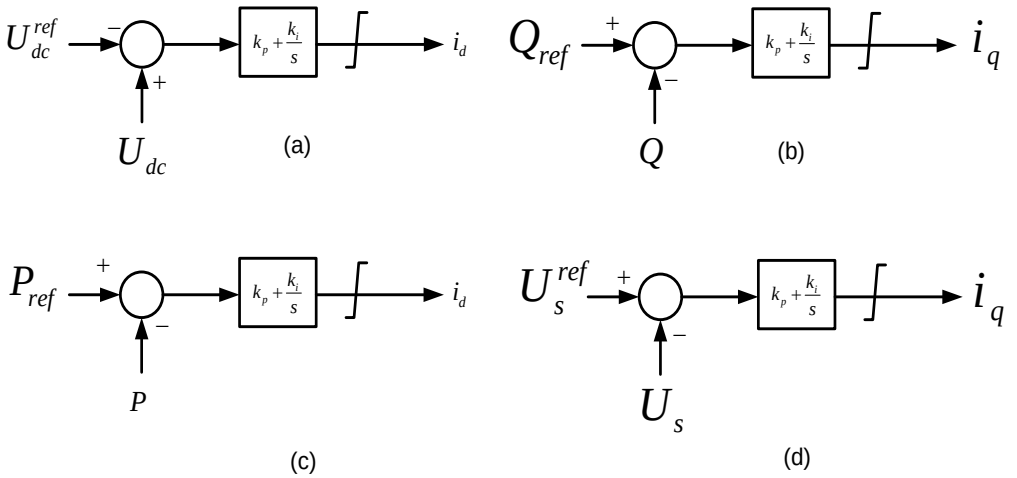

Figure 5. 3: Control modes of the Grid side converter station a) dc voltage control mode b) reactive power control mode and c) active power control mode d) ac voltage controller

The PSS-type POD includes a wash-out block which is responsible to filter low frequency changes ensuring that the POD will not affect the steady state operation of the converter station. It includes also phase shift blocks which are by means of inserting a phase shift between the input and the output signal [**35**]. Last, limiters are included in order to restrict the output signal at acceptable levels.

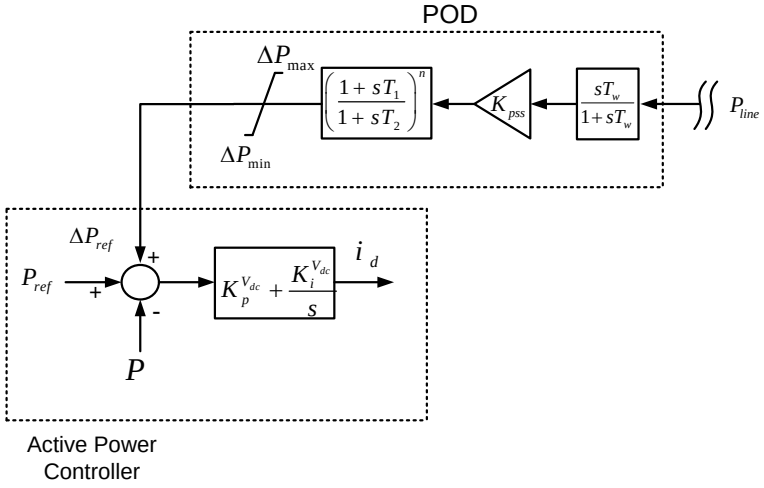

Figure 5. 4: Classical PSS type POD for application in VSC stations

The limiter margin is important because it determines the variations of the dc voltage at the dc capacitor of the VSC as a result of active power modulation. It is worth mentioning that the modulation of active power injection of the GSVSC by the POD creates dc voltage variations in the dc network. The effect of the POD in the dc voltage of the MTdc network will be discussed in following paragraph introducing as well the relevant simulation results.

The main concept of the VSC-based proposed POD controller is based on the capability of the GSVSC to modulate the active power. The controller introduces a net damping effect to the nearby generators. Following a disturbance the synchronous generator connected close to the GSVSC station will start to oscillate against the external (large

and infinite) network. As a result of oscillations the POD will modulate the GSVSC active power following the generator oscillations introducing a net damping effect.

Consequently, when the GSVSC decreases its active power, the generator will increase its active power to cover the load and the rotor speed of generator will decrease introducing in such a way a net damping effect. This type of controller has advantages not only in terms of design but also because it introduces equivalent inertia to the system, as it has been mentioned in [**42**] [**24**].

5.3.2 Simple proportional POD controller

The classic PSS type POD that has been introduced in Figure 5. 4 gives adequate results in terms of damping power system oscillations and has been applied in a number of papers that discuss the modulation of active power of VSC-HVDC transmission systems that operate in parallel to ac transmission lines [**27**] [**24**] [**43**]. However the application of such POD needs careful selection of parameters especially when they are facilitated in converter stations. The main reason is the phase shift that PSS-type POD introduces to the input signal.

In the case of PSS application on the excitation system of a synchronous generator, where the input signal is the speed deviation, this phase shift is required in order to increase the damping torque component of the generator. Actually this is the reason that the PSS have been designed, to contribute a phase shift to the generator torque with respect to speed deviation increasing thus the damping torque component which had been reduced by the excitation system operation [**35**].

However, in the case that the PSS-type POD is applied in GSVSC stations where the input signal is the active power of a transmission line or even the active power of the nearby generator there is no actual need for a phase shift. Furthermore, if not carefully tuned it may contribute damping power in wrong phase. In order to tackle this problem optimization algorithms that use sophisticated methods have been introduced in [**27**] [**28**]. These methods define the optimum parameters of PSS-type POD for VSC-based applications which contribute maximum damping without introducing negative effects on the other modes.

Another solution, originally adopted for the design of power system stabilizers facilitated in full converter direct drives wind turbines [**44**] [**24**], will be proposed in this project. The proposed controller is introduced in figure 5.5. The controller employs a simple wash-out filter with time constant T_w, so that the power set point is not affected in steady state. The output is fed directly to the active power controller of the grid side converter, as illustrated in Figure 5. 5.

The operation of the present controller is based on simple physical considerations and doesn't require the design of special lead/lag compensators as in the PSS type. A typical wash-out time constant of 10s can be applied and the only degree of freedom is K_{dmp}, which determines the introduced damping. Therefore, it can be facilitated without sophisticated tuning studies simplifying its application.

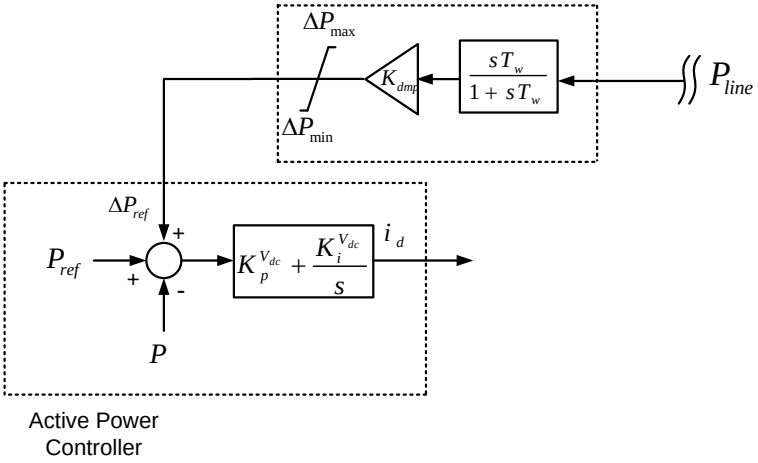

Figure 5. 5: Simple proportional POD controller for application in VSC stations

5.3.3 Proposed band-pass POD for utilization in VSCs

Finally, another proposal will be given in this paragraph for introducing damping of inter-area oscillations. More specifically given the frequency of oscillation it is possible to design a POD controller that will modulate active power of the converter only for the given frequency of inter-area oscillation.

For that reason a band-pass controller with a very narrow band around the central frequency of oscillation that appears in the AC system can be facilitated. At centre frequency the amplitude is maximized. With this method the grid side converter station can provide extra energy to the system in phase only with a specific frequency. In such a way it is possible to suppress only the particular mode of electromechanical oscillation. In addition, the band-pass filter design for a given frequency is an easy and well known procedure. The 3rd order Band-Width filter POD suggested is introduced in figure 5.6.

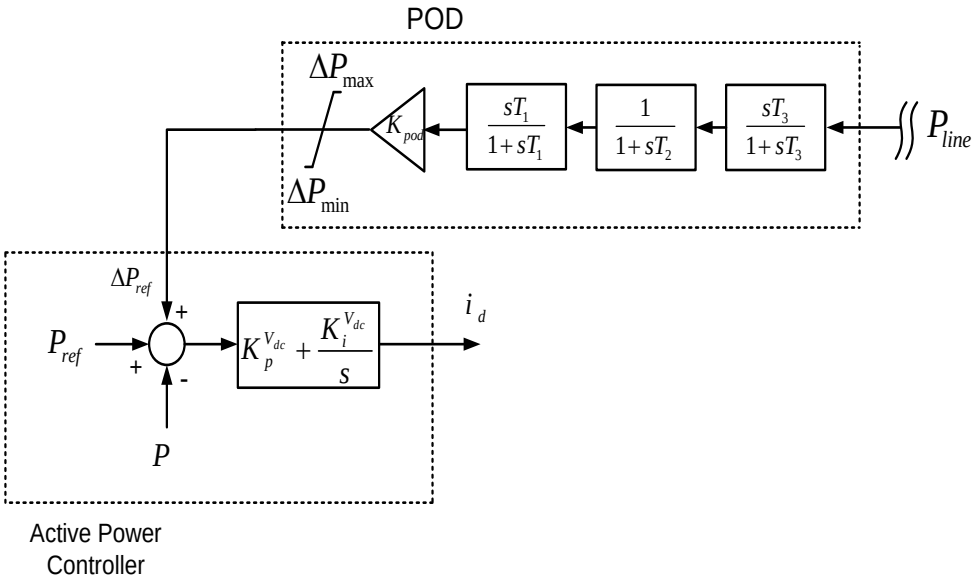

Figure 5.6: Band-pass type POD

5.4 Application in a two area asynchronous systems connected via a multi-terminal VSC-Based dc network

The three proposed controllers will be validated with the test system introduced in Figure 5. 7. It consists of two asynchronous areas connected via a VSC-Based MTdc network. The original system for each asynchronous area is considered to be the three-generator IEEE system [**45**]. Additionally, in this work a GSVSC is introduced at bus 509. Each synchronous generator is rated 400MVA in both areas and represented by the 6th order standard model with standard excitation system (SEXS) and governor (TGOV1). All loads are represented as static loads with constant impedance. All GSVSCs and WPVSCs are rated at 400MVA. The dynamic parameters of the generators and VSCs are same with test system of figure 4.7 and are given in Appendix E.

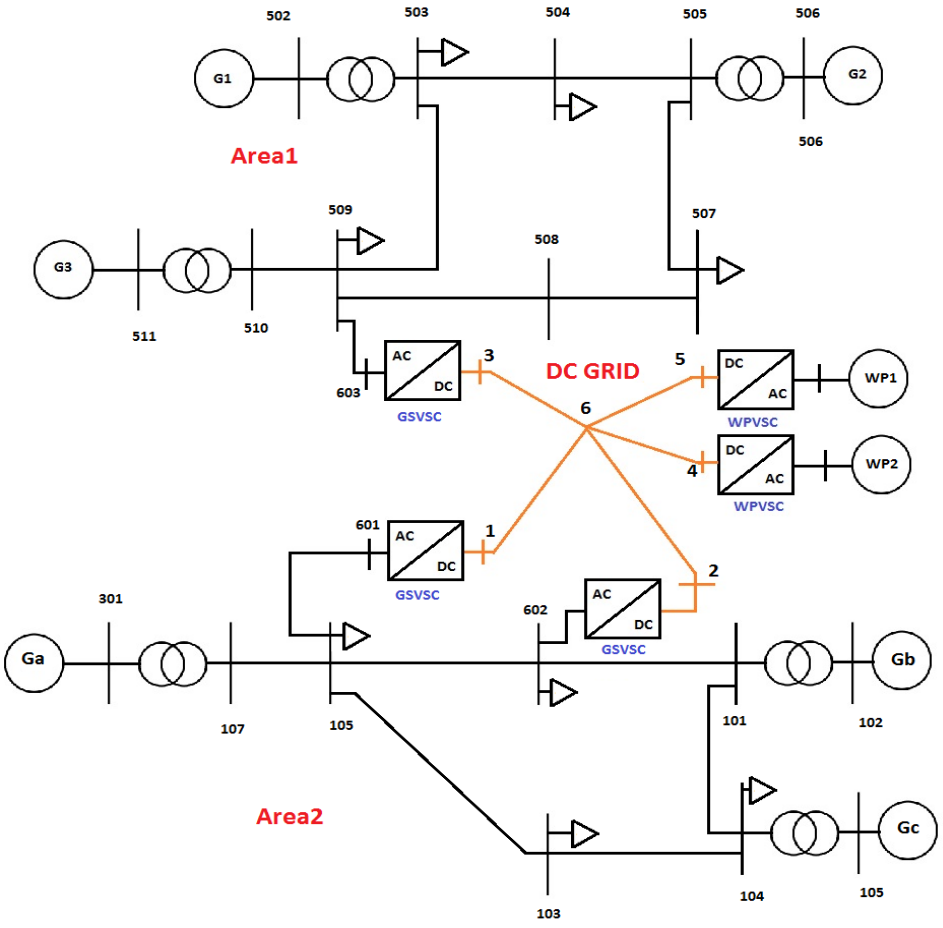

Figure 5. 7: Two asynchronous Power Systems connected via a MTdc network

Two offshore wind farms are considered for this test system both rated at 400MW. For each farm DFIG wind turbines models have been used represented by standard dynamic models from the PSSE library [**6**]. More specifically the wind turbine consists of the generator model, converter model, mechanical and pitch control model.

Area1			Area2		
	bus #	MW		bus #	MW
SG	*502*	**300**	SG	*301*	**300**
SG	*506*	**270**	SG	*102*	**300**
SG	*511*	**300**	SG	*105*	**300**
GSVSC	*603*	**340**	GSVSC	*601*	**150**
LOAD	*503*	**200**	GSVSC	*602*	**200**
LOAD	*504*	**200**	LOAD	*602*	**250**
LOAD	*507*	**300**	LOAD	*104*	**300**
LOAD	*509*	**500**	LOAD	*103*	**400**
N/A	-	-	LOAD	*105*	**300**

Table 4: Generation and load for the selected snapshot of the test system

Table 4 introduces the selected operational point or else known as snapshot for the test system of Figure 5. 7. More specifically for the present case study, GSVSC603 is operated in active power control mode whereas GSVSC 601 and GSVSC602 are in dc voltage control mode facilitating a droop controller. Hence, the POD is installed in GSVSC 603. Its input signal is considered the active power flowing in line 510-509. Last, the slack bus of Area 1 is generator 506 while for Area2 generator 105.

5.5 Simulation results and discussion

In this paragraph the three POD controllers will be tested with the power system of Figure 5.7. For the selected snapshot, a three phase fault disturbance at bus 506 will be introduced. The POD is in operation at GSVSC603. The input signal is the active power at line 510-509. The scope is to investigate the improvement in power oscillation damping at asynchronous Area 1, and more specifically at generator G3 (bus 301) by the operation of the POD installed at grid side converter 603.

5.5.1 PSS-type POD

For the selected parameters of the PSS type POD (K_{pss}=20, T_w=10, T_1= 2.2, T_2= 1.4 and n=2), figure 5.8 introduces its Bode diagram. More specifically as it can be seen, the POD adds 25^o phase shift to the input signal at 0.3Hz. At1Hz, which is the common frequency of local oscillations of synchronous generators the phase shift introduced by the POD is 10^o.

The active power profile of G3 (at bus 511) is given in figure 5.9 for a 200ms three-phase fault at bus 506. From simulation results it can be concluded that the damping introduced by the POD installed at GSVSC603 to G3 (area1) is significant. What is more, it is comparable to the damping introduced by a classical power system stabilizer (PSS) operating at the excitation system of the G3. The design of the PSS of the excitation system is performed by classic conventional method [**35**]. By observation of active power of G2 and G1, there is also slight improvement of oscillations at these generators, as a result of net damping effect. Last, the output signal of the POD is given in figure 5.10.

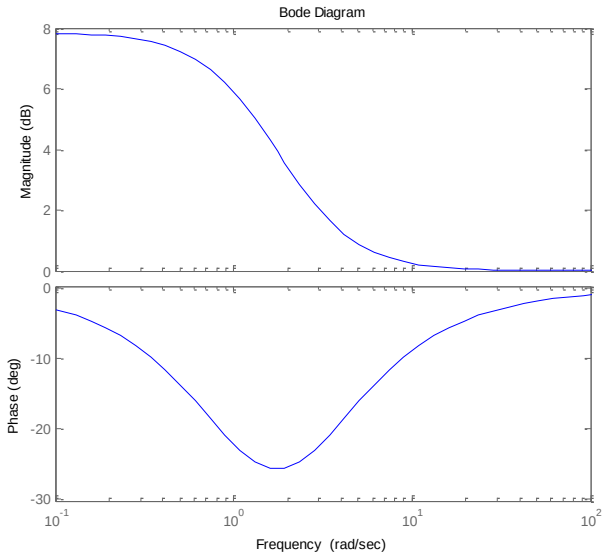

Figure 5. 8: Bode diagram of for the PSS type POD for selected parameters

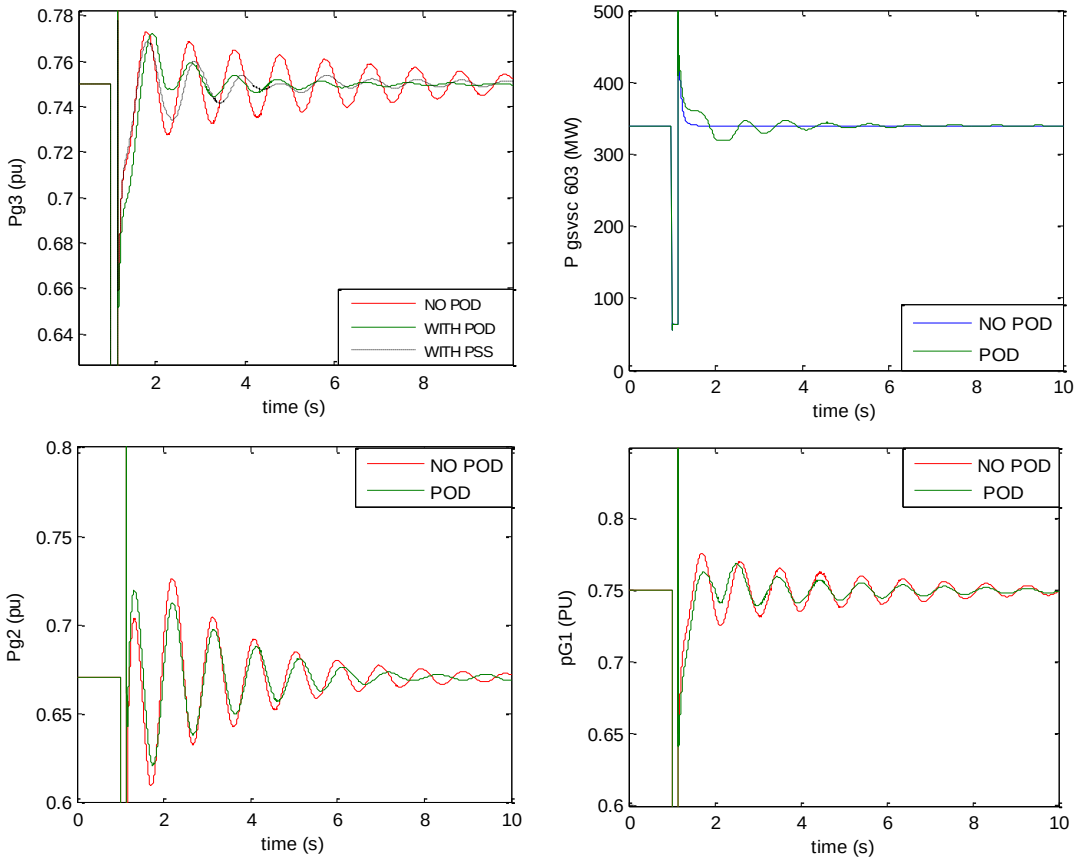

Figure 5. 9: Active power of G1, G2 and G3, GSVSC 603

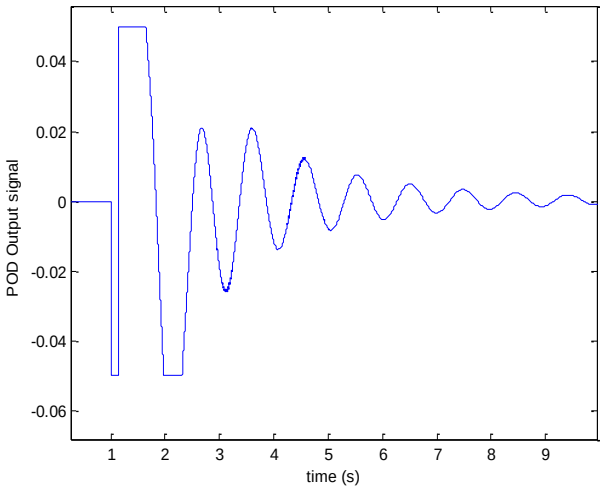

Figure 5. 10: Signal at the output of the POD installed at GSVSC603

From figure 5.9, the disturbance created in G2 triggers power oscillations in G3. The power oscillation of G3 is the input signal of the POD. The POD based on the G3 oscillations modulates the grid side converter active power contributing thus a damping effect to G3. More specifically when the generator decelerates, the POD controller will reduce the injected from the converter station active power. As a result, the generator will increase its active power in order to supply the load. The total effect is a net damping introduced to the system of Area1.

Additionally, figure 5.11 illustrates the sensitivity of the G3 active power set point in the ability of the GSVSC to damp power oscillations. The conclusion from the simulation results is that the GSVSC provides damping effect to G3 for different operational points of G3. Furthermore, the capability of the GSVSC and its POD to damp power oscillations is only related to the limiter margin of the POD and to the upper current limit of the grid side converter station. The higher the limiter margin introduced at POD the bigger the modulated active power from the converter station. However, the POD limiter margin cannot be made significantly high because it would create unstable direct voltage oscillation in the dc network.

Let us know focus on the dc voltage at the dc capacitor of the GSVSC station. As it can be seen in figure 5.12, there are dc voltage oscillations which are triggered due to the operation of the POD on the GSVSC 603. The reader should recall that the dc voltage and active power injection are closely related. Furthermore, the GSVSCs in area2 which operate in dc voltage control mode will try to control these dc voltage variations by modulating accordingly the converter's active power.

Figure 5.13 introduces active power response of the GSVSC601 and GSVSC602 operating in Area2. Both converter 601 and 602 are in dc voltage control mode implementing a droop control method. It can be seen that the POD operation on GSVSC 603 triggers dc voltage oscillations which via the droop controller are propagated to the active power injection of the GSVSCs in Area2.

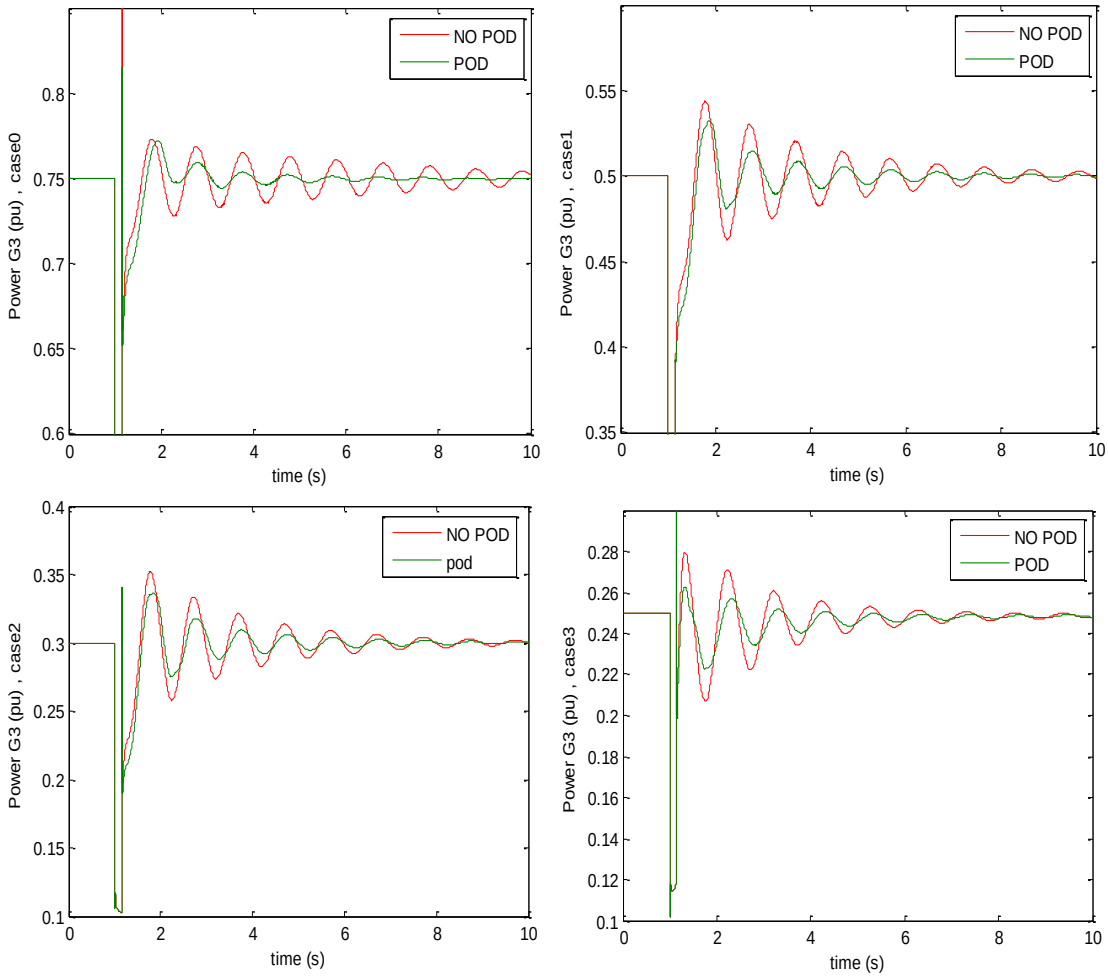

Figure 5. 11: Sensitivity of G3 active power set point

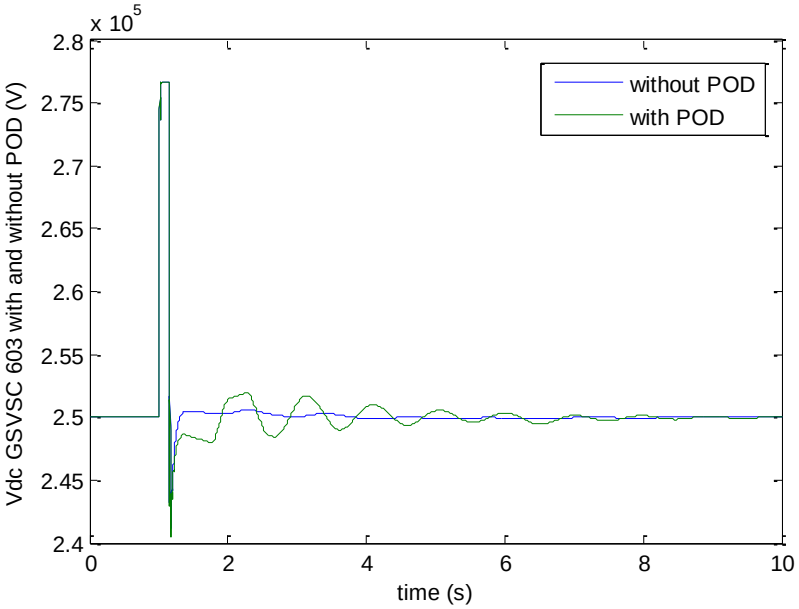

Figure 5. 12: DC voltage at the DC capacitor of the grid side VSC

Additionally, the short circuit in Area1 will create an overvoltage at the dc network, as it can be seen in Figure 5. 12. This comes due to loss of power balance at the converter's dc capacitor followed by instant storage of power at the dc capacitor. The instant power storage will increase the dc voltage in the dc network. As soon as the dc voltage reaches the threshold value, (1.1pu in this project) the dc chopper will be activated and will start dissipating power in order to keep the voltage at constant value during the fault.

The overvoltage that appears in the MTdc network will create an overshoot in the active power injected at grid side converters in Area2. More specifically, due to the fact that these converters are operating in dc voltage control mode, facilitating a droop controller, the dc overvoltage will increase active power injection in Area 2. That is the main reason of the active power overshoot in figure 5.13.

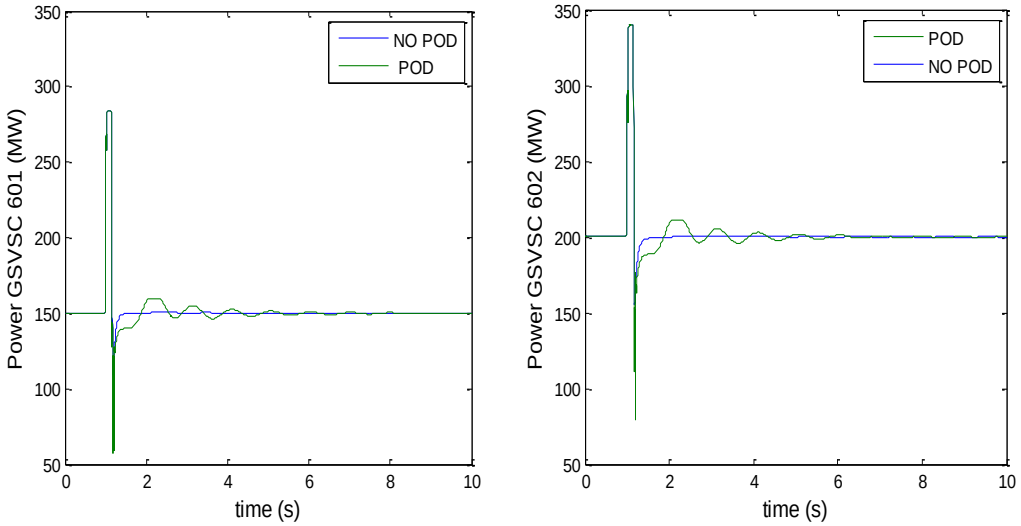

Figure 5. 13: Active power injection of the grid side converters at Area2

The grid side converter in area 1 is capable of damping power system oscillations improving power system stability in the particular area. However, the operation of the POD creates dc voltage variations in the dc network which could create power oscillations of the grid side converters operating in area2. These dc voltage variations are not present in the dc network in the situation where the POD is not in operation. Furthermore, a short circuit in Area1 will trigger a large overshoot in the GSVSCs active power in area 2.

5.5.2 Simple POD

In this paragraph, the simple type POD that has been described in 5.2.2 will be compared with the PSS type POD, described in 5.2.1. The POD is operating at the converter 603 similar to the case of the PSS type POD. Figure 5.15 illustrates the active power profile of the G3 with simple and with PSS type POD.

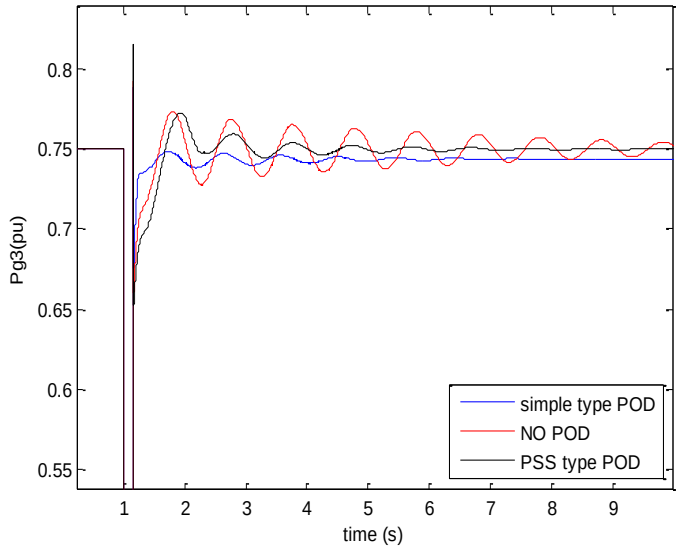

Figure 5. 14: Active power of G3

Comparing the damping performance between the two controllers, it can be concluded that they both provide a net damping effect in Area1. What is more, the advantage of simple POD against the PSS type is that the implementation of such controller is easier. The only degree of freedom is K_{dmp} gain which determines the damping performance. The output signal of simple type POD is given in figure 5.15. There is a steady state error that can be seen in the POD output which is related to the proportional characteristic of the simple type POD.

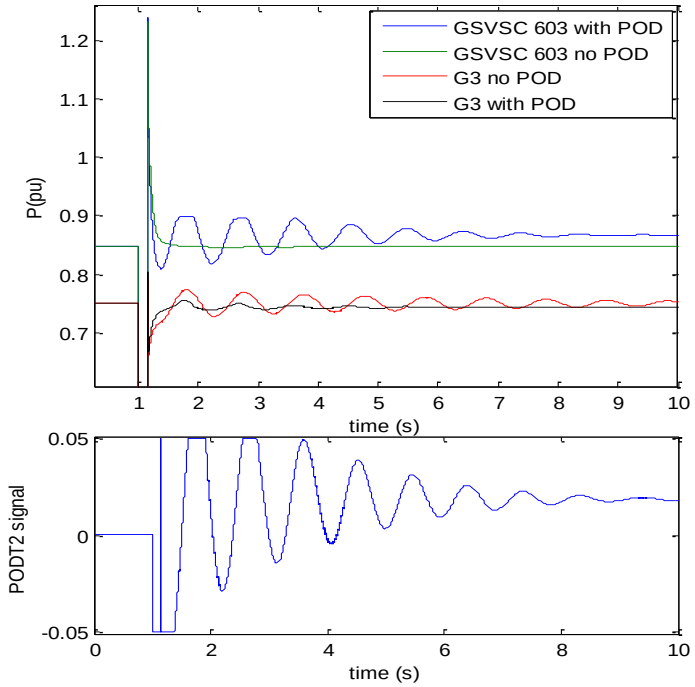

Figure 5. 15: Up: active power of G3 and grid side converter. Down: POD output

5.5.3 Band-pass POD

Finally, the band-pass POD type is going to be investigated. More specifically, the controller can be tuned in such a way that the centre frequency is the frequency of electro-mechanical oscillation of G3, 1.05Hz for this case study. For the particular frequency of electromechanical oscillation and the selected parameters of POD, figure 5.16 introduces the Bode plot of the particular controller.

As it can be seen from the Bode plot, the proposed controller consists of a band-pass zone around the centre frequency. In other words the controller will modulate the grid side converter active power only for the range of oscillation frequencies within the band width. As a result, there is zero amplification for frequencies outside the band-width of the controller.

Figure 5.17 introduces the response of the G3 when a band-pass POD controller is facilitated. Additionally, the modulated by the POD grid side converter output is introduced in figure 5.18. From the response it can be seen that the proposed controller manages to damp power oscillations of the G3 generator. However, there is different dynamic response which has mainly to do with the spectra of frequencies that Band-pass POD operates.

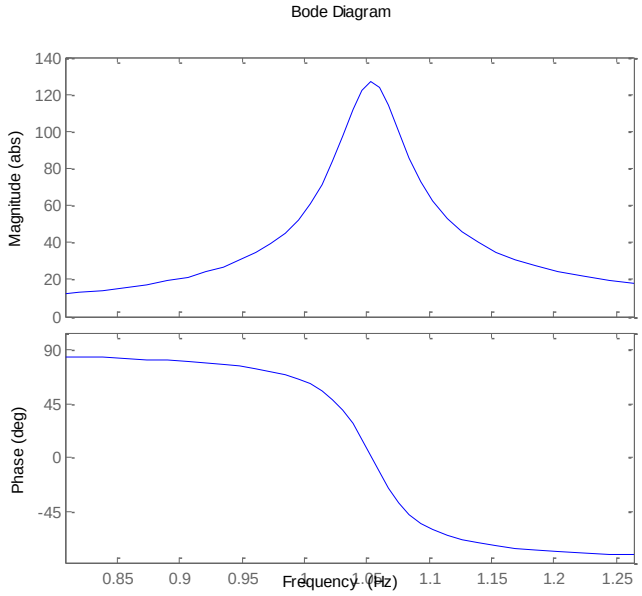

Figure5. 16: Band-pass controller tuned for damping the electromechanical oscillations of G3

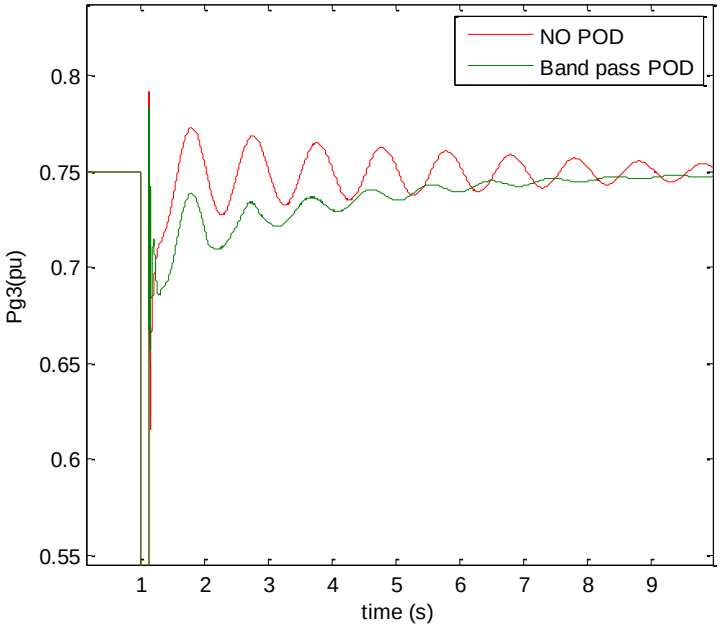

Figure 5. 17: Active power of G3

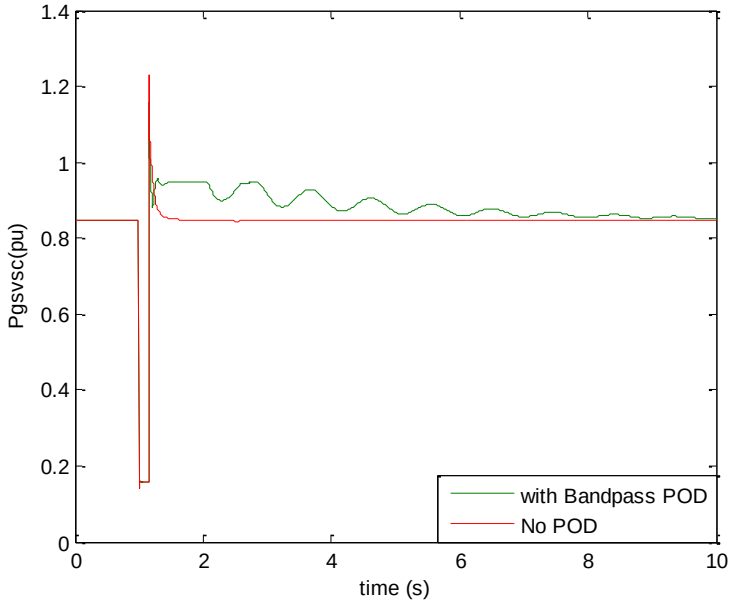

Figure 5. 18: Modulated active power by Grid Side converter 603 with Band type POD

5.6 Conclusions

This chapter relates the capability of VSC-based HVDC MTdc networks to introduce damping of power oscillations in ac power systems that operate meshed with MTdc networks. Three control strategies have been introduced for damping of power oscillations. The POD controller is added to the active power control loop of the GSVSC. Each of the three controllers introduced a damping effect in the power system they operate by active power modulation of the GSVSC station.

The best performance is achieved with the simple POD type controller as it can be seen in Figure 5. 14. Furthermore, the particular controller can be tuned easily and can be used without the need for parameter optimization. Additionally, a band-pass controller is proposed for damping only a specific mode of electromechanical oscillations. The advantage of the band-pass POD is that the controller is activated only for a specific frequency of electromechanical oscillation. This makes it interesting for applications where the POD introduces damping only at a specific frequency such as an inter-area oscillation.

From the simulation results with the selected test system, it can be concluded that the utilization of POD controller that operate at GSVSC 603 introduced damping of power oscillations in Area 1. However, the interaction of the POD with the direct voltage droop controller at buses GSVSC601 and 602 demands special attention. Moreover, the modulation of active power by the POD triggers direct voltage oscillations in the MTdc network which would carry the power oscillations from area 1 to area 2. For that reason the modulation of GSVSC active power by the POD should be kept within acceptable limits in order to prevent stability problems in the second asynchronous system.

Finally, it is important to stress that in the two-area test system a short circuit in area1 triggers a large overshoot in the dispatched active power by the GSVSCs in area 2. This is primary related to the dc overvoltage and the droop controller response. The overshoot of active power will be extensively discussed in chapter 6 where a transnational MTdc network is interconnected with the onshore power system.

Chapter 6: Analysis of transient stability of the Dutch power system with meshed offshore VSC-HVDC networks

6.1 Overview of the Dutch high voltage transmission system

The Dutch high voltage transmission system consists of four types of high voltage levels: 380kV, 220kV, 150kV, and 110kV high voltage level. The 380kV and 220kV transmission lines are mainly responsible to transport the majority of power through the Netherlands while the 150kV and the 110kV are functioning as sub-transmission systems. The main ring is at 380kV level with several radial branches. In the Northern part of the country there is a second ring at 220kV level. Figure 6.1 gives the present situation of the Dutch power system [**46**].

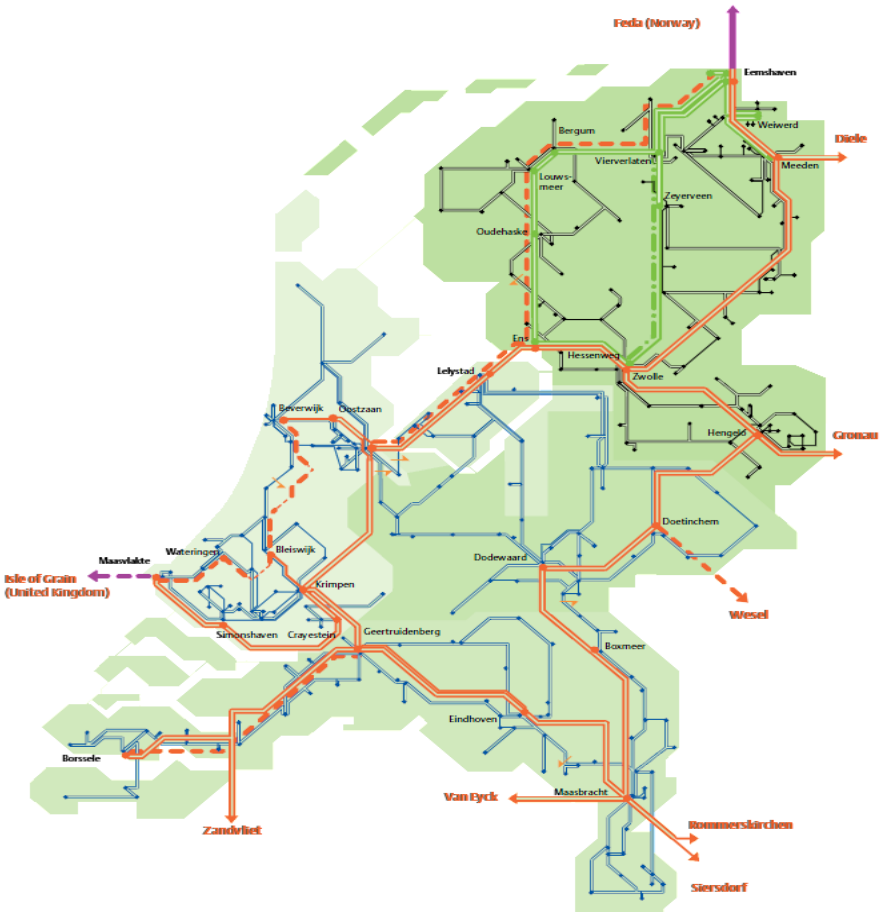

Figure 6.1: Present Dutch high voltage transmission system at 380kV, 220kV, 150kV, and 110kV level. Red: 380kV, Green: 220kV, Blue: 150kV and black 110kV

6.1.1 Network Reinforcements

The transmission system of Netherlands is about to undergo certain grid reinforcements in order to ensure the quality and security of supply for 2025-2030. Currently, another ring at 380kV level in the Western part of the country and more specifically at the industrial area of *Randstad* is under construction. This ring will connect the substations Westerlee, Wateringen, Bleiswijk, Beverwijk, Ooszaan and Diemen.

Furthermore, the new 380kV ring will increase the transmission capacity in the Randstad area. It will enhance the ability to safely integrate large amounts of offshore wind power at the Beverwijk substation, which is planned as one the three connection points of the offshore wind projects [**5**]. In addition, the construction of new power plants in the Eemshaven substation along with the sustainable energy projects and planned interconnectors demand for further grid reinforcements in this region. For that reason a new 380kV line from Eemshaven to Diemen will be constructed [**46**].

6.1.2 Dutch Power system interconnectors

The Dutch transmission system is currently connected to Germany and Belgium, through totally five interconnectors at the level of 380kV. Plans are at hand to build a sixth interconnector with Germany which will be in operation by 2020. In addition, there are asynchronous HVDC interconnections with Norway (through the NorNed HVDC cable since 2007, with capacity of 700MW) and with UK (through BritNed HVDC cable commissioned since 2011, with a full capacity 1000MW). Furthermore, a second interconnector with Norway will be constructed and an interconnection with Denmark, both utilizing HVDC transmission technology.

6.2 The North Sea Transnational Grid project

As it has been described in chapter 1, the NSTG project investigates the most efficient technical solutions for the integration of large amounts of offshore wind power to the national grids.

The main focus of this thesis is contribution to the NSTG project firstly showing that the proposed model is capable to study the stability of heavily meshed ac/dc networks and secondarily drawing conclusions about the transient stability of the Dutch power system and more specifically how the first swing or rotor stability of critical generators can be affected in situations with high wind penetration connected onshore via VSC-HVDC transmission systems. To that effect, selected snapshots will be evaluated through time domain simulations which include case studies with high offshore and onshore wind and low conventional generation.

Three types of VSC-HVDC transmission configurations will be evaluated [**47**] [**5**]. The first type includes individual connection of the offshore wind farms via point-to-point VSC-HVDC transmission lines. The second type introduces the connection of the offshore wind farms in a Multi-terminal VSC-HVDC offshore network connected at a country. The last type considers the transnational connection of the German-Dutch-Belgian offshore wind farms via a multi-terminal HVDC network that extends from the German to the Belgian offshore wind area.

6.2.1 National plans of the Netherlands for offshore wind power

Since the focus in this project is to investigate the interaction of the multi-terminal VSC-HVDC offshore networks with the interconnected Dutch power system from transient stability point of view, the total 6000MW planned offshore wind capacity for Netherlands will be divided into modules of 1200MW, corresponding to the capacity of the VSC-HVDC station. Three offshore wind zones are considered in the Dutch power system for the development of the offshore wind farms [**5**].

Concerning the grid feed-in points, three substations are selected, namely Eemshaven 380kV, Beverwijk 380kV and Borssele 380kV [**3**], [**5**]. Table 5 introduces the assumptions taken for this study about the network feed-in points, the capacities and distances measured from the centre of the offshore zone to shore.

Location	Area (km^2)	OWF capacity	Network feed-in substation	Distance to shore (km)
Eemshaven I	150	1200MW	Eemshaven 380kV	90
IJmuiden I-II	150	1200MW	Beverwijk 380kV	80
IJmuiden V	300	2400MW	Beverwijk 380kV	120
Borssele II	150	1200MW	Borssele 380kV	50

Table 5: *Locations and grid connection point of the Dutch offshore wind farm projects*

6.2.2 National plans of Germany for offshore wind power

There are five defined offshore zones for the construction of the German offshore wind farms with a total planned capacity of 25 GW. Table 6 illustrates the capacities for each of those areas with the feed-in points into the German transmission system and the distances to shore [**5**].

Location	Area (km2)	Capacity	Network Feed In	Distance (km)
Nordlich Borkum I,II,III	550	4560MW	Diele 380kV	90
Ostlich Austemgrund	400	3420MW	Unterweser 380kV	180
Sudlich Amrumbank	400	3420MW	Unterweser 380kV	130
Hochsee Sud	800	6840MW	Conneforde 380kV	150
Hochsee Nord	800	6840MW	Conneforde 380kV	210

Table 6: *Locations and grid connection point of the German offshore wind farm projects*

6.2.3 National plans of Belgium for offshore wind power

An area of 225km^2 is devised at the Belgian section of the North Sea. Table 7 introduces the wind farm modules considered as well as the distance from shore.

Location	Area (km^2)	OWF Capacity	Network feed-in substation	Distance to shore (km)
NW-Thorntonbank	225	1710MW	Eeklo-Nord 380kV	60

Table 7: *Locations and grid connection point of the Belgian offshore wind farm projects*

6.3 Overview of 2010 Network Dynamic Model of TenneT

The 2010 dynamic model of TenneT in PSSE includes the interconnected continental European high voltage transmission system network and is based on the UCTE model from 2001. However, even if there is a full load flow model only the Dutch, Belgian, German and part of the French generators are represented by dynamic models.

6.3.1 The Dutch Part of the model

In the 2010 dynamic model, there is a detailed description of the Dutch high voltage transmission system at the levels of 380kV, 220kV, 150kV and 110kV for the 2010 network situation, illustrated in Figure 6.1.

Most of the power generation is located in the west part of the country near the coast at Maasvlakte and Borssele. Large generators are also located in the North, connected to Eemshaven substation. In the 2010 model made available by TenneT, conventional generators are modeled by 6th order IEEE standard models with dedicated parameters along with excitation systems, governors, and prime movers [**6**]. All the generators in the Dutch system larger than 100MW are modeled with their excitation system and governors.

The majority of dynamic parameters of the generators in the Dutch part of the model are known. Loads are represented as static loads with fixed impedance. There is no dynamic model of BritNed and NorNed, because there is no representation of UK and Norway transmission system. For that reason all asynchronous interconnectors are considered in the load flow model as static loads, with positive or negative value according to the direction of power flow.

6.3.2 The German Part of the TenneT model

In the German part of TenneT model, there is a description of the high voltage transmission system at 380kV, 220kV and 110kV level. Only large generators connected to 380kV, 220kV and 110kV level are modeled by IEEE standard models along with excitation system. For simplicity reasons standard generator parameters have been facilitated for the German part of the model.

6.3.3 The Belgian and French Part of the TenneT model

The Belgian part of the ENTSO-E model includes the high voltage transmission system at 380kV, 220kV and 150kV. Only power plants connected to the above mentioned high voltage levels are represented by dynamic models. For the Belgian part, standard generator models and excitation systems have been used with standard parameters.

The French part of the model consists of the 380kV transmission system only. Merely the large generators are connected to the 380kV level are represented by standard models with standard parameters.

The rest of the countries in the ENTSO-E system are represented by equivalent load flow models. The slack bus of the TenneT model is considered a 380kV bus in Italy.

6.4 A 2025-2030 version of TenneT dynamic model in PSSE

With the ultimate goal to study the transient stability of the interconnected Dutch power system for the 2025-2030 network situation, the present 2010 dynamic model of TenneT needs to be upgraded with the major network reinforcements. Up to date there is no available dynamic model that represents the 2025-2030 situation of the Dutch power system in PSSE. For that, all the planned network reinforcements in the 380kV level of the Dutch transmission system for 2025-2030 as given by TenneT have been included into the existing dynamic model as shown by the dashed lines in figure 6.1.

6.4.1 Conventional Generation

According to TenneT planning for 2025-2030, very old generators will become outdated and non-operational. In addition, new generators will be constructed at certain locations of the system.

However due to the fact that the dynamic model parameters of all the generators in the Dutch power system for the 2010 situation are known (model parameters given by the producers) it was considered more reasonable not to use standard models and parameters for the new generators that are going to be in operation for 2025-2030 network situation.

Consequently in the unit commitment of the 2025-2030 model the main assumption considered is that very old generators are de-committed and only generators that are now in operation and will still be by 2025-2030 are taken into consideration. This situation is feasible because only snapshots with minimum conventional generation and large wind penetration will be studied.

6.4.2 Selected snapshots of the Dutch power system for dynamic simulations

In the project at hand a 2025-2030 version of the TenneT dynamic model is used. For that reason the operation point of the Dutch power system or otherwise known as snapshot should be a case study that reflects a 2025-2030 network situation. Three snapshots have been selected for the dynamic simulations in this study. Figure 6.2 introduces a graphical representation of the three selected snapshots.

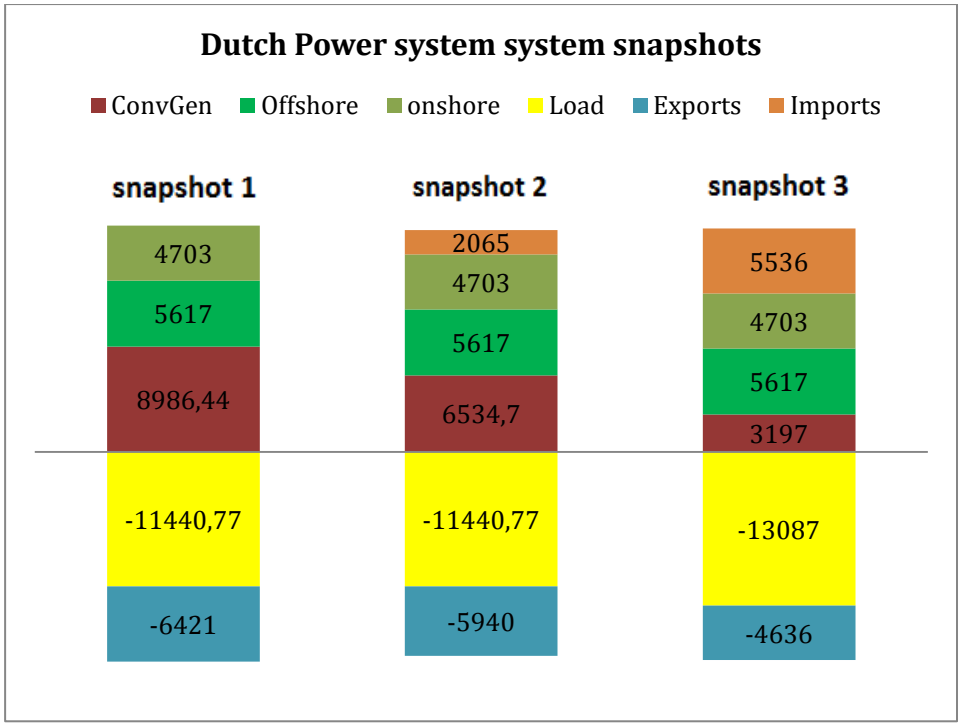

Figure 6.2: Selected snapshots of the Dutch power system (all powers in MW), negative means exports and load

6.4.2.1 Snapshot 1 of the Dutch power system

From stability point of view an interesting snapshot would be one with low conventional generation, minimum load and maximum wind penetration. This operating point represents a situation with low inertia in the system especially when large amount of offshore wind power is transported onshore via VSC-HVDC transmission systems.

A graphical representation of the selected snapshot is introduced in Figure 6.2. Snapshot 1 reflects a situation of the network where there is large amount of onshore and offshore wind generation, large export to Belgium, Denmark, Norway, UK and Germany in combination with minimum conventional generation and load. No imports are considered for the case study of Snapshot 1. Figure 6.3 introduces the exports as given from the ac power flow.

It is important at this point to notice that the load for the 2025-2030 situation is selected based on market model simulation done by TenneT for 2025-2030 and is similar for the first two snapshots. More specifically the maximum load for 2025-2030 is estimated at 25.6GW while the minimum load at 11GW. In addition, in the capacity plan study of TenneT for 2020, there is a scenario in which the minimum load in the Dutch power system is considered to be 7.53GW. Thus extrapolating with a normal rate of 2% per year we conclude that the selected load is not far from the estimated minimum load for 2030. Concerning conventional generation, market results for 2030 reveals a minimum generation of 8.2GW. Thus the selected conventional generation is close to the market model resullts as well.

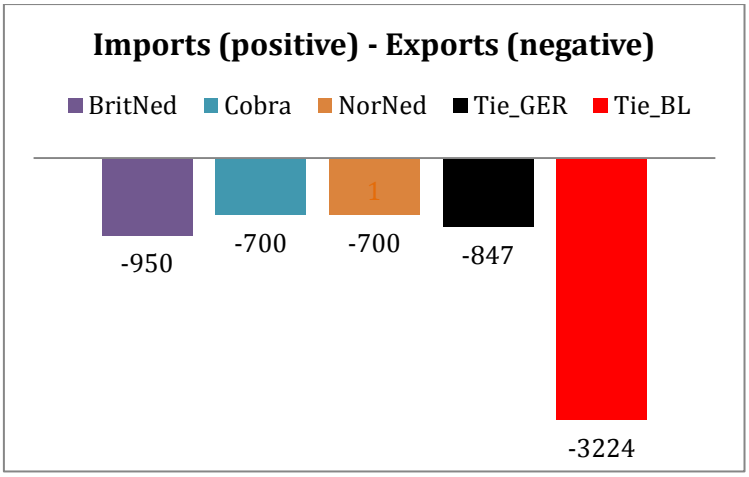

Figure 6.3: Snapshot 1of the Dutch Power system (all Power in MW)

This snapshot is interesting from stability point of view for numerous of reasons. First, there is large generation of power from both onshore and offshore wind farms and thus great amount of wind power penetration in the system. Second, conventional generation is low, lower than wind penetration which may impair transient stability.

Furthermore, in the case of offshore wind power transported onshore via VSC-HVDC links (or MTdc networks as well) this problem can be even worse. The reason for this is the full decoupling of offshore wind turbines kinetic energy from the ac system frequency. Finally, the large amount of power injected by converters operating in the power system and their dynamic interaction during ac disturbances also needs investigation in such a situation. For all the above reasons the selected snapshot is attractive from power system stability point of view and will provide an overview of the behavior of the interconnected Dutch power system under high wind penetration both onshore and offshore.

		Snapshot 1&2	Snapshot 3	Snapshot1	Snapshot2	Snapshot3
	Zone	**LOAD (MW)**	**LOAD (MW)**	**Gen (MW)**	**Gen (MW)**	**Gen (MW)**
1	**UTRECHT**	844	980	372	235	159
2	**FLEVOLAND GE**	1625	1887	1050	635	593
3	**GDO**	1599	1855	442	337	0
4	**ZUID HOLLAND**	903	1048	916	112	112
5	**NOORD-BRABANT**	1633	1894	760	760	0
6	**LIMBURG**	1067	1237	444	235	0
7	**ZEELAND**	237	275	1152	1132	925
8	**NOORD HOLLAND**	2182	2531	690	630	630
9	**220kV**	489	577	1366	665	0
10	**380kV**	0	0	1793	1793	778
11	**FRIESLAND**	372	236			
12	**CRAYESTAIN**	489	567			
TOTAL		**11441**	**13087**	**8986**	**6535**	**3197**

Table 8: Generation and load per zone of the Dutch power system for each snapshot

The dynamic model of Dutch power system, is divided into 12 zones. Table 8 introduces the generation and load per zone that has been chosen for the simulations. As it has already been discussed, old power plants that are considerered out of operation for 2025-2030 have not been used in the unit commitment. In addition the conventional generation per zone is based on extrapolated values of TenneT capacity plan (CSD) for 2020.

6.4.2.2 Snapshot 2 of the Dutch power system

The second selected snapshot, Figure 6.2, introduces an operational point with low conventional generation for the 2025-2030 grid situation of the Dutch power system. The difference between snapshot 1 and 2 is that in the second, conventional generation is lower and both import and export flows or else transit flows are taking place. More specifically, as it can be seen in Figure 6.4 there is 2065MW imports from Germany combined with exports to Belgium and to the asynchronous interconnectors.

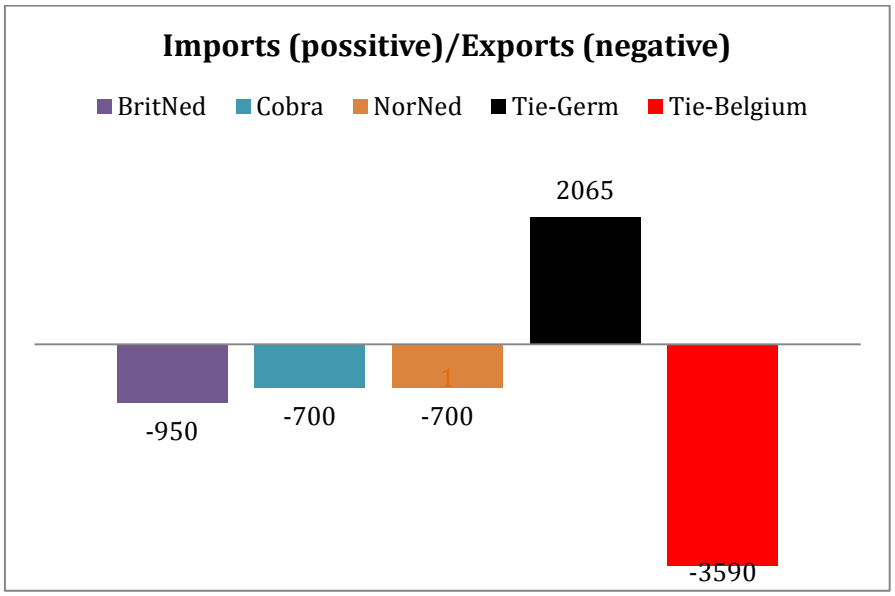

Figure 6.4: Snapshot 2 of the Dutch Power system (all Powers in MW)

This grid situation represents an operating point with high wind penetration in the Netherlands combined with minimum load, and import from Germany. Exports through asynchronous interconnectors are kept at high level while there is low conventional generation due to imports from Germany.

6.4.2.3 Snapshot 3 of the Dutch power system

Snapshot 3 represents a network situation where imports from Germany are high. In addition, there is high wind in Netherlands followed by exports to other countries. This is a situation that occurs when there is large amount of low cost production in Germany, mainly wind and solar generation. Large amount of wind generation in Netherlands combined with exports to UK, Norway and Denmark. Load in this situation is considered higher whereas conventional generation in Netherlands is extremely low.

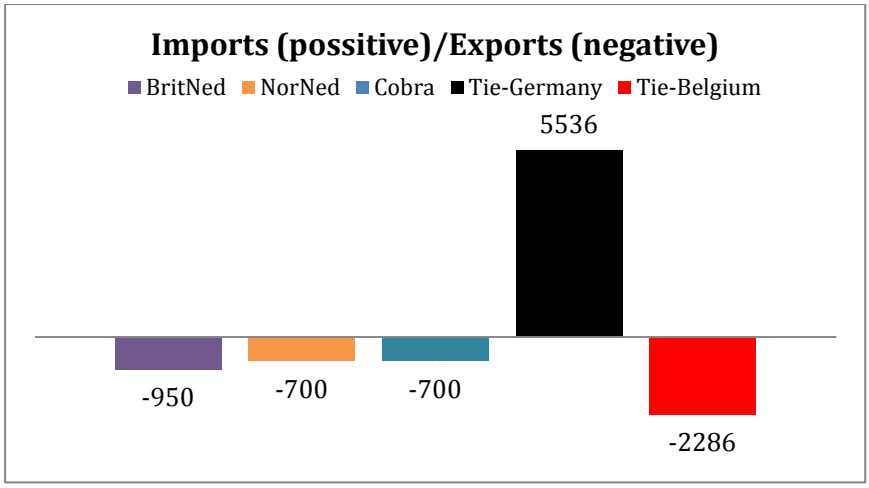

Figure 6. 5: Snapshot3 of the Dutch Power system (all Power in MW)

6.4.3 Selected snapshots of the German and Belgian power system for the dynamic simulations

For the above selected snapshots, Table 9 introduces the total generation and load in Germany and Belgium. What is of great importance to notice is that in both countries all the generation is conventional and no onshore wind or solar generation has been considered, especially in Germany where there is large solar and onshore wind installed capacity.

	Snapshot 1&2		Snapshot 3	
	Germany	**Belgium**	**Germany**	**Belgium**
Load (MW)	49670	12810	49670	12810
Conv Generation (MW)	56018	13024	63094	13382

Table 9: Generation in Germany and Belgium for the selected snapshots

Consequently, a realistic grid situation in Germany should include at least 25GW installed solar power capacity (which is up-to-date in operation). In addition 29 GW onshore wind power is already installed since 2011 which is not included in the model.

For that reason, the assumption of only conventional generation in the German part of the TenneT model gives an inherent error with regard to the total equivalent power system inertia in Germany. More specifically in the present case study the German power system is operating as a large and stiff network with high system inertia. The same applies also for Belgian part of the model where only conventional generation is considered as well.

6.4.4 Onshore wind farm models and planned onshore wind capacity for 2025-2030

Looking further into the future and the 2025-2030 situation of the Dutch power system a total 6000MW onshore wind power capacity has been planned to be connected at certain locations of the power system. Within the present project 4700MW installed capacity of onshore wind power is considered to be in operation in the Dutch power

system by 2025-2030. Within the 2010 dynamic model of TenneT there is only a total 470MW installed onshore and offshore wind capacity.

Standard PSSE dynamic models for Double Fed Induction Generator (DFIG) and direct drive (DD) wind turbines have been facilitated for the planned onshore wind farms. More specifically, standard electrical control model of direct drive wind turbine (WT4E) has been used with standard generator and power converter model (WT4G) as given in PSSE library [**6**]. For the case of the DFIG type, standard generator model have been facilitated (WT3G1) with standard electrical control model (WT3E1), pitch angle model (WT3P1) and mechanical system model (WT3T1).

Table 10 introduces the connection points of the onshore wind farms in the Dutch power system along with the type of wind turbine model used. For the 2025-2030 onshore wind capacity, only 300MW is considered to facilitate DFIG turbines while the rest utilize DD turbines.

Total onshore & offshore installed Wind Power			**Planned Onshore Installed wind Power**		
2010 grid situation	**Capacity**	**WT type**	**2025-30 grid situation**	**Capacity**	**WT type**
Connection Point	**MW**		**Connection Point**	**MW**	
RLL10B/A 10,6kV	14,58	DD	Bergum 21kV	300	DFIG
BSL10/B 10,6kV	20,19	DD	Meeden 380kV	993	DD
Q8 WINDPARK 34kV	116,29	DD	Maasvlakte 380kV	450	DD
T-EEMS 10,5kV	168,75	DD	Oterleek 150kV	800	DD
T-WPHFDPLTPR 10,6kV	11,22	DD	Lelystaad 150kV	800	DD
VLN Q7 1 22kV	64,61	DD	Beverwijk 380kV	300	DD
VLN Q7 2 22kV	64,61	DFIG	Geertruidenberg 380kV	590	DD
WAP10KV 10,6kV	10,1	DD			
Total installed by 2010	**470,35**		**Total installed by 2025-2030**	**4703,35**	

Table 10: Onshore wind farms connection points for the 2025-2030

The dynamic behavior of the DFIG and Direct drive wind turbines differ in terms of angular stability. More specifically, in the case of direct drive wind turbines, the turbine recovers quickly after the fault while it is introducing very small power oscillations. In the direct drive type with full converter grid interface the generator is fully decoupled from the network frequency. There is no angular stability problem and the power conversion is controlled by the wind turbine grid side converter.

On the other hand, in the case of the DFIG wind turbines the stator is directly connected to the network. Thus the generator is more vulnerable to network disturbances which in some cases can lead to rotor instability. For that reason it is expected that for the 2025-2030 network situation the percentage of direct drive wind turbines in operation will be higher than the DFIG turbines. This justifies the choice of using a higher capacity of direct drive wind turbines for the present stability study.

6.5 Offshore VSC-HVDC transmission system configurations

As it has already been mentioned, three types of VSC-HVDC transmission system configuration have been considered and will be described in this paragraph. The main assumption that has been taken is that an aggregate wind turbine dynamic model has been utilized to represent each offshore wind zone per country. The reason for this simplification is that the main focus will be the interaction among the ac and dc network. Furthermore there is no available information about the type of wind turbines and how wind farm modules will be connected per zone. A standard direct drive type dynamic model has been used for each area. In addition, every area is connected through a converter to the multi-terminal network.

6.5.1 Type 1: 2025-2030 model with Individual connection of offshore wind farms

In this configuration, every offshore wind location per country (Netherlands, Germany and Belgium) is connected via point-to-point VSC-HVDC link to the relevant feed-in onshore substation. Therefore, there are VSC-HVDC point-to-point links transporting offshore wind power from the offshore zones to the feed-in points.

6.5.1.1 Individual connection of the Dutch offshore wind zones

In Netherlands three large offshore zones have been considered for this project [**5**]. Figure 6.6 gives a graphical overview of these locations and the feed-in connection points at the Dutch transmission system. An amount of 1140MW is planned to be connected to Eemshaven (EEM) 380kV substation. For that reason the rated power of the EEM grid side converter (as well as the wind park converter) is chosen for this study to be 1200MW.

NAME	Eemshaven I	IJmuiden	Borssele II
Connection1 _WP	Eemshaven I	IjmuidenV	Borssele II
Connection2_AC Grid	EEM/380kV	BVW/380kV	BSL/380kV
Length (km)	90	120	50
VSC Rated Power (MW)	1200	3000	1200
DC Voltage (kV)	±450	±450	±450
DC Current (A)/Cable	1335	1656	1335
Number of parallel HVDC cables	1	2	1
Polarity	Bipolar	Bipolar	Bipolar
AC voltage (kV)	380	380	380
R_{dc} (Ohms/km)	0.03	0.03	0.03
L_{dc}(μH/km)	200	200	200
C_{dc}(nF/km)	220	220	220

Table 11: Point-to-Point VSC-HVDC connection of Dutch Offshore wind farms

For the case of Beverwijk 380kV substation a rated capacity of 3000MW offshore wind power is considered to be fed into the 380kV transmission system. More specifically due to the fact that at present there is no commercial converter station with 3000MW rated capacity, for offshore applications, in general three parallel converters can be facilitated. However for the present study an aggregate model with rated capacity 3000MW is considered. Finally, a 1200MW VSC-HVDC link is considered to connect the Borssele II offshore area to Borssele substation.

All the parameters and capacities of the three VSC-HVDC systems have been illustrated in Table 11. In addition, the same control gains have been facilitated for all VSC controllers. Of course the length of each HVDC line is different, reflecting the distance of each area to shore.

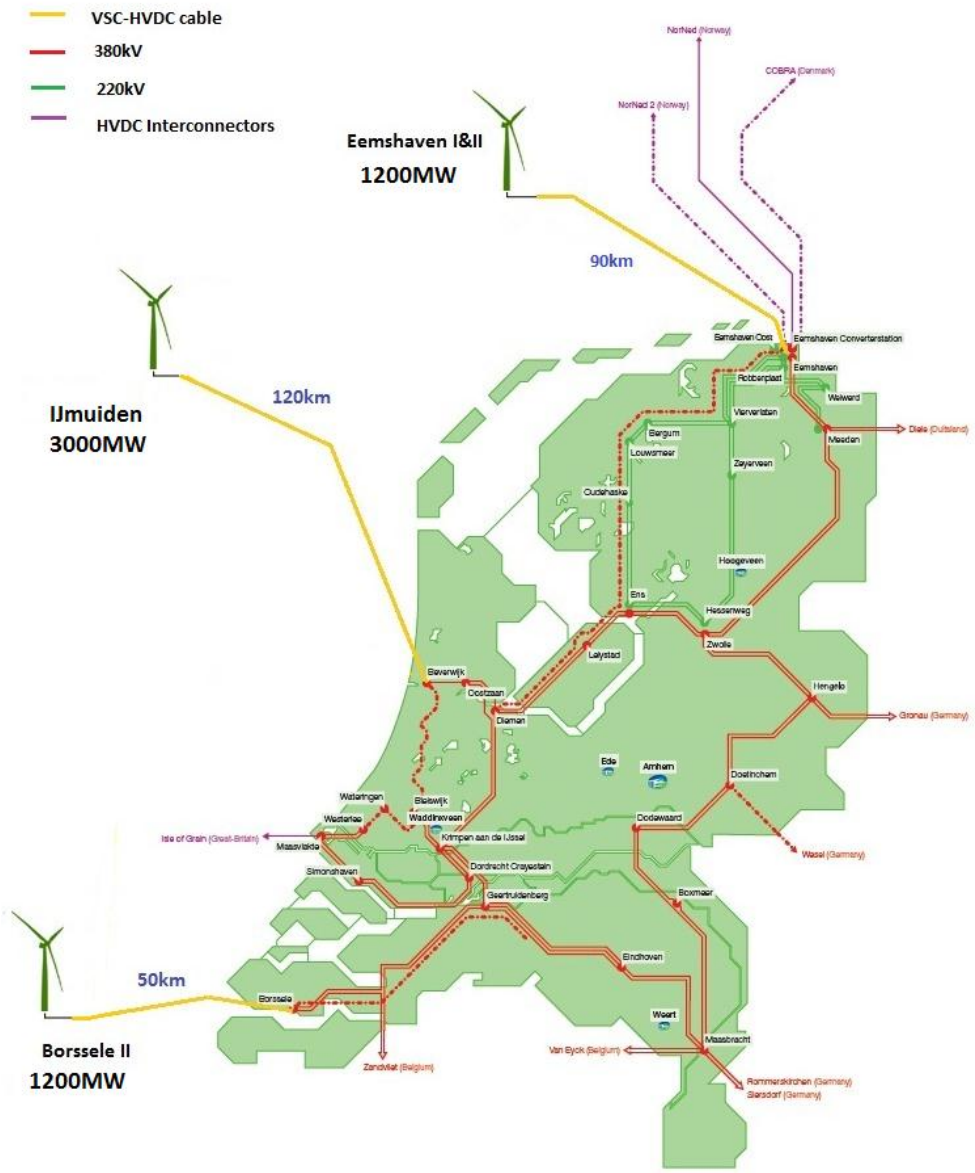

Figure 6.6: Point-to-point connection of the Dutch offshore wind zones (type 1)

It is important to mention that the selected dc voltage levels for the HVDC cables is ±450 kV. Currently the largest commercial application facilitating VSC-HVDC

technology for offshore applications is ABB HVDC light and Siemens Plus. This technology utilizes +/- 320kV direct voltage level at 1200MW and 1500MW. However due to the fact that high voltage technology is progressing, it is not unlikely that higher levels can be reached in the near future [**19**].

More specifically up to date there is a commercial application of VSC-HVDC at ±450kV for overhead lines. ENTSO-E predicts even higher dc voltage levels for VSC-HVDC cables [**3**]. More specifically Cigre [**19**] does not foresee technical obstacles in developing and construction of VSC-HVDC converters for every high voltage and power (i.e. 600kV and 3000MW) facilitated in offshore wind industry. In addition, according ENTSO-E [**3**] there is at least one manufacturer that is confident that can deliver an 1800A IGBT-based VSC-HVDC system for offshore application. Combining it with ±500 kV it allows 1800MW VSC-HVDC system to be ordered and commissioned by 2014-15.

6.5.1.2 Individual connection of the German offshore wind zones

In table 2 the national plans for offshore wind power development in Germany according to the NSTG project have been given for 2025-2030. However, for the German transmission system in order to be able to integrate the planned amount of offshore wind power for 2025-2030 there is a need to undergo a great amount of grid reinforcements especially near the feed-in locations. More specifically with the present situation of the German power system at the three connection points it is not possible to feed the discussed in Table 6 amount of power at the German feed-in points. The main reason for that is the limited capacity of the present high voltage transmission lines between the substations Diele-Conneforde-Unterweser.

In order to make a reasonable case study for 2025-2030 it is important to include the German grid reinforcements in order to consider the German offshore wind zones for the transnational offshore wind multi-terminal network. However, there is no available information about the German grid reinforcements. There is only limited amount of publications [**48**] introducing the plans for grid reinforcements without providing exact high voltage line parameters. More specifically, in this German system operators report, an overview of 2032 situation of the German network is given, with many South-North HVDC corridors with multiple GW of connection capacity.

Figure 6. 7: Point-to-Point connection of the German wind parks (type 1)

For the above reasons, in this project a total 7.5GW offshore wind power is considered for the German part of the NSTG project. This number is chosen because it is the estimated offshore wind capacity for 2020 in Germany. More specifically only three zones will be taken into account. The first includes Sudlich Amrumbank zone, with a total capacity of 1000MW, the second Hochsee Sud with capacity 5000MW, and last Nordlich Borkum with 1500MW.

Certain assumption has been made in order to include 7.5GW offshore wind power in the present calculations. It includes the reinforcement of 380kV and 220kV transmission lines between the substations Diele, Conneforde and Unterwesser that have been considered as the feed-in points for the German part. More specifically the transmission capacity of these high voltage lines has been doubled by considering extra circuits with the same electrical parameters.

Consequently, it becomes evident that all the conclusions will be based on this specific assumption. However, the main focus is not to study the German power system neither to introduce the grid reinforcements for the German part of the network but rather to include the effects that transnational multi-terminal offshore grids may have on the Dutch power system. The Dutch transmission system is the main item of interest, which level of detail is considered high enough. Finally Table 12 introduces the parameters for the VSC-HVDC connection of the German offshore wind zones. Again equivalent models are considered for every converter.

NAME	Nordlich Borkum	Hochsee Sud	Sudlich Amrumbank
Connection1 _WP	Nordlich Borkum	Hochsee Sud	Sudlich Amrumbank
Connection2_AC Grid	Diele/380kV	Conneforde/380kV	Unterweser/380kV
Length (km)	90	150	130
VSC Rated Power (MW)	1500	5000	1200
DC Voltage (kV)	±450	±450	±450
DC Current/Cable (A)	1670	2737	1335
Number of parallel VSC-HVDC lines	1	2	1
Polarity	Bipolar	Bipolar	Bipolar
AC voltage (kV)	380	380	380
R_{dc} (Ohms/km)	0.03	0.03	0.03
L_{dc}(μH/km)	200	200	200
C_{dc}(nF/km)	220	220	220

Table 12: Point-Point VSC-HVDC connection of German Offshore wind farms considered in the simulations

6.5.2 Type 2: 2025-2030 model with connection of wind farms per country into a dc network configuration

In this particular type of VSC-HVDC configuration, the offshore wind farms per country, as described in type 1, will be connected in a MTdc network for each country. The reason for considering such a case is that the development of a transnational offshore MTdc network will be realized in stages, first with MTdc networks for each country and then in a transnational connection [**5**]. In addition, a comparison will be made among the type 1 and type 2 configuration in order to draw conclusions about onshore power system rotor angle stability and the ac-dc network interaction for each transmission system configuration.

6.5.2.1 Connection of Dutch offshore wind farms in MTdc network

In type 2 HVDC transmission system configuration, the three areas assigned for development of offshore wind in Netherlands (Eemshaven, IJmuiden and Borssele) will be connected to a multi-terminal VSC-HVDC network as illustrated in Figure 6.8. The capacity of the HVDC cables is assumed equal to cable capacity of BVW cable in Table 11. The same onshore power system connection points have been considered as in the point-to-point connection. In addition, in order to compare type1 with type2 HVDC transmission configuration the active power set points of the grid side converters are the same with active power injection of the converters in the type 1 configuration.

The dc voltage in the MTdc network is controlled by the three grid side converters. Thus, all three grid side converters (EEM, BVW and BSL) are in dc voltage control mode. The droop method is considered as control strategy of dc voltage controllers as has been described in chapter 4. The market power dispatch scheme implemented is proportional power sharing. In addition, all grid side converters are equipped with ac

voltage controllers that regulate reactive power injection based on the ac voltage levels at their PCC.

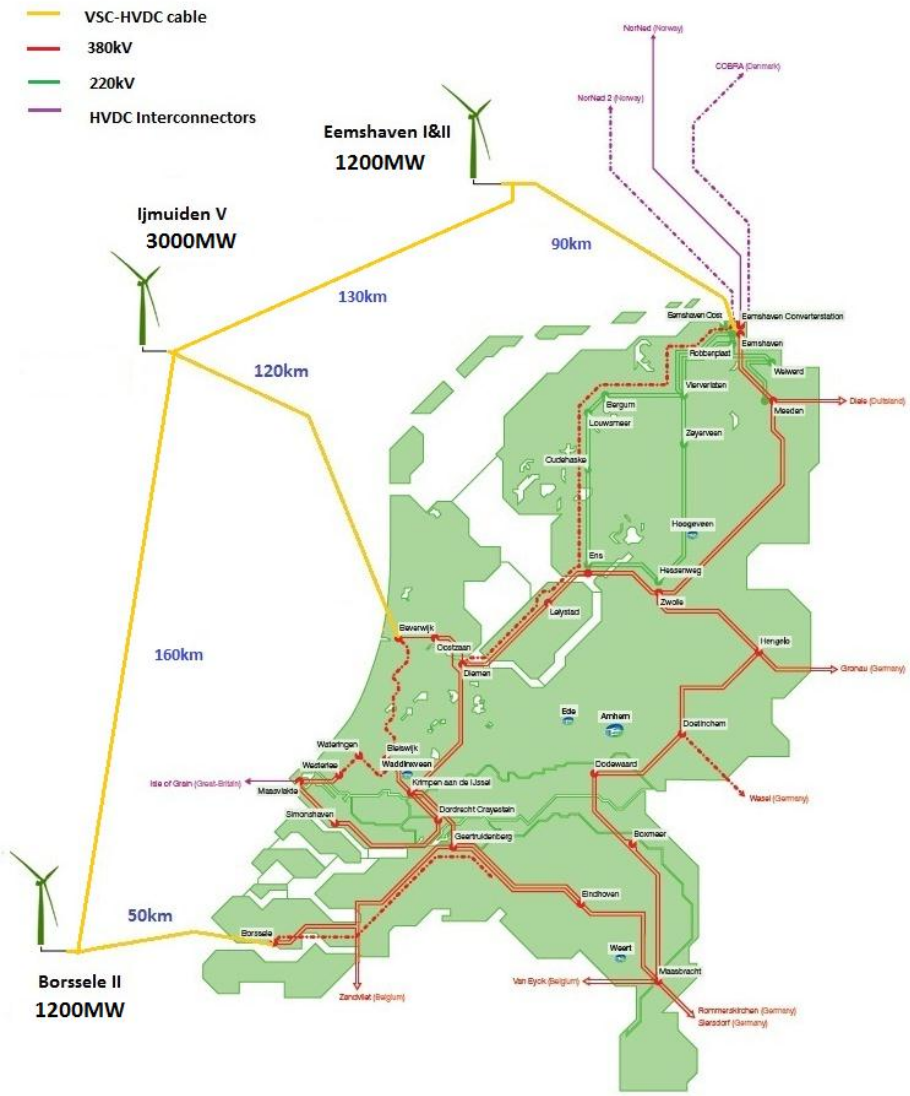

Figure 6.8: Multi-terminal VSC-HVDC network for interconnection of the Dutch Offshore wind farm zones (type 2)

6.5.2.1.1 Dutch MTdc network snapshot

The assumption that is made in the Dutch part of the MTdc network is that dc power flows in the dc network are in radial direction from the wind farm zones to the grid side converters. Thus at this snapshot there is almost zero dc power flow between the wind farm zones. With this assumption the steady state dc voltages and dc currents of the Dutch MTdc network has been calculated for the given snapshot from the dc power flow. More specifically, Table 13 and Table 14 introduce the converter stations dc voltages and currents as given from dc power flow for this particular snapshot.

No	Node	U_{dc} (kV)	P (MW)
1	WPVSC_EEM	900.962	1140
2	WPVSC_IJmuiden	900.960	3000
3	WPVSC_BSL	900.950	1140
4	GSVSC_EEM	899.255	1135
5	GSVSC_BVK	899.255	2980
6	GSVSV_BSL	900.000	1140,72

Table 13: Direct voltages at the Nodes of the Dutch MTDC network

From	To	I_{dc} cable (A)
1	2	2.38
2	3	2.135
1	4	1262.93
1	5	3330
1	6	1262.46

Table 14: Direct current in the cables of the Dutch MTDC network

6.5.2.2 Connection of German offshore wind farms in MTdc network

Similar to the case of the Dutch offshore wind zones, the three assigned German offshore wind zones are connected in a multi-terminal network as introduced in Figure 6. **9**. The capacity the HVDC cables are assumed equal the capacity of largest converter station which in this case is Hochsud-Conneforde.

Figure 6. 9: Multi-terminal VSC-HVDC network for interconnection of the German Offshore wind farm zones (type 2)

Similar to the Dutch MTdc network, all grid side converters are in dc voltage control mode. The droop method is applied in the German MTdc network. In addition ac voltage controllers are in operation for all grid side converter stations.

6.5.2.2.1 German MTdc network snapshot

The power flow results for the selected snapshot of the German MTdc network are introduced in Table 15 and Table 16. Similarly to the Dutch MTdc network, dc power is flowing in a radial way from the wind farms to the feed-in connection point.

No	Node	U_{dc} (kV)	P_{vsc} (MW)
1	WPVSC_SudAmr	902.259	1000
2	WPVSC_HochSud	902.255	5000
3	WPVSC_NorBorkum	902.252	1500
4	GSVSC_Unterweser	900.102	995
5	GSVSC_Conneforde	889.794	4928
6	GSVSV_Diele	900.000	1501.56

Table 15: Dc voltages at the Nodes of the German MTDC network

From	To	I_{dc} (A)
1	2	2.64
2	3	5.9
1	4	1105.686
1	5	5538.405
1	6	1668.409

Table 16: Dc current in the cables of the German MTDC network

6.5.3 Type 3: 2025-2030 model with transnational interconnection of the Dutch, German and Belgian wind farms into a MTdc network configuration

The last type of VSC-HVDC transmission system configuration that has been considered in this project consists of the transnational MTdc network. More specifically the German, Dutch and Belgian offshore zones considered in the type 1 and type 2 configuration are now connected to a transnational offshore MTdc network as introduced in Figure 6.10.

The ac power set points of the converter stations are considered to be the same as the type 2 and type 1 configuration. All grid side converter stations are selected to be in dc voltage control mode, applying droop control strategy.

Figure 6.10: Type3 configuration – Transnational MTDC network (type 3)

6.5.3.1 Transnational MTdc network snapshot

In this selected snapshot of the MTdc network all the wind farms are connected into the transnational network however there is no flow in the dc lines between countries. Furthermore Table 17 and Table 18 introduce the snapshot A of type3 network.

No	Node	U_{dc} (kV)	P (MW)
1	**WPVSC_SudAmr**	900.48	1000
2	**WPVSC_HochSud**	900.477	5000
3	**WPVSC_NorBorkum**	900.473	1500
4	**WPVSC_EEM**	900.46	1140
5	**WPVSC_Ijmuiden**	900.437	3000
6	**WPVSC_BSL**	900.407	1140
7	**WPVSC_Eekl-Noord**	900.4	390
8	**GSVSC_Unterweser**	898.319	995
9	**GSVSC_Conneforde**	887.99	4928
10	**GSVSV_Diele**	898.23	1492
11	**GSVSC_EEM**	898.754	1135
12	**GSVSC_BVK**	894.439	2980
13	**GSVSV_BSL**	899.458	1138
14	**GSVSV_Eekl Noord**	900.0	400

Table 17: Dc voltages at the Nodes of the Transnational MTdc network

From	To	I_{dc} cable (A)
1	2	2.63
2	3	5.59
3	4	9.69
4	5	12.08
5	6	12.1
6	7	12.1
1	8	1107.88
2	9	5549.66
3	10	1661.68
4	11	1263.63
5	12	3331.69
6	13	1266.09
7	14	445.24

Table 18: Dc current in the cables of the Transnational MTdc network

6.6 Simulation Results and Analysis

In this paragraph the three types of VSC-HVDC transmission system configurations that has been introduced in paragraph 6.5 will be analysed for a 150ms three phase bolted short circuit at the Eemshaven converter station. The duration of the fault is selected because it is the typical protection rating for a normal fault clearing. EEM substation is selected because there is a large amount of conventional generation connected at the specific substation. In addition, asynchronous interconnectors such as NorNed II and Cobra will be in operation for the 2025-2030 grid situation. EEM is electrically close to the Diele and Unterweser converters in the German part of the ENTSO-E grid. Thus a disturbance in EEM will create a voltage drop in the Diele and Unterweser converter stations with effects on the MTdc network operation.

	Snapshot 1	**Snapshot 2**	**Snapshot 3**
Type 1	x		
Type 2	x		
Type 3	x	x	x

Table 19: Performed simulations for different types of VSC-HVDC and snapshot

The three types of the VSC-based HVDC configurations will be evaluated with the three selected snapshots of the Dutch Power system. Only selected simulations will be illustrated and additional results can be found in the appendix. Table 19 introduces the case studies which will be investigated with time domain simulations for 150ms three phase fault in Eemshaven. Based on these case studies and the predefined assumptions conclusions will be drawn about the interaction and the transient stability of the Dutch power system meshed with VSC-based HVDC transmission systems. All the assumptions made in this chapter are grouped and presented in Appendix D.

6.6.1 Type 1: Simulation Results for Dutch Power system Snapshot 1

For the type 1 VSC-HVDC transmission system figure 6.11 illustrates the AC terminal voltage profiles of the GSVSCs at the relevant connection points. Concerning the Dutch power system, the fault in EEM converter creates voltage drop at the other two converter stations as depicted. As soon as the fault is cleared, the voltage recovers very quickly at BVW and BSL.

In addition, all the grid side converters react to the voltage drop by injecting reactive power to the relevant ac bus they are connected to. More specifically, the ac voltage controllers will detect the voltage drop and increase automatically the amount of reactive power the converter injects to the onshore network as shown in Figure 6.12. The higher the reactive power, the higher the voltage support and thus the more positive the impact from voltage stability point of view.

However, one very important constraint for the short circuit power contribution of the grid side converters is the protection scheme and circuit breaker requirements. The protection scheme is related to the maximum operating current that the IGBTs are designed to withstand. This has in principle to do with thermal limits of the

semiconductors. More specifically, GSVSCs can provide fault current as long as the short circuit ac current does not damage the IGBTs (or GTOs). For that reason in the present study all the GSVSCs are modeled along with current limiters [**8**] [**7**]. The purpose of current limiters is to protect the switching devices of the converter by limiting the current at the maximum acceptable value.

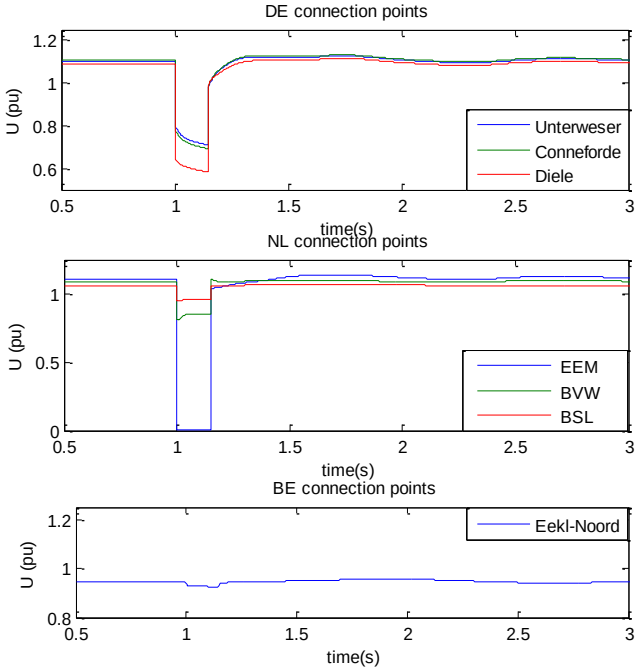

Figure 6.11: AC Voltage levels of the grid side converter stations

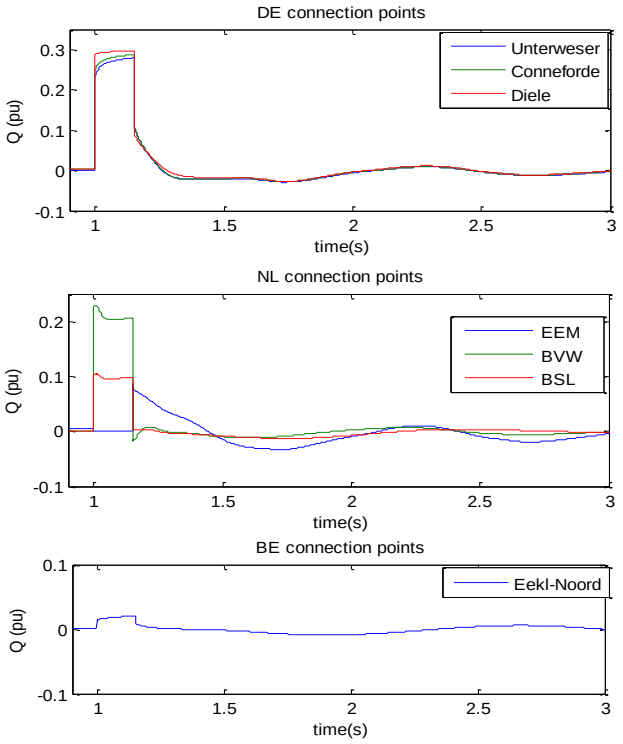

Figure 6.12: Reactive power of Grid Side voltage source converters (S_b=100MVA)

Normally the IGBTs cannot withstand more than 115% of the rated ac current at rated output voltage. For that reason in this project a 15% over-current is considered acceptable and has been introduced to the model. In addition, there are three options that can be used as a limiting strategy. The first gives priority to active power (or i_d current component), the second to reactive power (or i_q current component) and the last equal priority. In this project equal priority is considered as the limiting current strategy. The value of the current limiter is important because it defines the participation of the GSVSC and more specifically the contribution it has to the short circuit current.

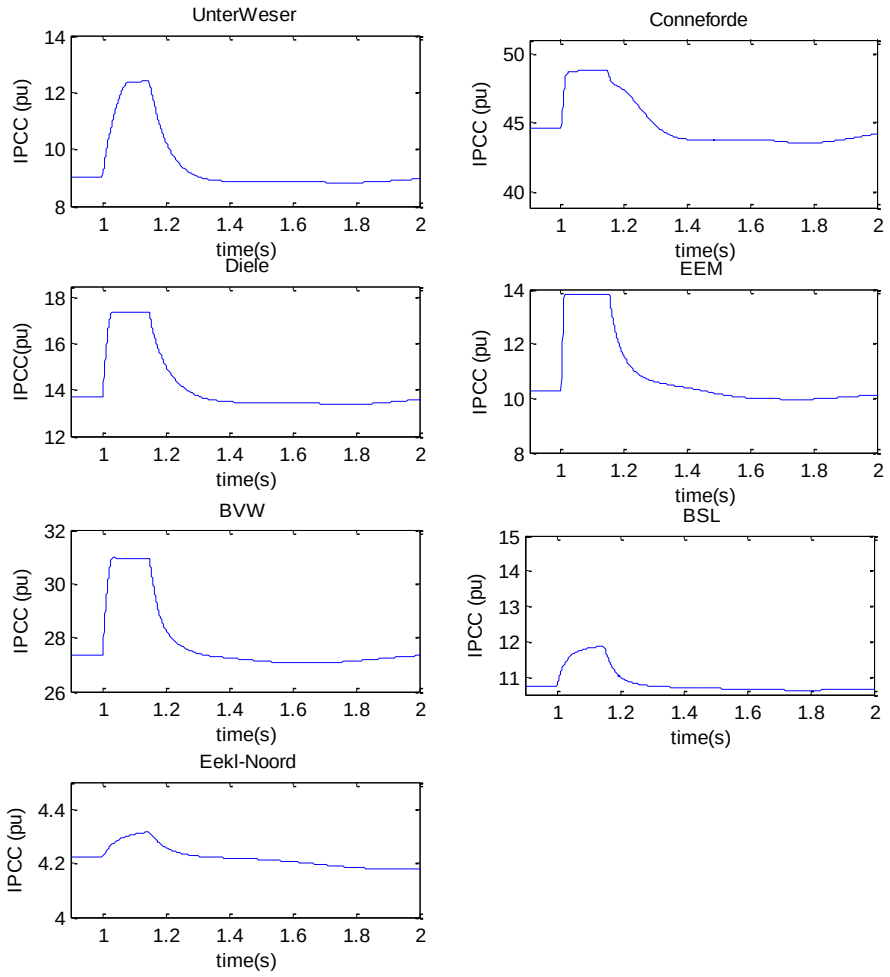

Figure 6.13: AC current injection of GSVSCs (S_b=100MVA)

As illustrated in Figure 6.13 ac currents increase instantaneously following the fault in EEM. In substation EEM and Diele the current reach its maximum value and it has been limited by the operation of the limiter.

Another important aspect is the active power of the VSCs and how it recovers after the fault is cleared. More specifically Figure 6.14 illustrates the active power as given from the computer model calculated at the PCC. From the simulation results it can be concluded that, as soon as the fault is cleared, the converter active power injection returns to pre-fault condition in very short time for all converter stations.

Thus, based on computer simulations it has been shown that it is possible for the VSCs to stay connected during the fault providing the system with fault current. Low-Voltage-Ride-Through (LVRT) capability is very important especially in the case that large amount of wind power is going to be transported onshore via VSC-HVDC transmission systems (either point-to-point or MTdc networks). TSOs will require not only LVRT capability but also contribution to short circuit current for all HVDC based transmission systems combined with a fast recovery after the fault.

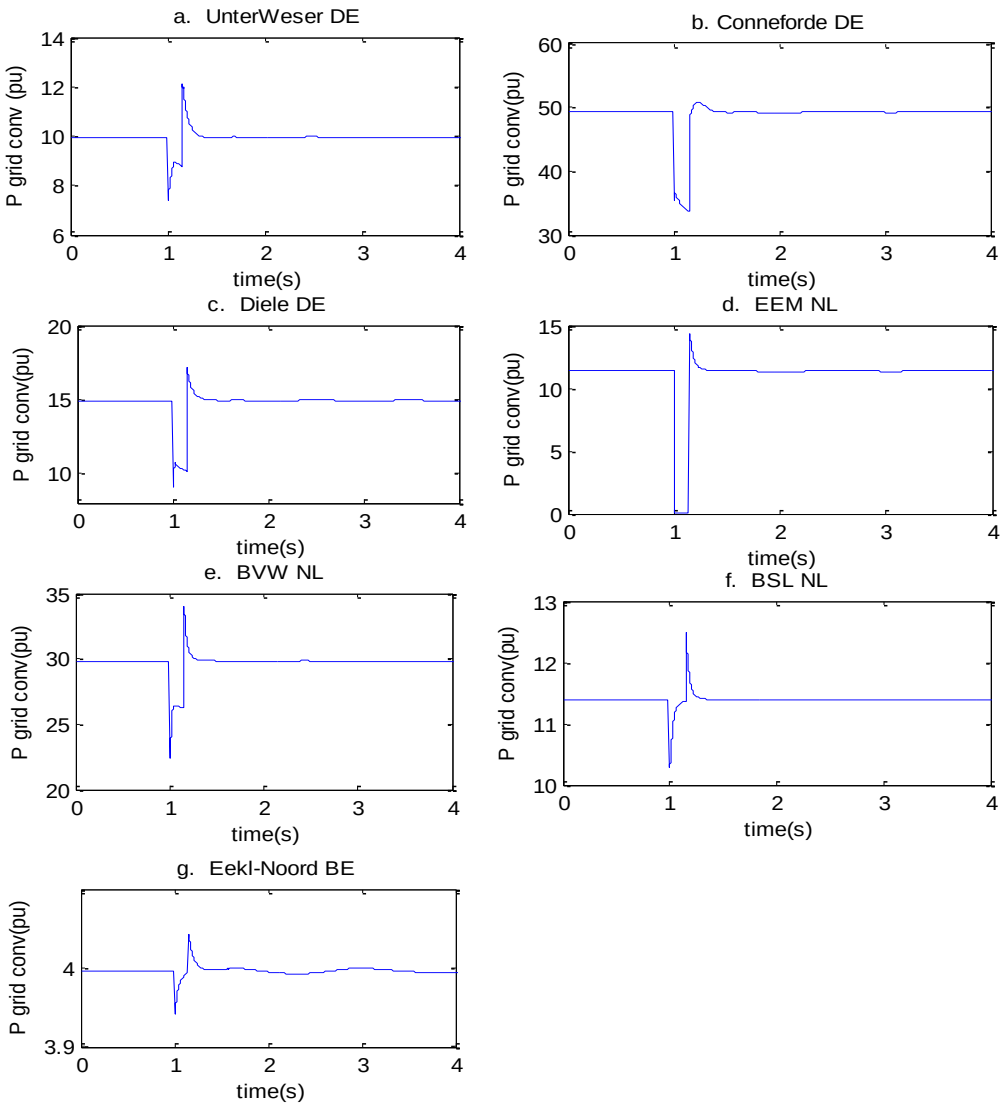

Figure 6.14: Active power injection grid side converters at connection points (S_b=100MVA)

In order to secure FRT capability for VSC-HVDC transmission systems it has to be ensured that the dc voltage of the HVDC cable is kept within operational limits [**23**]. More specifically, during the fault, the power balance at the dc side capacitor is lost as a result of reduced (or even zero) active power flow to the ac network. This loss of power balance leads to over-voltage in the dc side of the VSC stations. The dc overvoltage challenge can be tackled by using dc choppers (or else known as breaking resistors) rated for the full wind farm power [**22**]. The latter approach has been adapted in the present project and will be further discussed.

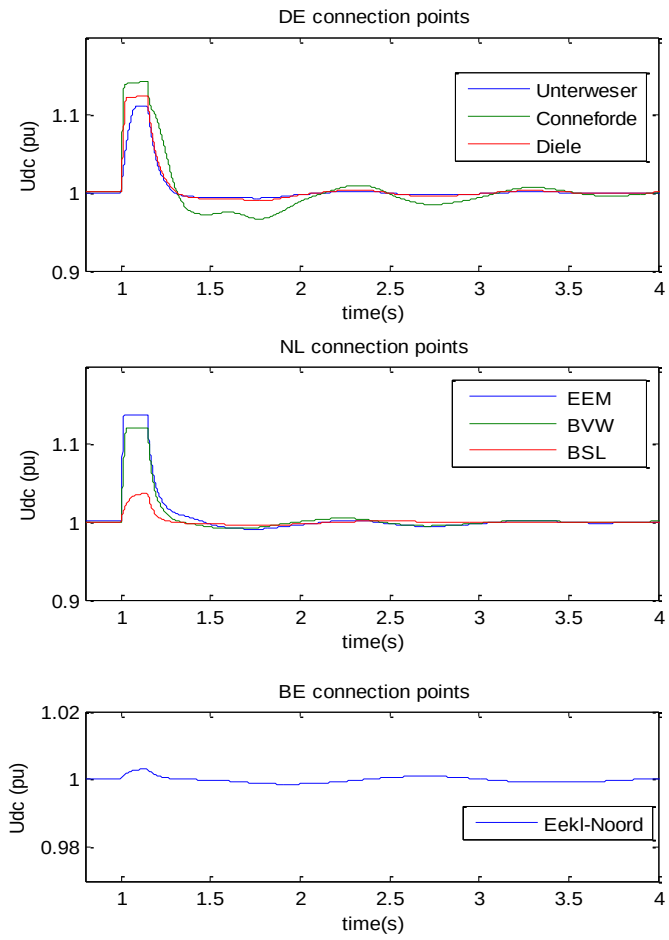

Figure 6.15: Dc voltages at Grid side VSCs

In figure 6.15 it is introduced the increase in the dc voltage at the dc side of the EEM GSVSCS during the fault. Additionally, the activation of the breaking resistors can also be observed in the particular situation as illustrated in figure 6.16. As long as the dc voltage reaches the threshold value (1.1p.u in this case study) the switching resistors are activated and active power that cannot flow to the ac network is dissipated.

As soon as the fault is cleared, ac voltage recovers and the converter station starts again injecting active power to the ac network. This recovery is followed by fast discharge of the dc capacitors. The discharge of the dc capacitors is responsible for the overshoot in the output power of the converter station that has been mentioned above. It would be possible to minimize the overshoots by lowering the threshold value which the dc chopper is activated. However this is not reasonable due to the fact that dc chopper can be activated at fast variations in wind power followed by dc voltage variations. As it has been discussed in chapter 4, the step-up of generated wind power will shift the dc voltage to a higher level when droop control is facilitated (it is advisable for the reader to recall Figure 4. 8 and Figure 4. 9) or create a dc overvoltage when VMM is used before the voltage recovers to the reference value (Figure 4.11).

The dc chopper method for achieving FRT is relatively simple in design and illustrates good performance in terms of active power recovery. However the bulk amount of power transported via VSC-HVDC transmission system requires for large capacity of dc

choppers, something that increases the cost of investments. For that reason there are also other ways to achieve FRT, such as coordinated control of the GSVSC and WPVSC in coordination with the wind turbines controls, facilitating fast communication [**49**].

One relevant example is given in [**50**] where fast communication can be used in order to lower the wind farms ac voltage set-point during the fault reducing in such a way active power injection from the wind farms to the VSC-HVDC transmission line. However even if this seems promising for point-to-point VSC-HVDC connection, in the case of MTdc network the fast communication which is required among offshore wind farms complicates the method and reduces reliability especially when there is large distance among the converters. On the other hand, the FRT method using dc breaking resistors do not need any communication link as all the information is present in the dc overvoltage [**22**] [**23**].

In general it can be concluded that the FRT method facilitating dc choppers has only theoretical interest. The large amount of energy to be dissipated makes it impractical. However for the purpose of at hand study, where the focus is more on the performance and interaction of the Dutch power system meshed with VSC-HVDC networks, the dc chopper method can be facilitated.

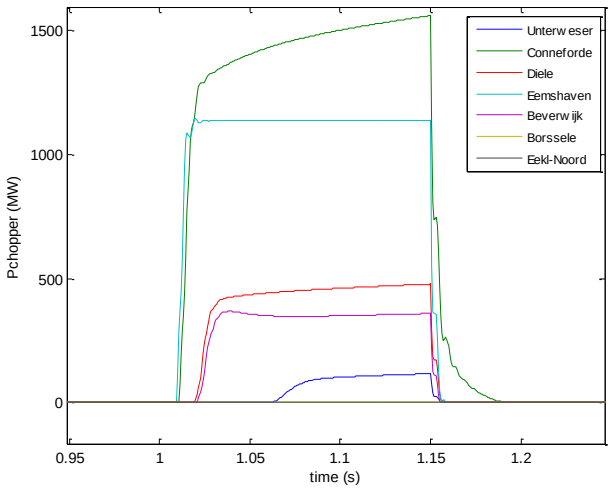

Figure6. 16: Power dissipated at breaking resistors for 150ms in EEM converter station

Following the description of the converters behavior, we are going to discuss how the ac network behaves at the specific fault. Therefore six large generators are selected for rotor angle stability analysis. In appendix B it can be found the location of the particular generators in the Dutch power system. Each one is located at a different zone of the transmission system (as given in Table 8). EC6 is the generator which is electrically closer to the fault connected at the EEM 380kV substation. It is shown in Figure 6.17 that the rotor angle of EC6 generator is increased as a result of the fault. As soon as the fault is cleared it recovers to pre-fault value. In addition, rotor angle oscillations that appear as a result of the disturbance are quickly damped out in all generators.

More specifically based on the simulation results the presence of the converter station in EEM substation does not negatively influence EC-6 generator. From the active power

response it can be concluded that there is enough damping torque available to damp out power oscillations quickly. In addition, the rotor angle response shows that the synchronizing torque component is satisfactory and rotor angle manages to recover in almost 10s at the pre-fault operating point.

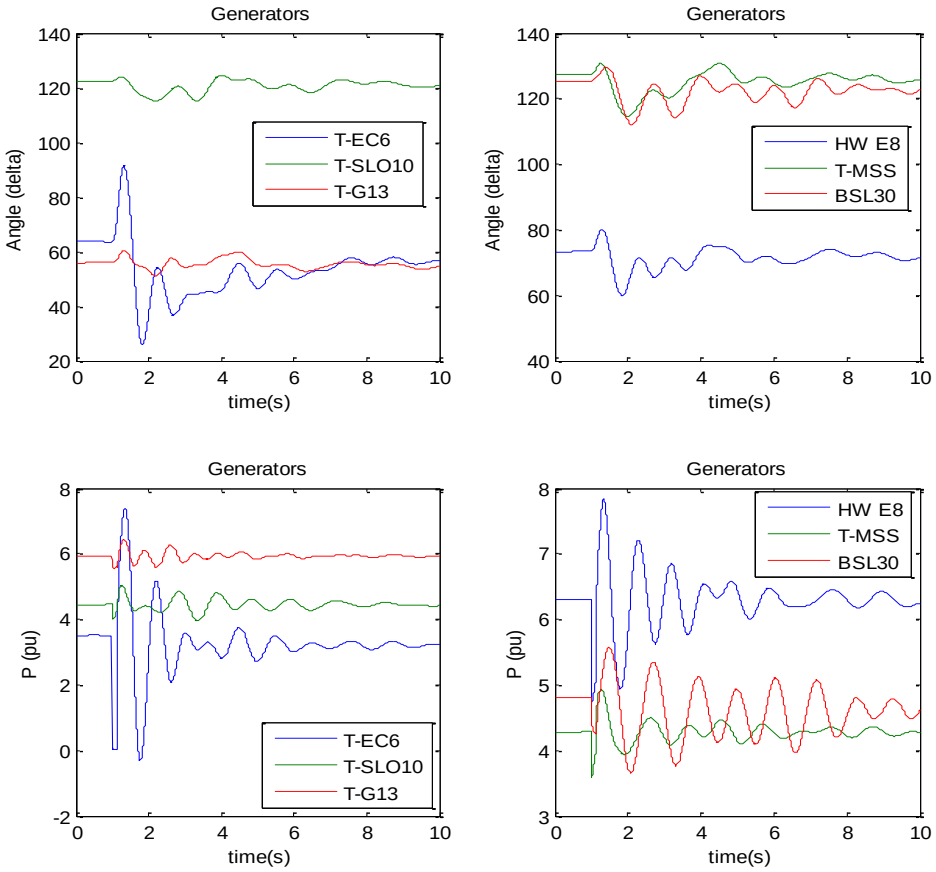

Figure 6.17: Angles and Active power of selected generators (S_b=100MVA)

It is important for the reader to note that all the rotor angle variables in the PSSE model are angle shifts from the slack bus (which is defined with angle zero) to the node or rotor shaft that is studied [**6**]. The angle shift of each generator includes also the phase angle shift of the step up voltage transformers. All the Dutch generators are modeled along with step up voltage transformers. This is the main reason of large values of rotor angles that appear in the SLO10, WH-E8 and MSS generators. Thus the inclusion of the phase shift that the voltage transformers add is irrelevant for stability assessment.

Finally, in figure 6.18 it is illustrated the reactive power profiles of the selected generators. It can be concluded from those responses that voltage recovers very quickly for all generators. In addition, all generators are contributing short circuit current and especially EC6 which is closer to the fault. Furthermore, EC6 voltage recovery is slower than the other generators. This has mainly to do with large contribution to short circuit current which leads to armature reaction that weakens the magnetic field in the generators gap.

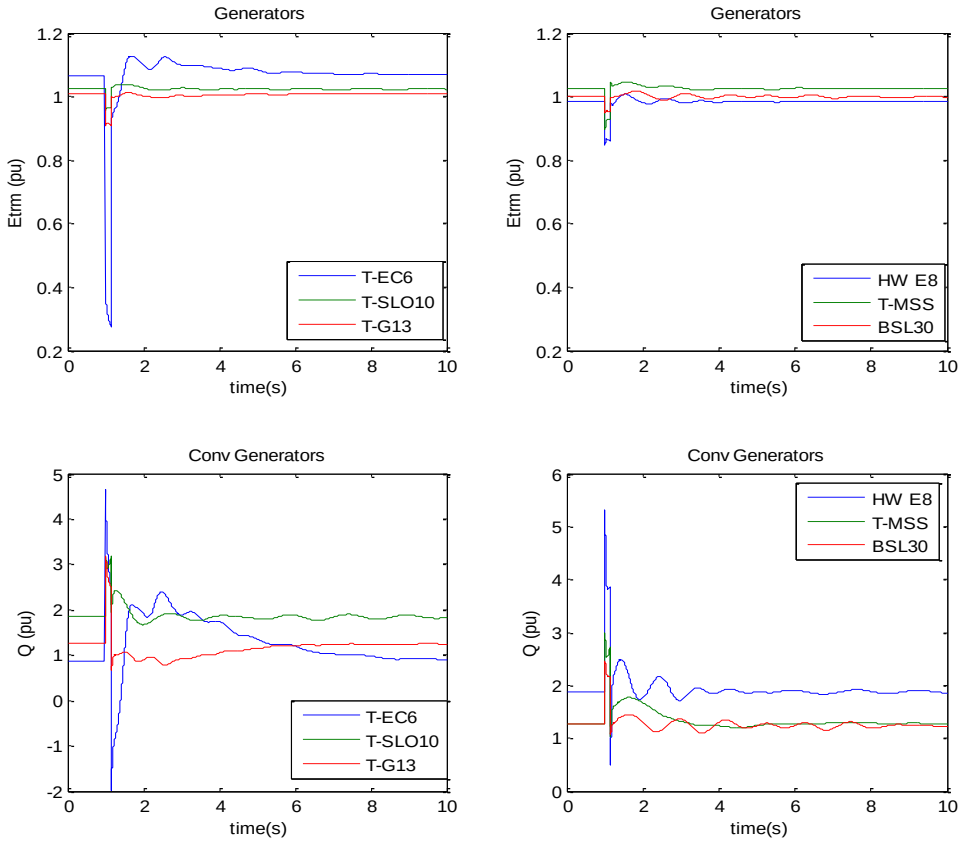

Figure 6. 18: Terminal voltage of selected generators and reactive power

6.6.2 Type 2: Simulation results with Power system Snapshot 1

In this paragraph the simulation results for the type 2 VSC-HVDC network will be discussed. The ac network snapshot is the same and also the amount of power injected onshore by GSVSC stations. The scope of this paragraph is to illustrate the main differences that appear between the individual connection of wind farms via point-to-point VSC-HVDC and multi-terminal configuration from the ac network stability point of view.

Figure 6.19 illustrates the response of active power at the three GSVSCs (EEM, BVW and BSL). From the plots, it is shown that both in the case of MTdc network and point-to-point connection, active power recovery is fast achieved within approximately 50-70ms. This indicates the FRT capability of the VSC without loss of control as explained in the previous paragraph. In addition, active power recovery is followed by a small overshoot, similar to the case study with the point-to-point connection. The cause of the overshoot is the over-voltage that appears in the dc side of the converter station followed by fast discharge of dc capacitors.

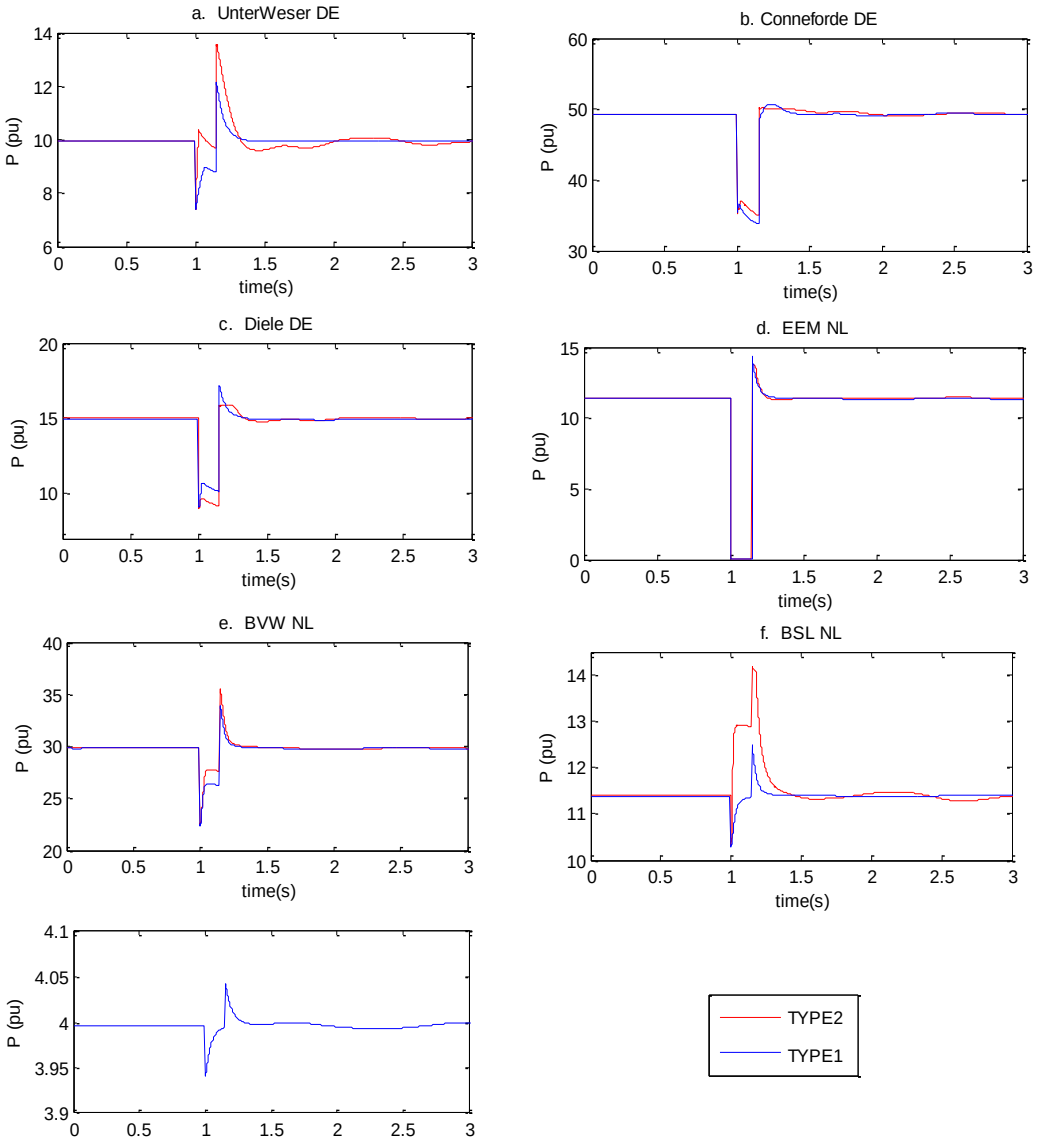

Figure 6.19: Active power at the grid side converter stations during a 150ms fault in EEM for the type2 VSC-HVDC network (S_b=100MVA)

In the case of multi-terminal network, there is an active power overshoot at BSL substation during the fault. In order to explain the reason for this overshoot we need to consider the over-voltage in the dc side of the converters in combination with the operation of the droop controller. The droop controller will respond to the dc overvoltage by increasing active power injection of the relevant converter station. In addition, figure 6.21 introduces the ac terminal voltage profiles of the GSVSC stations. As it can be seen in the case of the BSL converter the ac voltage drop is small in comparison to other converters. This small voltage drop in combination with the dc overvoltage is the main reason of active power overshoot at the BSL GSVSC station.

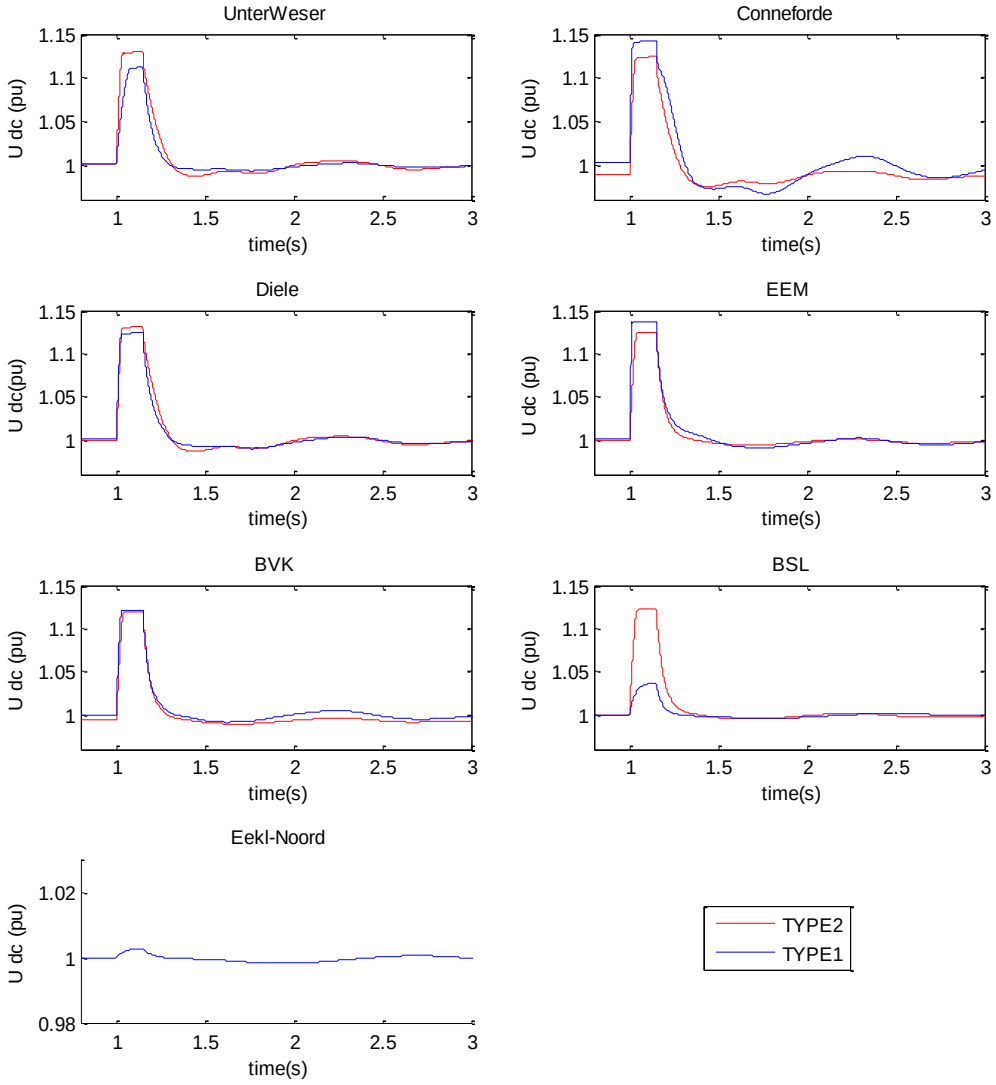

Figure 6.20: DC voltages at the grid side converters during 150ms fault in EEM

Furthermore, when the dc voltage reaches the threshold value the dc chopper will start dissipating power. Figure 6.20 illustrates the dc voltage profiles at the converter stations. The difference in the initial steady state values with type 2 network are due to the dc power flow result whereas in type 1 the dc voltage at GSVSCs is always 1pu. Additionally from the dc voltage response it can be concluded that the dc voltages of the converters in the MTdc network are increased by the same margin during the fault. Of course this varies with the size of the relevant converter and the dc capacitance. Last Figure 6. 21 introduces the voltage profiles at the ac terminals of the grid side voltage source converters.

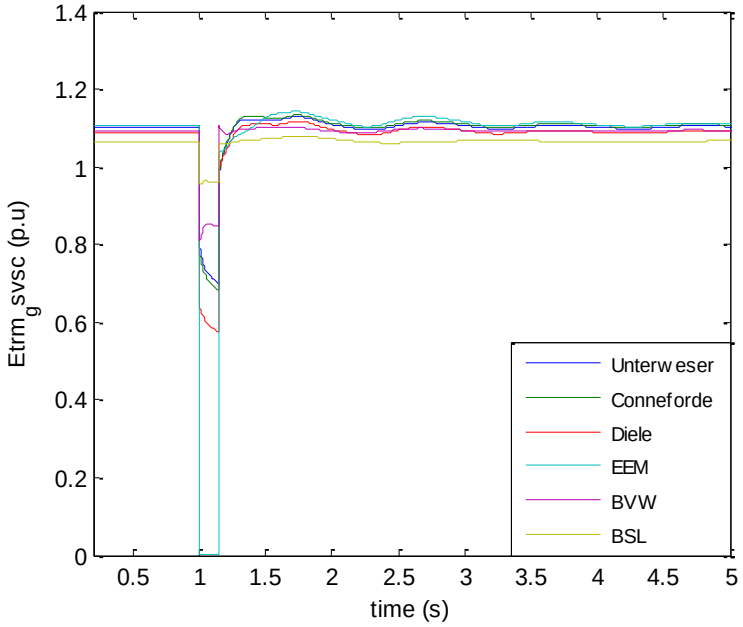

Figure 6. 21: AC voltage at the terminal of the grid side converter stations

Thus one major conclusion that it could be drawn is that in a multi-terminal VSC-Based HVDC configuration the dc side voltages of the converters are coupled together and vary in the same direction. So it becomes clear that the dynamic behavior of the multi-terminal network for the connection of the offshore wind farms depends strongly on the control strategy implemented on the converter stations. More specifically the dc voltage controller (droop controller in this case) plays a significant role and determines the active power response of the converter station. During the fault in EEM part of power that cannot flow to the AC network will be dissipated from the breaking resistors while part will flow as overshoot at the other converter stations.

With regard to the reactive power response of the converter station there is no difference between the two types of transmission system configurations. There is no sensitivity of the ac voltage controllers to the dc voltage and thus no difference in reactive power response. The responses of the GSVSCs are nearly the same for the two types of HVDC transmission as it can be seen in appendix A.

However the contribution of the converter stations to the short circuit current can be affected by the current limiters. More specifically due to the overshoot that appears in active power, as a result of the dc voltage controller operation, the dc voltage and the ac voltage controller “compete” each other in terms of available current increase. Thus the strategy followed by the current limiters (priority to active or reactive power) needs special consideration in the case of MTdc networks. In this study equal priority to active and reactive power is chosen. Figure 6.22 introduces the AC current measured at the PCC point of the converters.

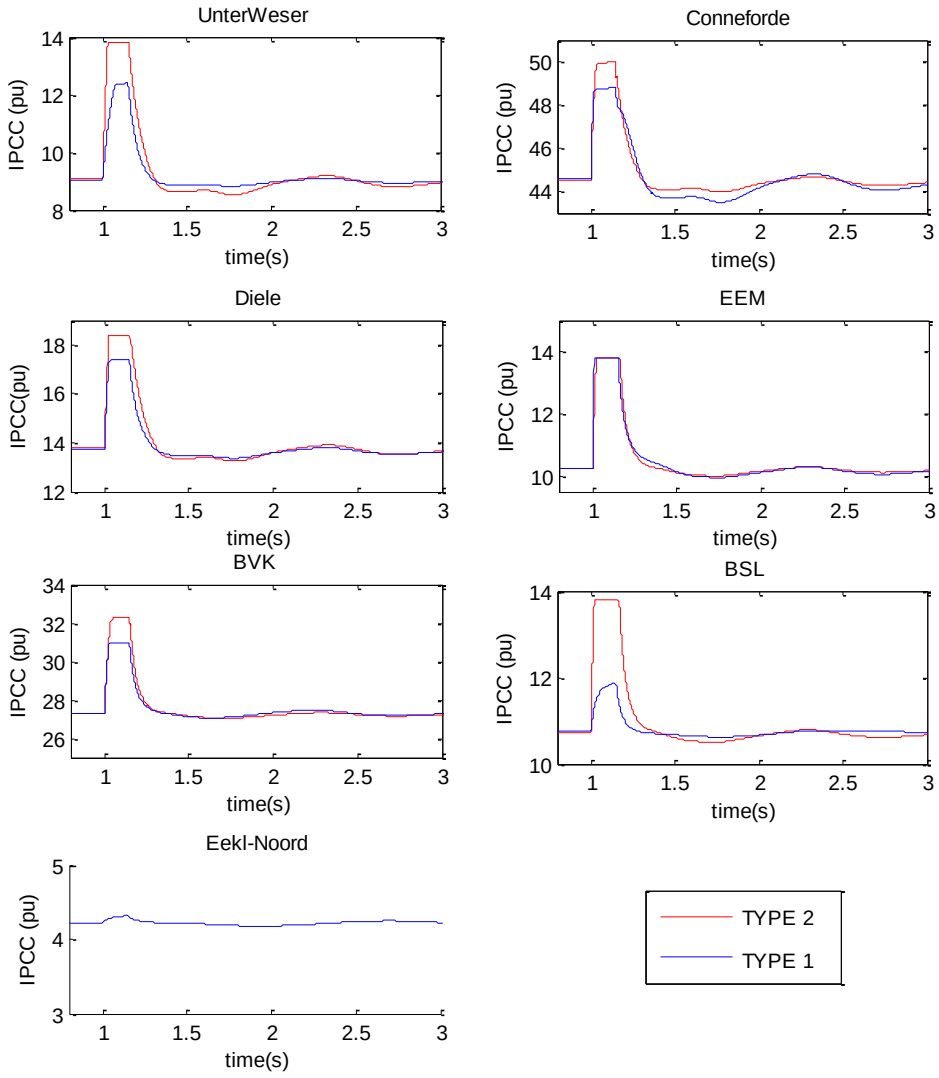

Figure 6.22: Ac current at the PCC of the grid side converters

From the previous discussion it becomes evident that the most important factors that determine the dynamic behavior of the VSC-HVDC multi-terminal system under AC side disturbances and the interaction with the AC network is the controllers implemented at the grid side converter stations.

Let us now discuss the dynamic performance of the selected generators with type 2 and type 1 transmission system. Figure 6.23 illustrates the active power of the selected generators for the two types of VSC-HVDC transmission system. From those it can be concluded that EC6 generator located at EEM shows similar response in both configurations. However in the case of BSL30 and TSLO10 generator (located in BSL) in type 2 configuration, it can be observed a different dynamic response. The main reason for that has to do with the converter station in BSL and the overshoot in active power that it introduces.

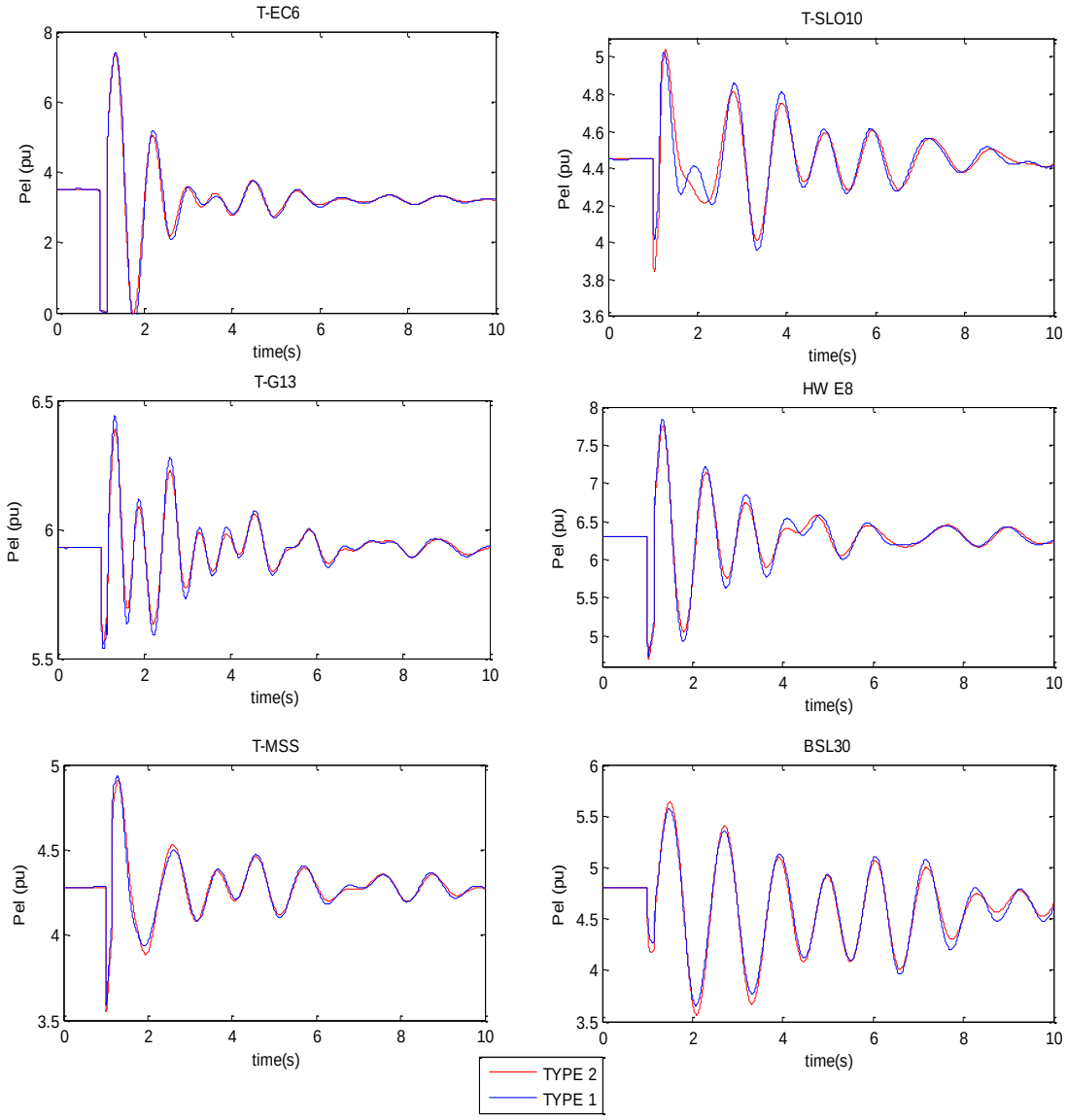

Figure 6.23: Active Power response of selected generators

6.6.3 Type 3: Simulation Results with Power system Snapshot1

Finally the simulation results with the transnational connection of the wind farms (type 3 transnational MTdc network) will be discussed. More specifically the results of the type 3 network will be compared with type1 (individual connection) and type 2 (MTdc network per country) in order to illustrate the differences in the dynamic behavior and interaction between ac-dc networks.

As it can be seen in Figure 6.24, comparing the dynamic response of the grid side converters with the same disturbance as in type 2 and type 3 it can be concluded that adding extra interconnection between the German and Dutch wind farms does not significantly change the dynamic response of the GSVSC stations in the Netherlands and Germany.

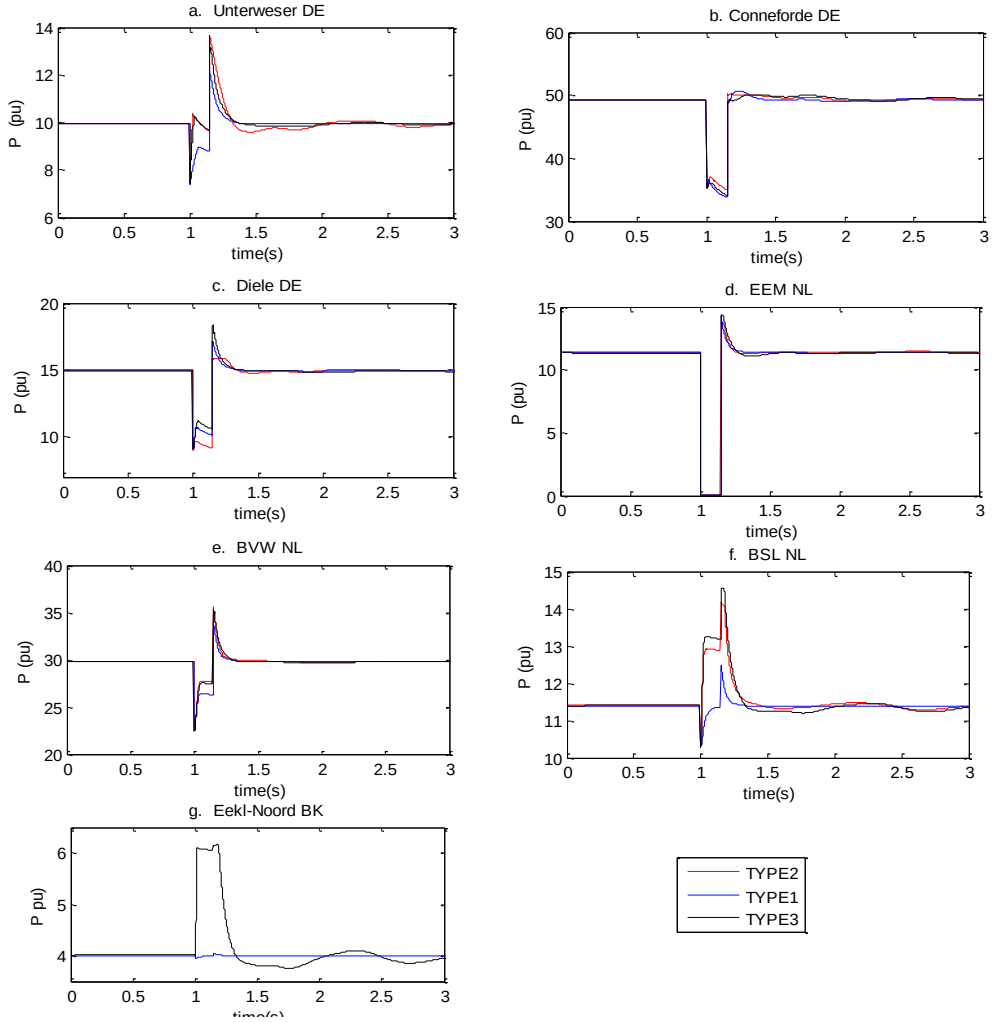

Figure 6.24: Active power of the grid side converters in Transnational MTDC network configuration (S_b=100MVA)

However, things are different in the case of the Eekl-Noord (Belgium) GSVSC station. More specifically as explained above, the AC voltage drop that the converter station in Eekl-Noord faces as a result of disturbance in EEM is very small, as it can be seen in Figure 6. 25 . Thus, the active power of the Eekl-Noord converter station would not drop significantly as a result of ac voltage drop. On the other hand the dc overvoltage is large as it can be seen in Figure 6.26. As a result of this overvoltage that appears in the dc capacitor of the Eekl-Noord

converter station the dc voltage controller would increase its active power injection during the fault. Normally what the dc voltage controller of the Eekl-Noord converter station will do is inject active power following the droop line characteristic. This is the main reason for the large overshoot of active power that appears at Eekl-Noord converter station.

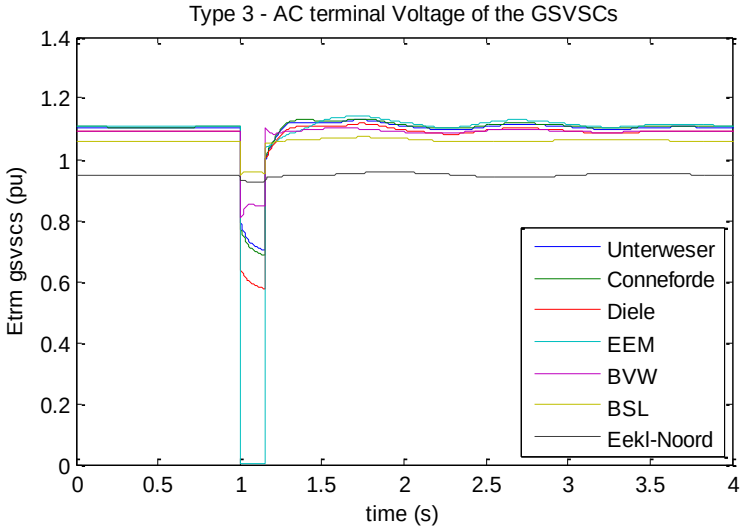

Figure 6. 25: Ac voltages at the grid side converters stations as a result of 150ms fault in EEM

This overshoot will be restricted by the current limiters of the Eekl-Noord converter station. More specifically as it can be seen in Figure 6.27, as soon as the ac current at Eekl-Noord converter station reaches the maximum acceptable limit it will be limited by the current limiter. In addition, dc breaking resistors will be activated and active power that cannot flow to the network will be dissipated in the resistors keeping the dc voltage at acceptable levels.

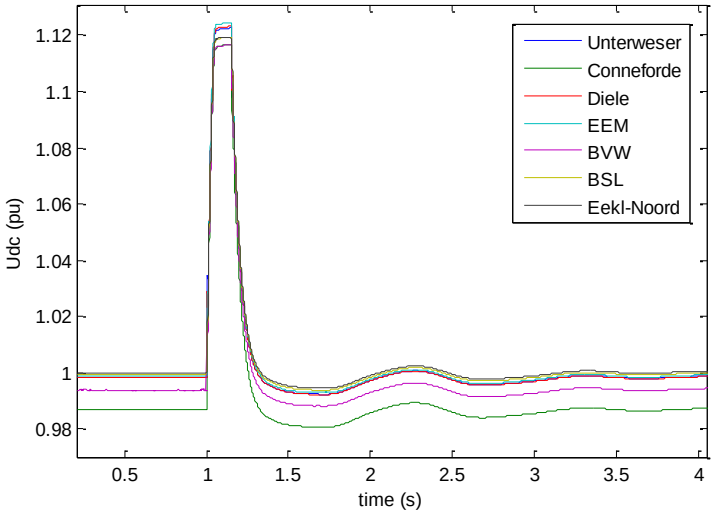

Figure 6.26: Dc voltages at the grid side converters stations as a result of 150ms fault in EEM

With regard to reactive power response of the converter stations, figure 6.28 introduces reactive power injection at the grid side converter stations. From the response it can be

concluded that all converter stations contribute reactive power to the AC network during the fault.

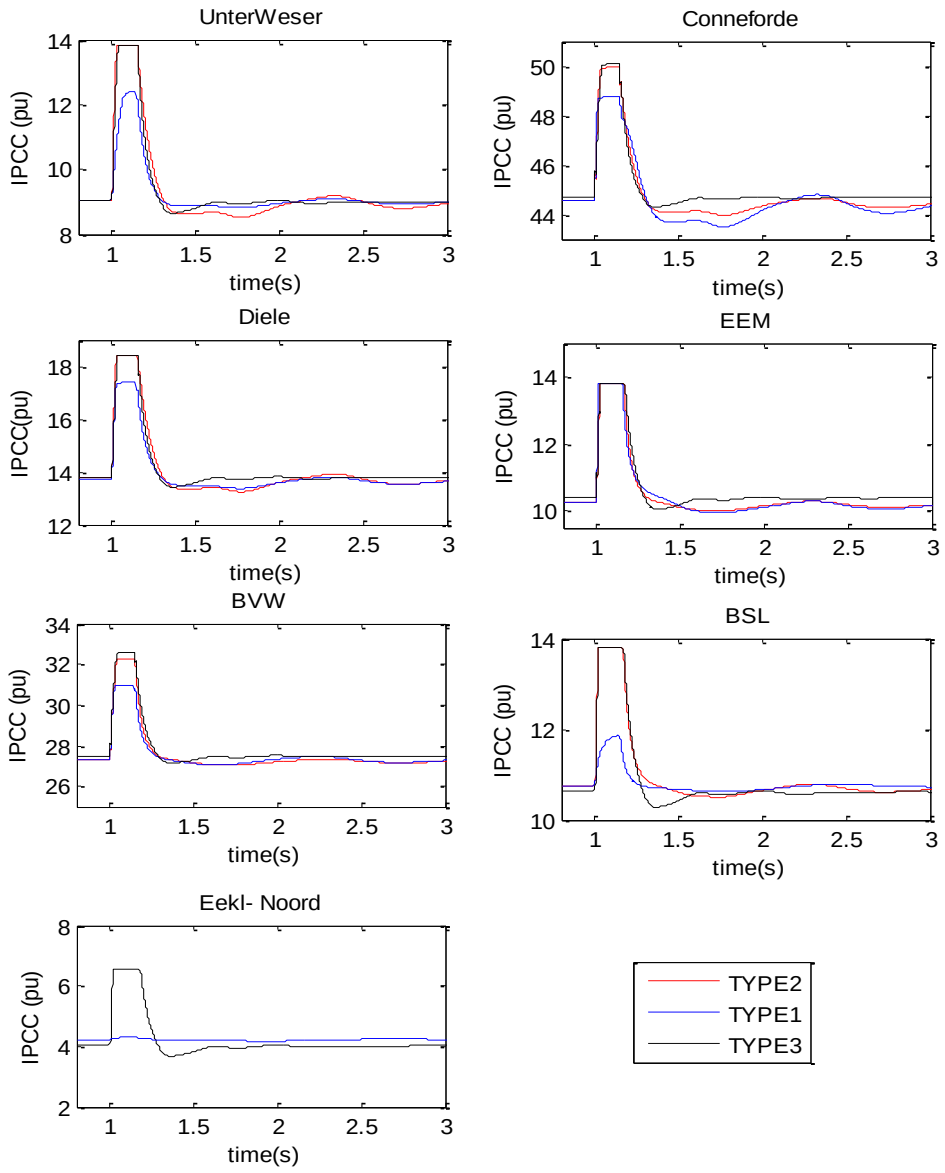

Figure 6.27: Ac current at PCC point of the VSCs (S_b=100MVA)

The conclusion is that the main difference that appears in the case of the transnational connection of wind farms is the overshoot in active power during the fault as a result of dc overvoltage. In addition, this overshoot is mainly closely related to ac voltage drop. The larger the electrical distance of the grid side converter from the fault, the bigger the overshoot (i.e. in the case of Eekl-Noord).

In terms of FRT capability, the grid side converters are capable to stay connected to the ac power system providing fault current. In addition, active power recovers in short time without loss of synchronization or control. Similar to the case of point-to-point converters dc breaking resistors are used as FRT method.

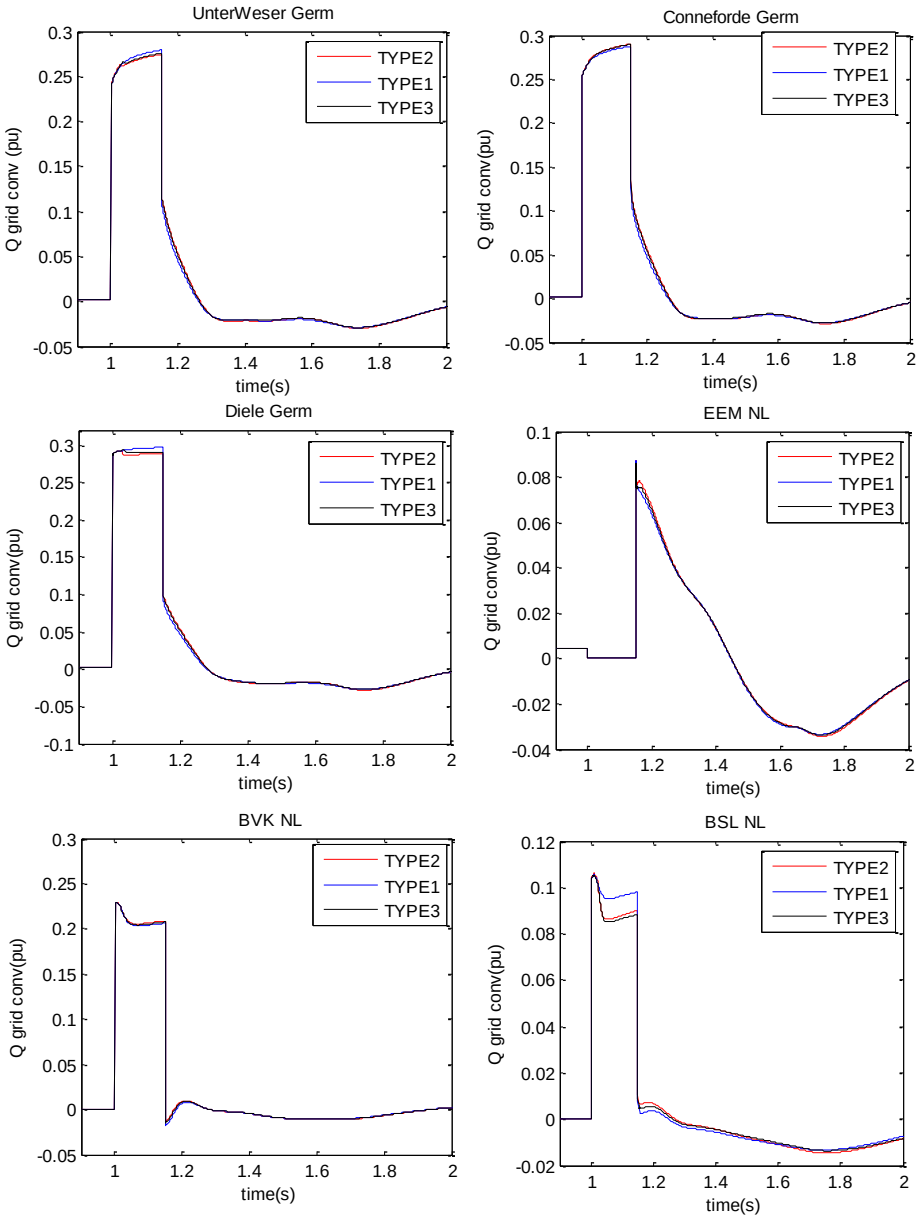

Figure 6.28: Reactive power of the grid side converters in the Transnational MTDC network configuration (S_b=100MVA)

With regard to the sensitivity of the selected generators on the three types of VSC-HVDC configurations, based on the initial assumptions it can be concluded that transient stability of generators in the Dutch power system is not affected from the VSC-HVDC configuration. More specifically as is shown in figure 6.29, the dynamic response of EC6, G13, MSS and HW E8 generators are same for all type of configurations. Whereas in the case of SLO10 and BS30 there is a slightly different response as a result of the overshoot that appears in the grid side converter station of BSL.

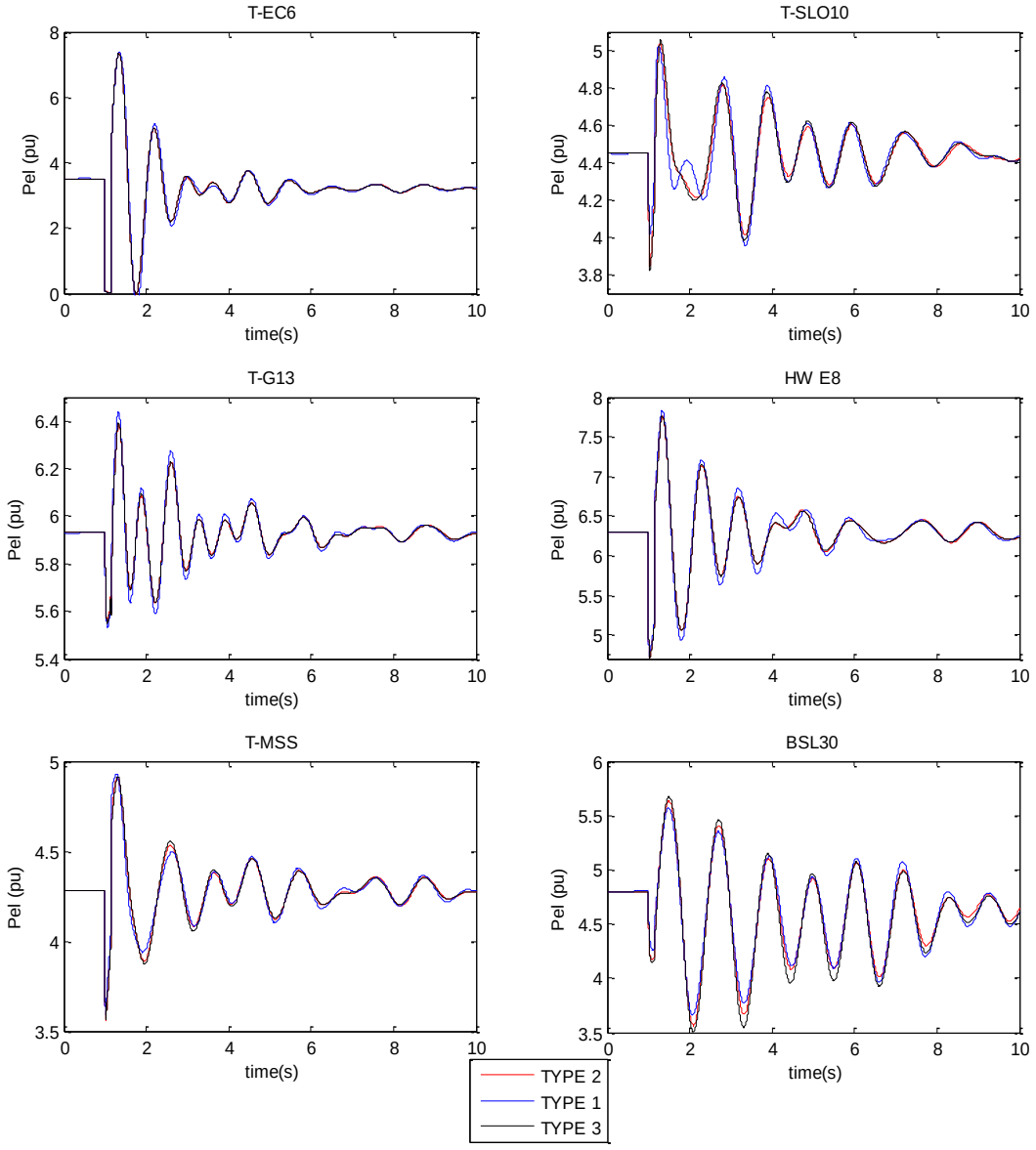

Figure 6.29: Sensitivity of the VSC-HVDC transmission system configuration on the transient stability of the Dutch power system synchronous selected generators

6.6.3.1 Sensitivity of the fault location for AC power system snapshot 1 and type 3

In this paragraph the sensitivity of the fault location on the performance of the transnational MTdc network (type 3) will be investigated. More specifically, a 150ms three phase fault will be considered in each of four selected converter stations. The ultimate goal is to evaluate the sensitivity of the location on the active power overshoot of the grid side converter stations during the fault. All converter stations are in dc voltage control mode facilitating droop control strategy.

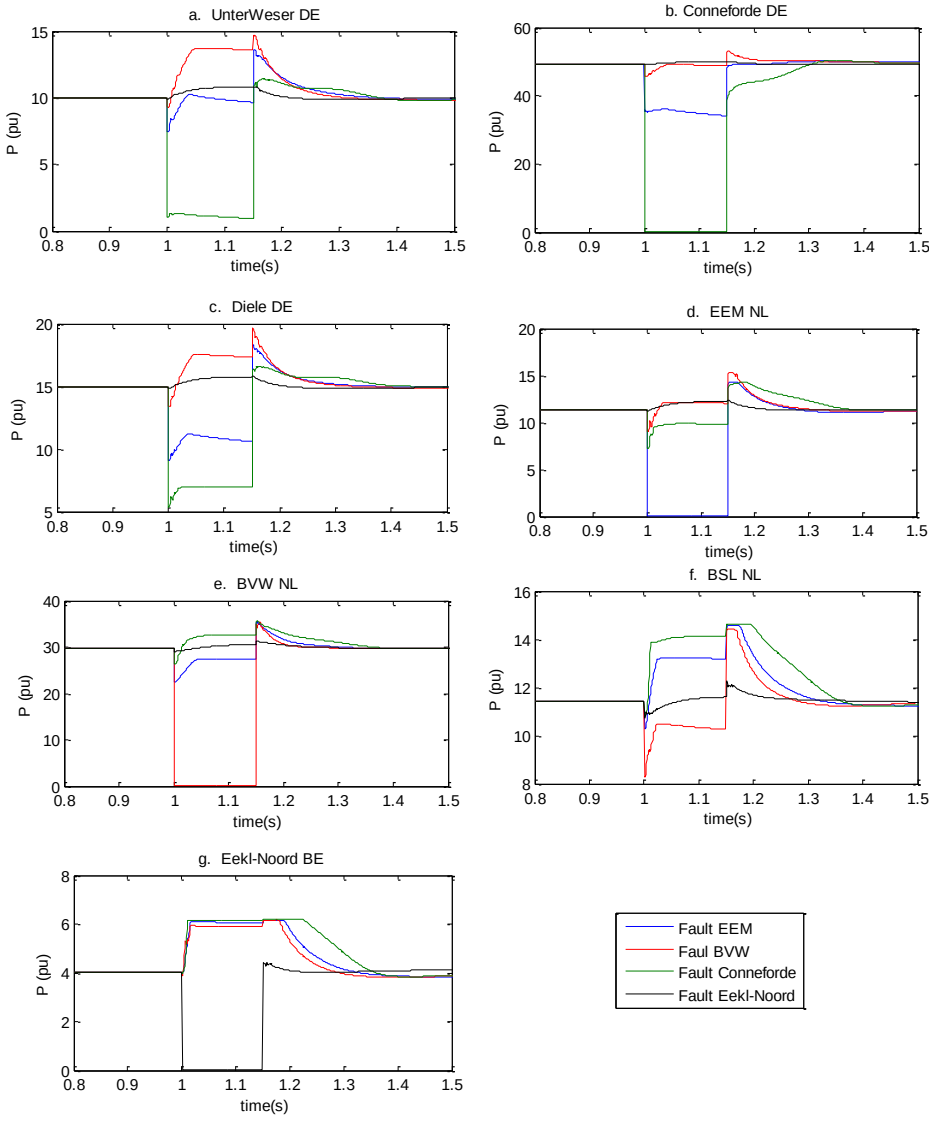

Figure 6.30: Sensitivity of the Fault location on the Grid side converter stations active power injection (S_b=100MVA)

It can be concluded from Figure 6.30 that the location of the fault plays a significant role in the dynamic performance of every converter station connected to the transnational network. The main reason for that has not only to do with the dc overvoltage that appears in the dc side capacitor of the converter stations, but also with the ac voltage drop of the relevant converter, as introduced in Appendix A.

According to the response of the Eekl-Noord converter station it can be concluded that the largest overshoot appears when the disturbance occurs in Conneforde. The main reason for that is the dc overvoltage in combination with the ac voltage drop at the Eekl-Noord converter station.

6.6.4 Simulation results Snapshot 1, 2 & 3 for the transnational MTdc network

In this paragraph the sensitivity of the transnational MTdc network (type 3) will be evaluated against the operational point of the ac power system. More specifically for the same transnational MTdc network and the same dc power flows in the dc network a common disturbance will be introduced. The target is to derive conclusions about both the stability of the onshore power system in each snapshot and also how the operation of the type 3 network is affected from the relevant ac power system snapshot.

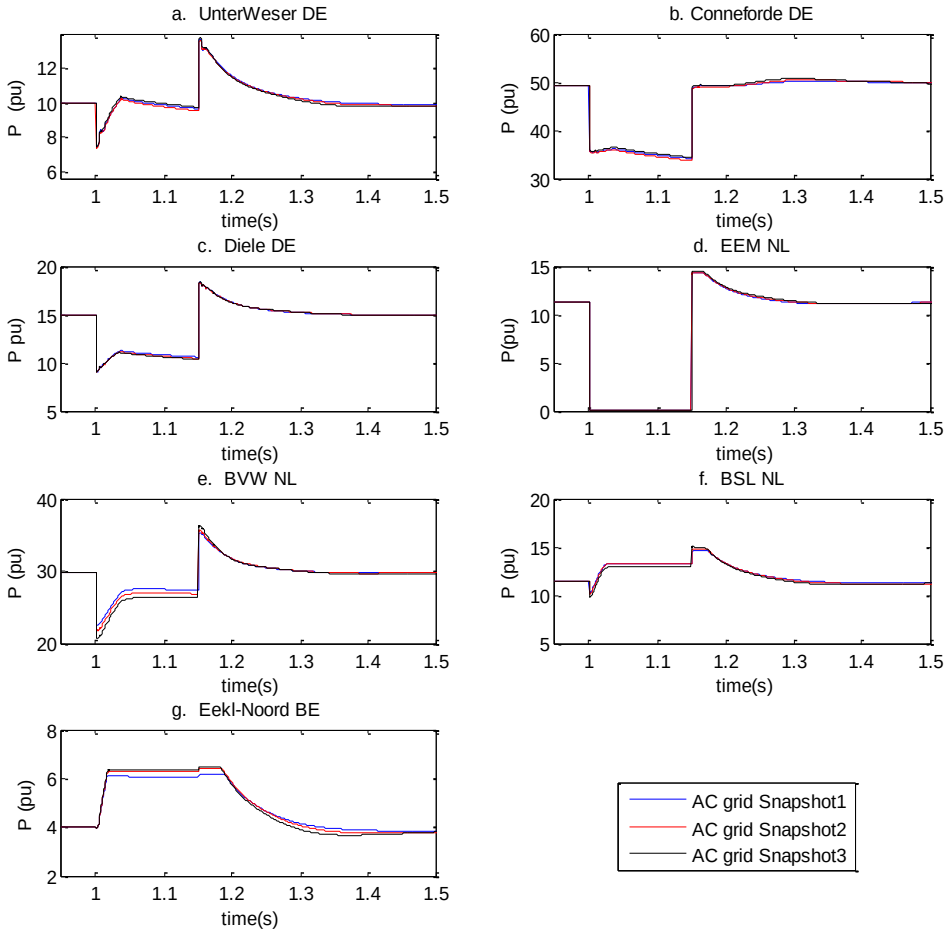

Figure 6. 31: Comparison of the Grid side converter stations dynamic response for snapshot1 and snapshot2 of the type 3 MTdc transnational network.

More specifically, a 150ms disturbance is applied at EEM converter station (same as in the previous case study). In Figure 6. 31 it is introduced the active power profiles of the grid side converters operating in the type-3 MTdc network (transnational connection) for the three selected onshore power system snapshots. As it can be seen, there are

minor differences in the performance of the converter stations during the fault. From that it can be concluded that the operation of the dc network is not affected by the ac power system snapshot.

Consequently, based on the predefined assumptions and the simulation results even if the conventional generation is much different between snapshot 1, 2 and snapshot 3, there is no such sensitivity in the responses of the GSVSCs. From that it can be argued that there is no large sensitivity of the MTdc network performance on the ac power system commitment.

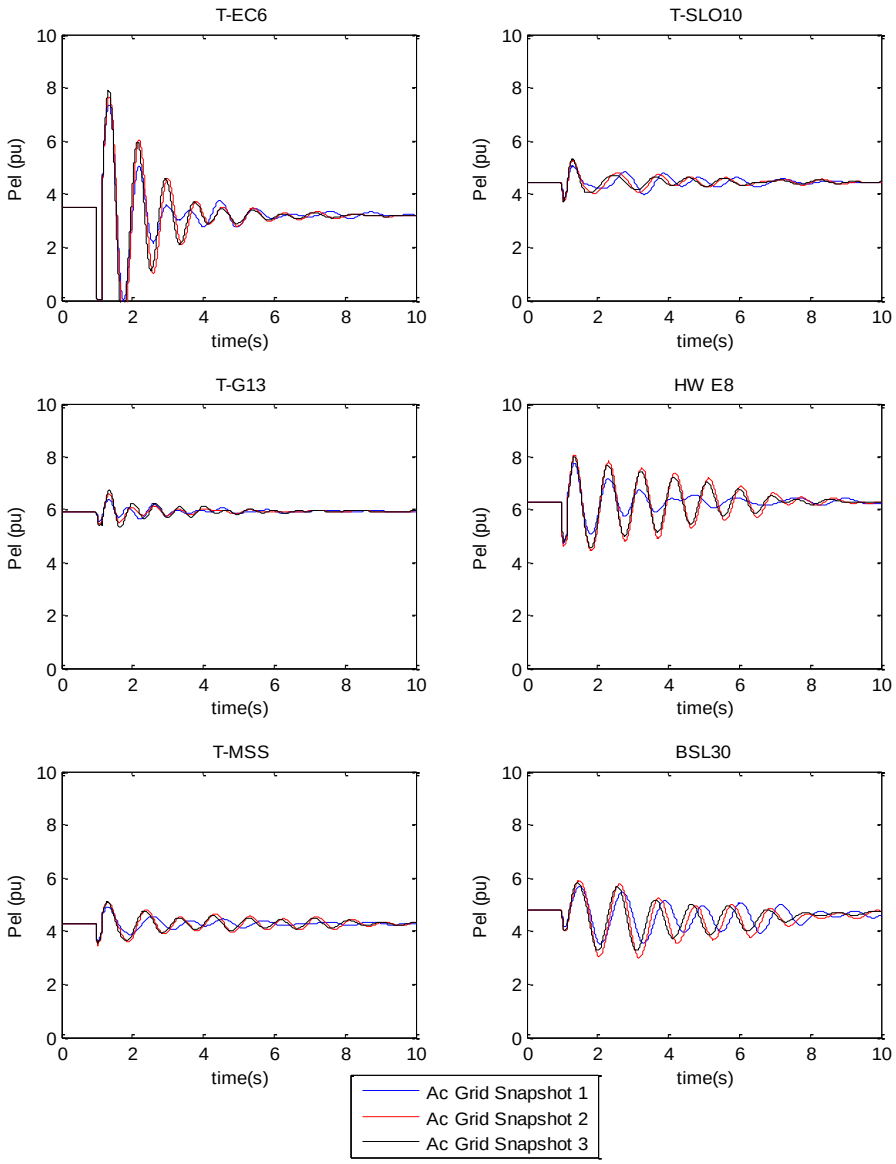

Figure 6. 32: Comparison of generators active power dynamic response for snapshot1, snapshot2 and snapshot 3 of the AC network for transnational MTdc

With reference to the ac network performance, Figure 6. **32** introduces the active power injections of the selected generators. From the simulation results it can be concluded that in snapshot 2 and 3, where there is low conventional generation, the selected

generators are undergoing larger oscillations. However, these oscillations are quickly damped out for the specific disturbance and do not create instability situation in the power system.

As a final conclusion for the three types of the HVDC transmission system configurations and the three ac power system snapshots, it can be argued that no unstable situation has been found.

6.6.5 Simulation results with power system snapshot 3, with three phase fault in EEM, and type3 MTdc network and critical clear time

In this paragraph the snapshot 3 of the Dutch power system (Figure 6. 5) will be tested against a three phase short circuit disturbance at EEM substation. The fault is cleared at the critical clear time (CCT) of EC6 generator (340ms). The CCT is determined by utilization of the dynamic model. What is more, the offshore wind farms are connected in transnational connection (Figure 6.10, type 3 connection).

Figure 6.33 introduces the rotor angles and the active power of selected generators for the described disturbance. It can be seen that the generator (EC6) recovers in adequate time without undergoing significant oscillations. The rotor angle recovers quickly indicating that there is sufficient synchronizing torque. Additionally, EC6 does not reveal un-damped or poorly damped rotor angle oscillations. It is worth mentioning that no PSS is installed at any generator in the present study.

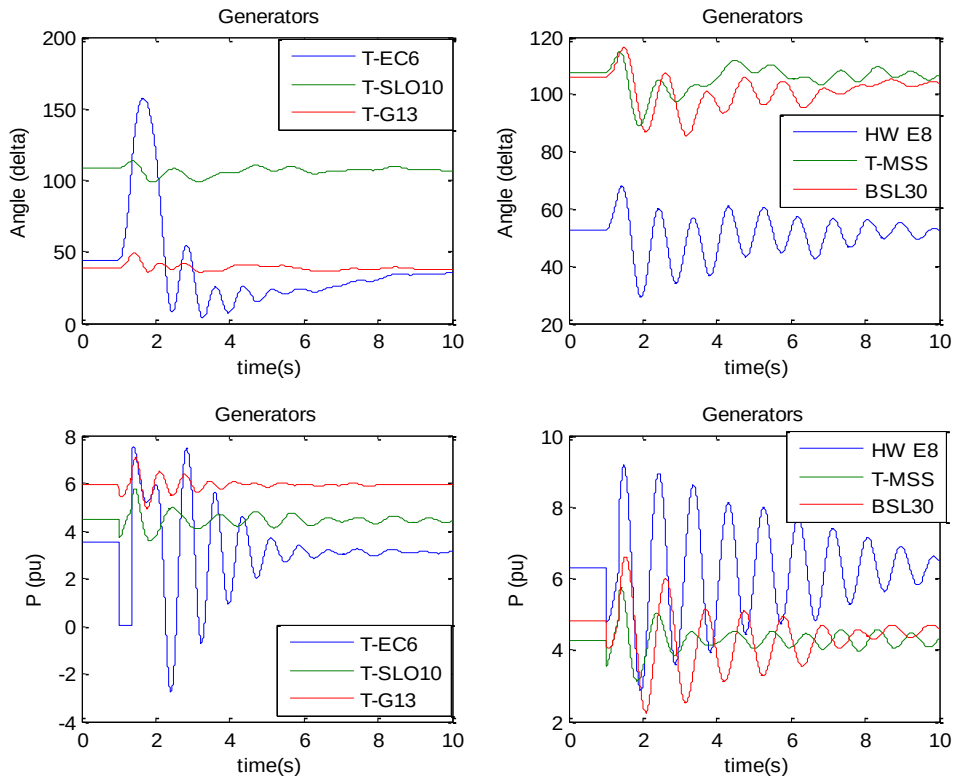

Figure 6. 33: Selected generators response for the critical clearing time of EC6 generator

Figure 6.34 introduces the voltage profile of the critical generators. As it can be seen, it takes around 2 s for the voltage at the terminal of the generator to recover completely.

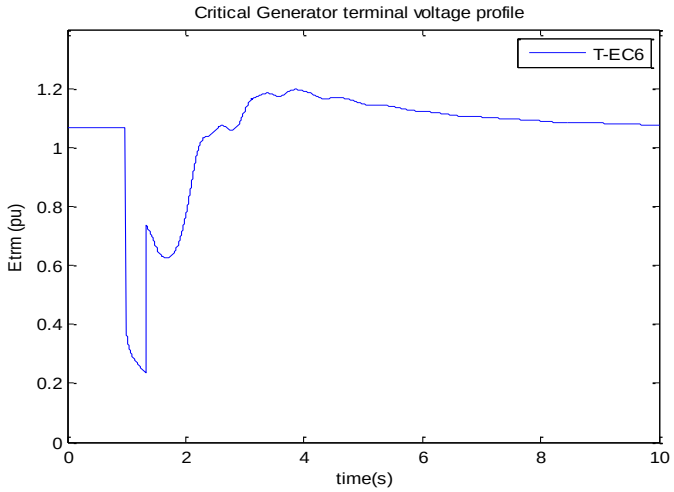

Figure 6.34: Voltage profile at the terminal of EC6 generator for the critical clearing time

Looking at the response of the other generators and based on the assumptions of this study it can be seen that SLO10 and G13 do not show highly oscillatory behavior following the fault. However, this is not the case for HW8. Following the disturbance this generator demonstrates large rotor angle oscillations. This is actually the generator that shows the most significant oscillations operating close to its stability limits. Such a poorly damped power oscillation is not acceptable. It causes significant stresses at the rotor and may trigger protection mechanisms and trip of the generator.

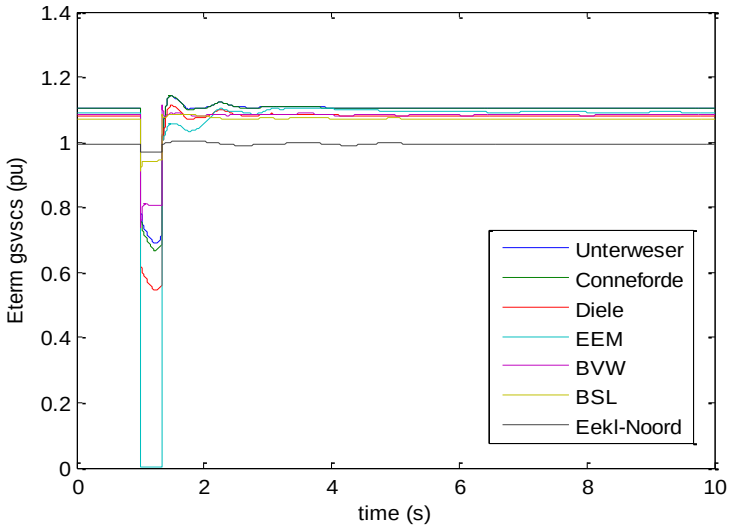

Figure 6. 35: Terminal voltage of grid side converter stations

It is worth to point out that the same oscillations are found also in type 1, 2 and 3. So it is not the connection of wind farms in MTdc transnational network where the problem can be found. It is more the low conventional generation of snapshot 3 that plays a role rather the configuration of the VSC-HVDC transmission system.

Figure 6. 35 introduces the voltage profiles of the grid side converters. From that it is apparent that the ac voltage at the EEM converter station recovers faster than the ac voltage at the EC6 generator. This illustrates again the ability of the converter to maintain synchronism and recover from a severe disturbance without loss of stability. The same applies to the other converter stations. They quickly restore pre-fault operation without introducing negative impact on the power system they operate to.

More specifically, the active power of the grid side converters is given in Figure 6. 36 while Figure 6. 37 introduces the reactive power response. The conclusion that can be drawn from those responses based on the predefined assumptions is that there is no transient stability problem concerning the dc network and the way that GSVSC stations recover the fault under the predefined assumptions.

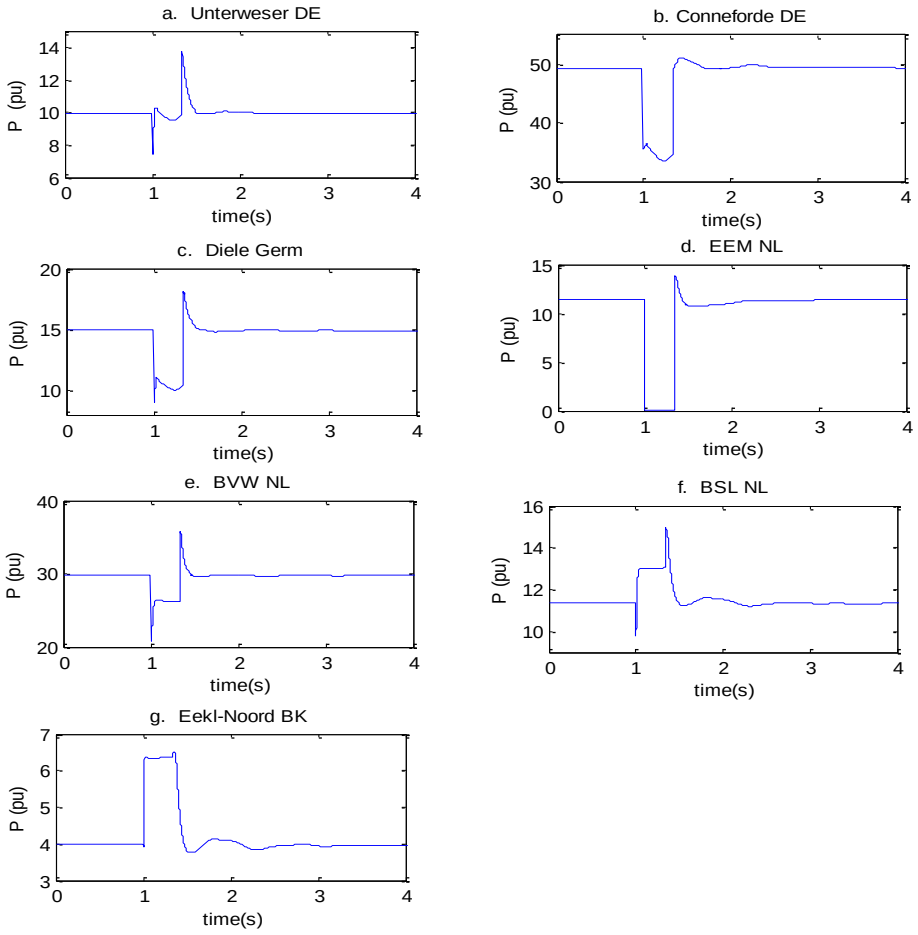

Figure 6. 36: Active power of the grid side converters for a three phase fault at EEM, cleared at critical clear time

From the reactive power response it is shown that there is reactive power contribution from the GSVSCs. In general, it has been illustrated, via time domain simulations for different dc network configurations and ac system snapshots that grid side converters can contribute fault current and reactive power at low voltage events that appear in their ac terminal. Additionally, it can be concluded that the MTdc network and more specifically the GSVSCs do not illustrate any rotor angle instability when a three phase bolted fault is applied in the EEM GSVSC station cleared at critical clear time.

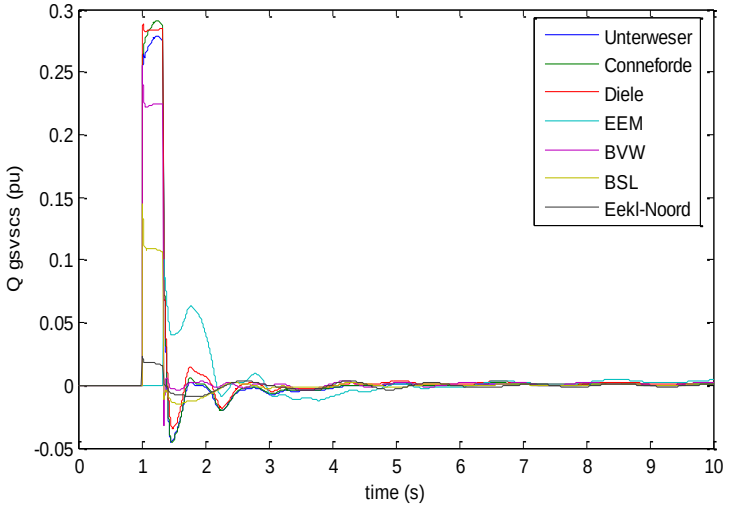

Figure 6. 37: Reactive power of the grid side converter stations for a three phase fault at EEM, cleared at critical clear time

6.7 Conclusions

In Chapter 6 the interaction of the Dutch power system meshed with VSC-based HVDC transmission systems for the integration of large amount of offshore wind power has been investigated. Three types of VSC-HVDC system configurations have been discussed. Additionally, three ac power system snapshots have been used which represent different operating points of the 2025-2030 grid configuration.

Comparing the three types of VSC-HVDC transmission configuration, it has been shown that the GSVSCs demonstrate FRT capability and provide limited short circuit current for all three configurations. Moreover, the current limiter of the GSVSC plays a significant role in the short circuit current participation of the GSVSCs. Each converter is capable to contribute to the fault current as long as it does not violate its acceptable over-current limit. Additionally, the control strategy followed to limit the current determines the reactive power contribution of the GSVSCs during the fault.

The main difference between the individual and MTdc network connection is the overshoot that appears in the active power of specific GSVSCs during the fault. The reason is the electrical distance (from the ac side) of the GSVSCs to the fault in combination with the dc overvoltage that appears in the MTdc network. Additionally, the sensitivity of the fault location to the active power overshoot of the particular GSVSCs has been illustrated in order to further support the above argument. The results revealed that the larger the electrical distance of the GSVSC from the fault location the higher the overshoot in active power.

The FRT method followed in the present project has shown satisfactory results and the GSVSCs are capable to maintain synchronism after a disturbance. However, the large amount of power that needs to be dissipated during an onshore disturbance makes the dc chopper FRT method impractical for real applications.

Concerning the critical generators in the Dutch power system it can be argued that according to Figure 6.29 there is no large sensitivity of the VSC-HVDC transmission system configuration to the generator rotor angle stability. The only factor that plays a role and alters

the dynamic behaviour of the generators for each VSC-HVDC configuration is the active power overshoot that occurs in particular GSVSCs in the MTdc network configuration.

Referring to the selected snapshots of the Dutch power system in the MTdc transnational connection, and based on the predefined assumptions it can be concluded that the specific onshore and offshore wind penetration do not introduce unstable operation of the synchronous generators for a 150ms three phase bolted fault at each of GSVSC stations. However with regard to snapshot 3 which represents a situation with extremely low conventional generation, a three phase fault in EEM cleared at the critical clearing time introduced significant power oscillations at HW8 generator. The last situation needs to be taken into account and tackled by facilitating power system stabilizers or by introducing damping by utilization of POD controllers operating at GSVSCs as discussed in chapter 5.

Finally, it is important to mention that only conventional generation is considered for the German and Belgian part of the former UCTE network. Thus a substitution of large amount of conventional generation in the German part with wind and solar power would probably create weakly damped or even unstable modes of electromechanical oscillations in the case of snapshot 3. However, such a case study is not possible to be evaluated in the present project due to data unavailability.

Chapter 7: Conclusions and future work

7.1 General Conclusions

This thesis focus on the transient stability analysis of offshore wind power connected to the Dutch power system by VSC-HVDC transmission system. For the MTdc network three market power dispatch schemes have been developed. The droop and the voltage margin method control strategy implement these market power dispatch schemes. Simulation results with test systems were performed to test the models and evaluate their performance. Additionally, Power oscillation damping controllers have been proposed which enhance damping of electromechanical oscillations in the power system.

As a realistic case study the transient stability of the Dutch power system meshed with VSC-based HVDC transmission systems has been investigated. The calculations were performed based on a developed version of 2025-2030 dynamic model of TenneT which represents parts of the former UCTE network in PSSE.

Three operating points of the Dutch power system have been considered representing different combinations of conventional generation, load and international power exchange. Additionally, three VSC-HVDC transmission system configurations have been compared in order to evaluate their performance and draw further conclusions about the interaction with the Dutch power system.

The main conclusions drawn in this thesis are:

- The main difference, based on the introduced scenarios, between individual and MTdc network configuration is the active power overshoot that occurs as a result of the dc overvoltage at the dc side of the GSVSCs.
- The active power overshoot is related to the response of the direct voltage controller to dc overvoltage in combination with the electrical distance of the GSVSC to the fault, hence to the ac voltage drop at the point of common coupling.
- From the selected snapshots of the Dutch Power system with 4700MW onshore wind and 5200MW offshore wind power which represents a 2025-2030 network situation it was shown that the system remained stable for a 150ms three phase fault at each of the GSVSC stations. The power oscillations of the selected generators are damped out satisfactory without introducing unstable situations.
- However significant oscillations at synchronous generators appeared in the situation where the fault in Eemshaven is cleared within the critical clear time. The system remained stable but the oscillations at certain generators need to be taken into consideration and tackled properly.
- The simulation results based on the described assumptions have illustrated that the operation of the MTdc network cannot be affected by the onshore power system inertia. Furthermore GSVSCs connected to the Dutch power system can operate

even if there is extremely low conventional generation, as in the snapshot with extremely low conventional generation.

- The GSVSCs that operate in individual connection or MTdc transnational network are capable to contribute to ac voltage and reactive power support at PCC.
- The short circuit current contribution of the GSVSCs is limited by the maximum terminal current that the GSVSCs can permit.
- The control strategy implemented to limit the current determines the reactive power contribution of the GSVSCs
- The droop control strategy facilitated at the GSVSC is capable to perform proportional power sharing and has illustrated significant results in terms of direct voltage and dc current performance. The direct voltage is controlled within rigid limits and the shift from one operation point to another is achieved without introducing unacceptable dynamic behaviour.
- The VMM is capable to implement fixed and priority power sharing. However special attention needs to be given to the direct voltage dynamic response, which varies from the droop control strategy due to the non linear character of the P_{dc}-U_{dc} characteristic.
- The application of the POD controller which operates in coordination with the active power controller of the GSVSC can introduce damping of electromechanical oscillations in the ac power system. However special attention needs to be given in the direct voltage variations that the POD introduces to the MTdc network. These variations can transfer the power oscillations from one power system via the MTdc network to another.

7.2 Recommendation for future work

In the present study fault ride through is achieved by means of braking resistors (dc choppers). However, it has been shown that in the transnational MTdc networks this method is impractical due to the large amount of energy that needs to be dissipated. For that reason, another proposal for further investigation would be to facilitate coordinated control between the grid-side and wind-park side converters in order to achieve reduction in the injected active power from the wind farms during onshore faults.

In chapter 5 a proposal to damp power system oscillations has been given by active power modulation of the grid-side converter. The major limitation of the proposed method is that the grid-side converter needs to be in active power control mode. For that reason a POD controller that could act on the dc voltage controller would be a better option as that would be combined with market power dispatch methods described in chapter 4. Future work in this direction is necessary.

Chapter 6 investigated the Dutch power system transient stability with respect to onshore power system disturbances. However, the effect of dc faults on the ac power system stability has not been investigated. The difficulty in this investigation is that a clear picture of the fault clearing mechanism and behaviour of IGBTs in a dc fault need to be defined in terms of technology. The effect of VSC diodes is very important in dc faults and need to be introduced in the models. Moreover, no consensus exists about the technical realization of isolating these faults.

The MTdc network considered in the present study expands from Germany via the Netherlands to Belgium. A future study should include the development of a benchmark model for UK which could be combined with an extended version of the MTdc network that includes also the UK offshore wind farms. This would give a better understanding about the operation of MTdc networks and the dynamic interaction between the former UCTE system and the UK system. Furthermore, once such a UK representation would be available then a dynamic model of BritNed could be facilitated.

Further work is needed for the implementation of power oscillation dampers (POD) at the grid-side converters of the Dutch power system. This problem is mainly a small signal stability problem and cannot be tackled only by time domain simulations. Even though in chapter 5 it has been shown that the proposed controller is capable to introduce damping in a small test power system, in order to facilitate the POD in large interconnected systems there is need for further work. The system needs to be linearised at a certain operating point and the controllability of the specific mode of electromechanical oscillation need to be determined. If the specific mode of electromechanical oscillation is controllable by the POD, then it is possible to introduce damping by proper selection of POD parameters.

Finally, in the German part of the dynamic model used in this thesis there is no representation of the connected onshore wind and solar generation. A future study should investigate and introduce these elements as well, to improve the accuracy of results.

References

[1] EWEA. (2010) Powering Europe: Wind Energy and the Electricity grid. [Online]. http://www.ewea.org/index.php?id=1976

[2] EWEA. (2012, June) Delivering Offshore wind Power in Europe. [Online]. http://www.ewea.org/index.php?id=1976

[3] ENTSOe. (2011) Offshore Transmission Technology. [Online]. https://www.entsoe.eu/resources/publications/

[4] EWEA. (2012, June) The European Offshore wind Industry key 2011 trends and statistics. [Online]. http://www.ewea.org/index.php?id=1976

[5] J.T.G Pierik, "NSTG Wind farm locations and development," ECN Technical support, 2009.

[6] Siemens PTI, *PSSE Operational Manual*.

[7] Paulo Chainho, Arjen A. Van der Meer, Madeleine Gibescu and Mart A.M.M. Van der Meijden, "General Modeling of Multi-Terminal VSC-HVDC Systems for Transient Stability Studies," , 2012.

[8] C. Ismunandur, "Control of Multiterminal VSC-HVDC for Wind Power Intergration ," *MSc thesis at TU delft*.

[9] Line Bergfjord, "Wind in the North Sea," MSc thesis at NTNY & TU Delft, 2011.

[10] C. M. Diaz Cano, "Impact Of Offshore Wind Power on the Stability of the Dutch Electrical Grid," MSc Thesis at TU Delft, 2010.

[11] J. A. Bos, "Connection of large-scale wind power generation to the Dutch electrical power system and its impact on dynamic behaviour," MSc Thesis at TU Delft, 2008.

[12] Nikos Flouretzou, Vassilios Angelidis and Georgios D. Demetriadis, "VSC-Based HVDC Power Transmission Systems: An Overview," *IEEE Transactions on Power Electronics, Vol.24, NO.3, March* , 2009.

[13] National Grid UK. (2012, April) [Online]. http://www.nationalgrid.com/uk/

[14] Colin C. Davidson, "Power Transmission with Power Electronics," Power Electronics and Applications (EPE 2011), Proceedings of the 2011-14th European Conference on , vol., no., pp.1-10, Aug. 30 2011-Sept. 1 2011.

[15] C.D. Barker and R.Whitehouse, "Autonomous Converter control in a Multi-terminal HVDC System," in *AC and DC Power Transmission, 2010. ACDC. 9th IET International Conference on , vol., no., pp.1-5, 19-21 Oct. 2010*.

[16] ABB. (2012, April) HVDC-Light. [Online]. http://www.abb.com/industries/us/9AAC30300394.aspx

[17] Lie Xu, Liangzhong Yao and Masoud Basargan, "DC grid Management of a Multi-terminal HVDC Transmission System for Large Offshore Wind Farms," in *Sustainable Power Generation and Supply, 2009. SUPERGEN '09. International Conference on* , p. 10.1109/SUPERGEN.2009.5348101.

[18] Ned Mohan,Tore M. Underland and William P.Robbins, *Power Electronics Converters, Applications and Design*.: John Willey & Sons, INC, 2003.

[19] CIGRE Workign group B1.10. (2009) Update of service experience of HV underground and submarine cable systems. [Online]. http://www.cigre.org/Publications/Scientific-papers

[20] Lidong Zhang, Lennart Harnefors and Hans-Peter Nee, "Power Synchronization Control of Grid-Connected Voltage-Source Converters," *IEEE Transactions on Power Systems, Vol.25, No.2,* 2010.

[21] Eduardo Prieto-Araujo, Fernando D, Bianchi, Adria Junyent-Ferre and Oriol Gomis-Bellmunt, "Methodology for Droop Control Dynamic Analysis of Multi-terminal VSC-HVDC Grids for Offshore Wind Farms," *IEEE Transactions on Power delivery, Vol.26, NO 4, October*, 2011.

[22] S. K. Chaudhary. R.Teodorescu, P. Rodriguez and P.C. Kjaer, "Chopper Controlled Resistors in VSC-HVDC Transmission for WPP with Full-scale converters," in *Sustainable Alternative Energy (SAE), 2009 IEEE PES/IAS Conference on , vol., no., pp.1-8, 28-30 Sept. 2009*.

[23] Weixing Lu and Boon-Teck Ooi, "DC Overvoltage Control During Loss of Converter in Multiterminal Voltage-Source Converter-Based HVDC," *IEEE Transactions on Power Delivery, Vol. 18, NO.3, July*, 2003.

[24] N.D. Calia, G.Ramtharan, J.Ekanayake and N.Jenkins, "Power Oscillation damping for fully rated converter wind turbines," *Universities Power Engineering Conference (UPEC), 2010 45th International , vol., no., pp.1-6, Aug. 31 2010-Sept. 3 2010*.

[25] F.Michael Hughes, Olimpo Anaya-Lara and Nikolas Jenkins, "Control of DFIG-based Wind Generation for power network support," *IEEE Transactions on Power Systems, Vol. 24, NO.4, November 2005*.

[26] R. Preece, A. M. Almutairi, O. Marjanovic and J. V. Milanovic, "Damping of Electromechanical Oscillations by VSC-HVDC Active power Modulation with Supplementary WAMS Based Modal LQG Controller," in *Power and Energy Society General Meeting, 2011 IEEE , vol., no., pp.1-7, 24-29 July 2011*.

[27] H. Latorre and M. Ghandhari, "Improvement of Power System Stability by Using VSC-HVDC," *Electrical Power & Energy Systems, vol. 33, NO.2, pp. 332-339, Feb*, 2011.

[28] H. Latorre and M. Ghandhari, "Improvement of Voltage Stability by Using VSC-HVDC," *Transmission & Distribution Conference & Exposition: Asia and Pacific, 2009 , vol., no., pp.1-4, 26-30 Oct. 2009*.

[29] Lidong Zhang, Lennart Harnefors and Hans-Peter Nee, "Interconnection of Two Very Weak AC Systems by VSC-HVDC links Using Power-Synchronising Control," *IEEE Transactions on Power Systems, Vol. 26, No1, February*, 2011.

[30] S. Cole and R. Belmans, "A proposal for standard VSC HVDC dynamic models in power system stability studies," *Electric Power system Research - Science Direct*, 2011.

[31] Pinto, R.T.; Rodrigues, S.F.; Bauer, P.; Pierik, J., "Comparison of direct voltage control methods of multi-terminal DC (MTDC) networks through modular dynamic models," in *Power Electronics and Applications (EPE 2011), Proceedings of the 2011-14th European Conference on* , 2011, pp. 1-10.

[32] Nilanjan Ray Chaudhuri, Rajat Majumber, Balarco Chaudhuri and Jiuping Pan , "Stability Analysis of VSC MTDC Grids Connected to Multimachine AC systems," *IEEE Transactions on Power Delivery, Vol. 26, NO. 4, October*, 2011.

[33] Drik Van Herten and Ronnie Belmans Jef Berteen, "VSC MTDC Systems with a Distributed DC Voltage Conrol - A power Flow Approach," in *PowerTech, 2011 IEEE Trondheim , vol., no., pp.1-6, 19-23 June 2011*.

[34] S.Cole, J.Berteen and R.Belmans, "Generalized Dynamic VSC MTDC Model for power systems stability studies," *IEEE Transactions on Power Systems, VOL 25. No3, pp 1655-1662* , 2010.

[35] Prabha Kundur, *Power System Stability and Control*.: McGraw-Hill Inc.

[36] Silvio Miguel Fragoso Rodrigues, "Dynamic Modeling and Control of VSC-based Multiterminal DC networks," MSc thesis TU Lisbon & TU Delft,.

[37] Jin Yang, John Edward and John O'Reilly, "Multiterminal DC Wind Farm Collection Grid Internal Fault Analsyis and Protection Design," *Power Delivery, IEEE Transactions on , vol.25, no.4, pp.2308-2318, Oct. 2010*.

[38] Jef Berteen, Stijn Cole and Ronnie Belmans, "A sequential AC/DC Power Flow Algorithm for Networks containing Multi-terminal VSC- HVDC Systems," in *Power and Energy Society General Meeting, 2010 IEEE , vol., no., pp.1-7, 25-29 July 2010*.

[39] Jun Linag, Oriol Gomis-Bellmunk, Janaka Ekanayake and Nicholas Jenkins, "Control of mulit-terminal VSC-HVDC transmission for offshore wind power,".

[40] Per-Eric Bjorklund, Kailash Srivastava and William Quaintance, "HVDC Light Modeling for Dynamic Performance," in *Power Systems Conference and Exposition, 2006. PSCE '06. 2006 IEEE PES , vol., no., pp.871-876, Oct. 29 2006-Nov. 1 2006*.

[41] Lingling Fan and Zhixin Miao, "AC or DC Power Modulation for DFIG Wind Generation with HVDC Delivery to improve Interarea Oscillations," in *Power and Energy Society General Meeting, 2011 IEEE , vol., no., pp.1-6, 24-29 July 2011*.

[42] Ekanayake, J. and Jenkins, N., "Comparison of the respons of doubly fed and fixed speed induction generators wind turbines to changes in network frequency," *Energy Conversion, IEEE Transactions on , vol.19, no.4, pp. 800- 802, Dec. 2004*.

[43] Joshua K. Wang, Robert M. Gardner and Yilu Liu, "Analysis of System Oscillations using wide Area measurements," Power Engineering Society General Meeting, 2006. IEEE , vol., no., pp.6 pp., 0-0 0.

[44] Georgios Tsourakis, Sotirios Nanou and Costas Vournas, "A power system stabilizer for variable speed Wind generators," in *18th IFAC World Congress*, Milano, 2011.

[45] Anderson, Paul M. and Fouad, A. A, *Power System Control and Stability*. Canada: IEEE press power engineering series, 2002.

[46] TenneT TSO B.V. Quality and Capacity Plan 2008-2014. [Online]. http://www.tennet.org/english/projects/index.aspx

[47] Oriol Gomis0Bellmunt, Jun Liang, Janaka Ekanaka, Rosemary King and Nicholas Jenkins, "Topologies of multi-teminal VSC-HVDC transmission for large offshore wind farms," *Electric Power Systems Research - Science Direct*, 2011.

[48] Netzentwicklungsplan strom 2012. Netzentwicklungsplan strom 2012. [Online]. http://www.netzentwicklungsplan.de/

[49] Arjen A. van der Meer, Ralph L. Hendriks and Wil L. Kling, "A survey of fast power reduction methods for VSC connected wind power plants consisting of different turbines types," *EPE-WE Seminar* , 2009.

[50] Christian Feltes, Holge Wrede, Friedrich Koch and Istvan Erlich, "Fault Ride-Through of DFIG-Based Wind farms connected to the Grid through VSC-Based HVDC link," *Power Systems, IEEE Transactions on V.24, Issue3, p.p 1537-1546* , 2009.

[51] A. Mendosa and J.A. Pecas Lopes, "Robust tuning of power system stabilizers to install in wind turbines conversion systems," *IET*, 2008.

[52] CIGRE, "Analysis and Damping Oscillations in the UCTE/CENTREL Power System," 2000.

[53] Per-Eric Bjorklund, Jiuping Pan, Chengyan Yue and Kailash Srivastava, "Anew approach for modeling complex power system components in different tools,".

[54] Vladimir Blasko and Vikram Kaura, "Anew Mathematical Model and Control of a Three-Phase AC-DC Voltage Source Converter," *IEEE Transactions on power electronics, VOL. 12, NO. 1, Jan*, 1997.

[55] G. Kabashi, K. Kadriu, A. Gashi, S. Kabashi, S. Pula and V. Komoni, "Wind Model for steady state and Dynamic Analysis," in *Word Academy of Science, Engineering and Technology*, 2011.

[56] Jun Liang, Tianjun, Oriol Gomis-Belmunt, Janaka Ekanayake and Nikolas Jenkins, "Operation and Control of Multiterminal HVDC Transmission for Offshore Wind Farms," *IEEE Transactions on Power Delivery, VOL. 26, NO. 4, October*, 2011.

[57] G. J. Lim T. T. Lie, G. B. Shrestha and K. L. Lo, "Impementation of coordinated multiple facts controller for damping pscillations," *Elevier- Electrical Power Systems*, 2000.

[58] Tatsuhito Nakajama and Shoichi Irokawa, "A control system for HVDC Trnasmission by Voltage Sourced Converters," *Power Engineering Society Summer Meeting, 1999. IEEE , vol.2, no., pp.1113-1119 vol.2, 1999*.

[59] Zheng Chao, Zhou Xiaoxin and Li Ruomei, "Dynamic Modeling and Transient Simulation for VSCbased HVDC in Multi-Machine System," in *Power System Technology, 2006. PowerCon 2006. International Conference on*.

[60] Lie Xu, Liandzhong Yao and Yi Wang, "The Role of Multiterminal HVDC for Wind Power Transmission and AC Network Support," in *Power and Energy Engineering Conference (APPEEC), 2010 Asia-Pacific*.

[61] Ooos, Etienne Veilleux and Boon-Teck, "Power Flow Analysis in Multi-terminal HVDC Grid," in *Power Systems Conference and Exposition (PSCE), 2011 IEEE/PES*.

[62] Nilanjan Ray Chaudhuri, Rajat Majumber, Balarko Chaundhuri, Jiuling Pan and Reynaldo Nuqui, "Modeling and Stability Analysis of MTDC Grids for offshore Wnd Farms: A case study on the North Sea Benchmark System," in *Power and Energy Society General Meeting, 2011 IEEE*.

[63] R. Preece and J.V Milanovic, "Comparisson of Dynamic performance of meshed networks with different types of HVDC lines," in *AC and DC Power Transmission, 2010. ACDC. 9th IET International Conference on* , p. 10.1049/cp.2010.1001.

[64] Dawei Xiang, Li Ran, Jim R. Bumby, Peter J. Tavner and Shunchang Yang, "Coordinated Control of an HVDC Link and Doybly Fed Indusction Generators in large Offshore Wind Farm," *Power Delivery, IEEE Transactions on power delivery*, vol. 21, no. 3, pp. 463- 471 , 2006.

Appendix A: Additional simulations results

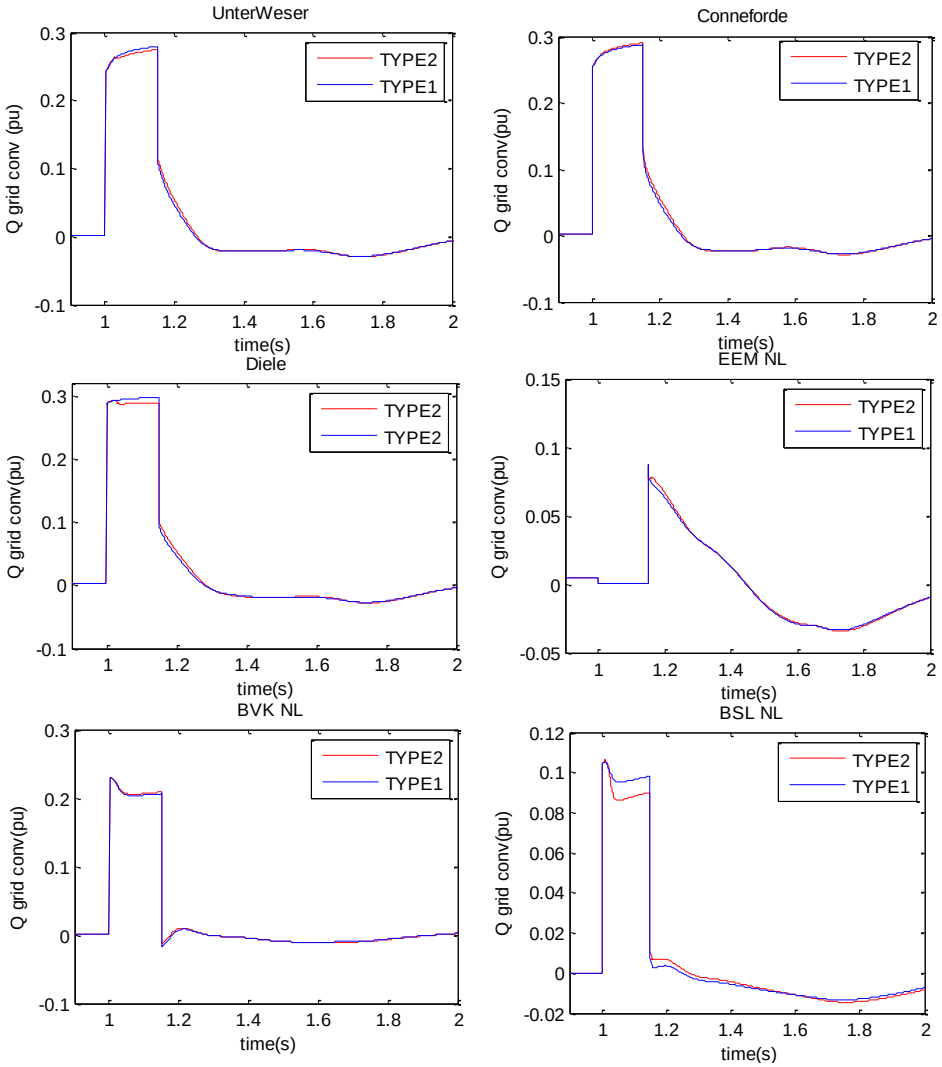

Figure A: Reactive power at the grid-side converter stations during a 150ms fault in EEM for the type2 VSC-HVDC network

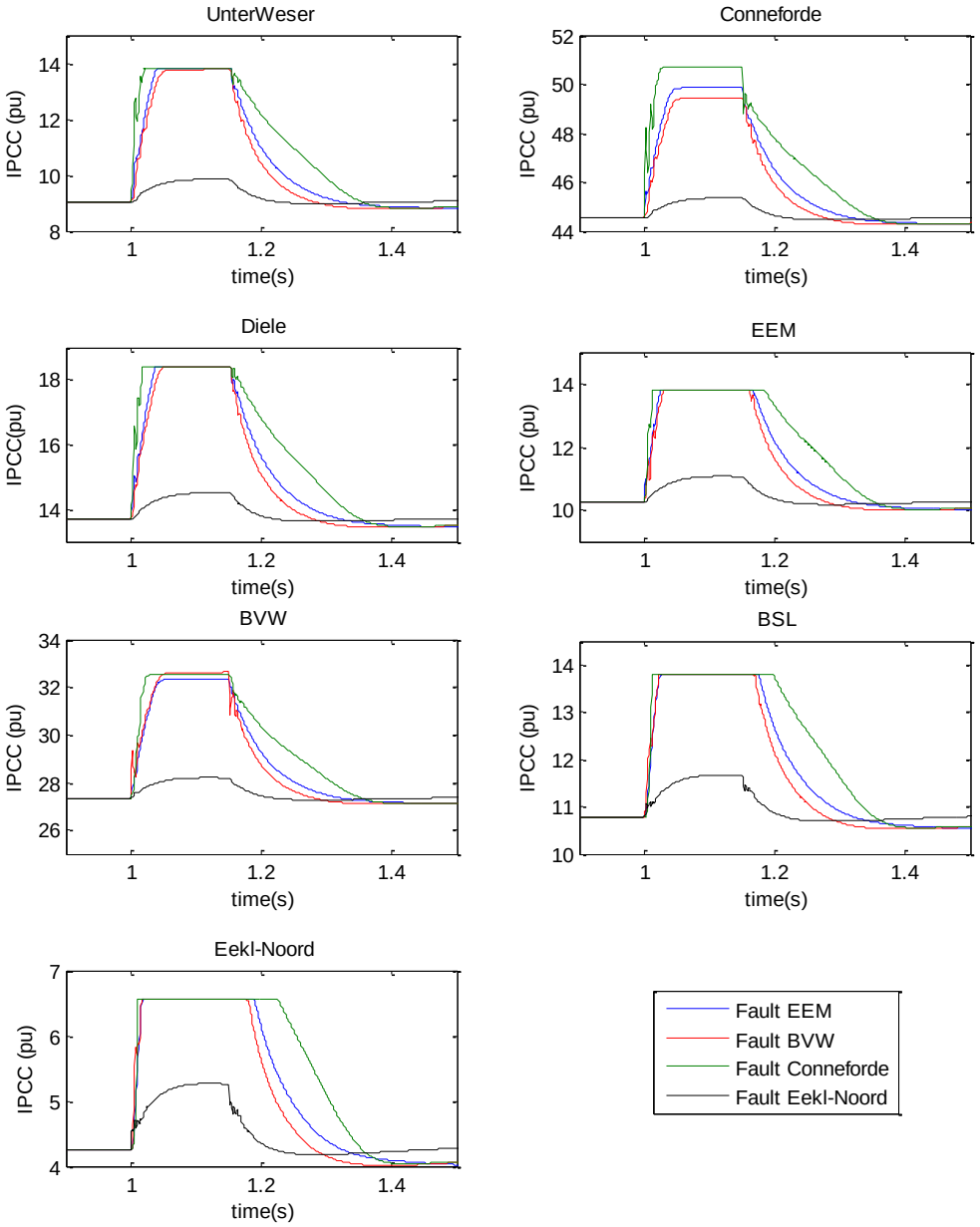

Figure B: Sensitivity of the Fault location on the Grid-side converter stations ac current at the PCC (Sb=100MVA).

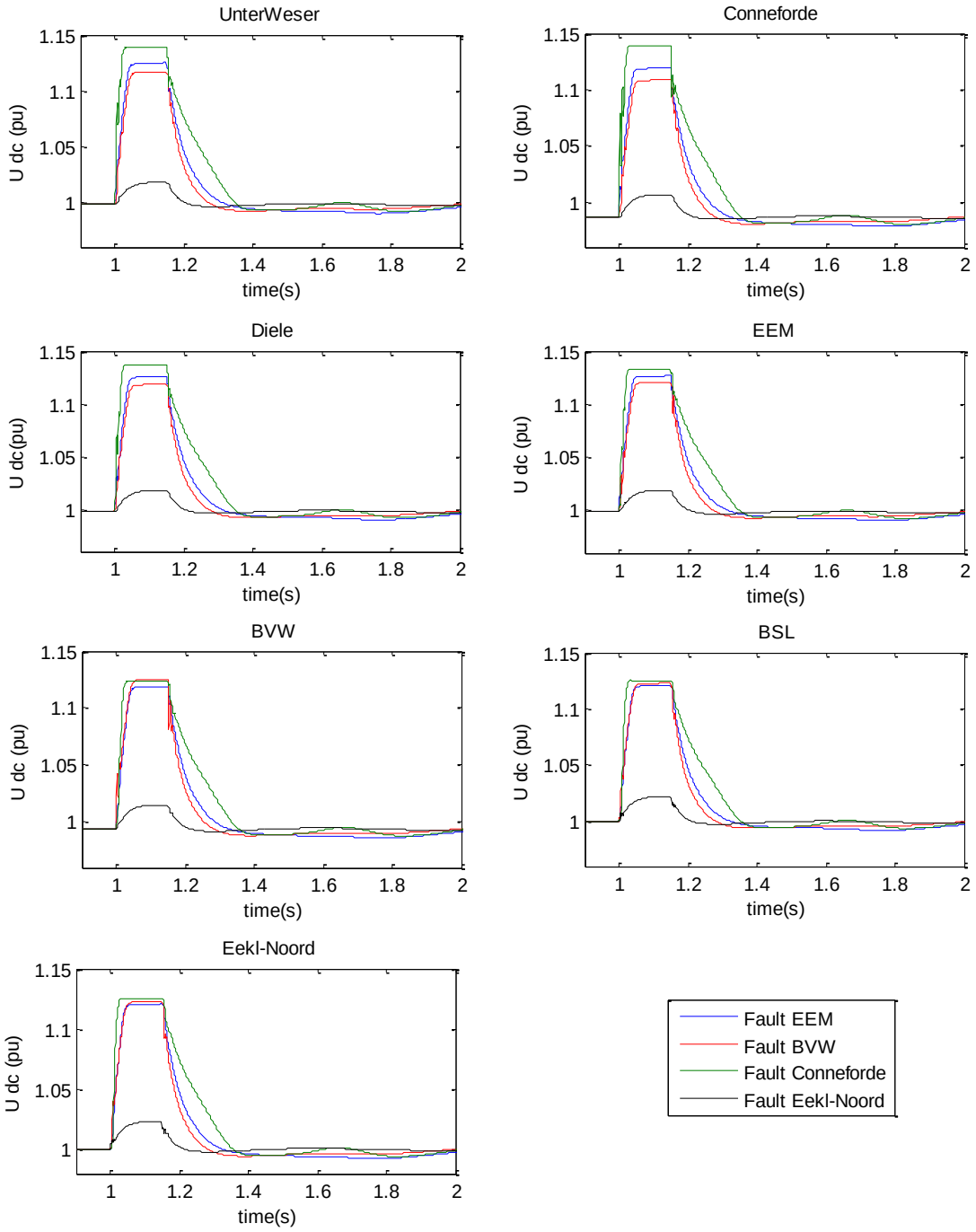

Figure C: Sensitivity of the Fault location on the Grid-side converter dc voltage

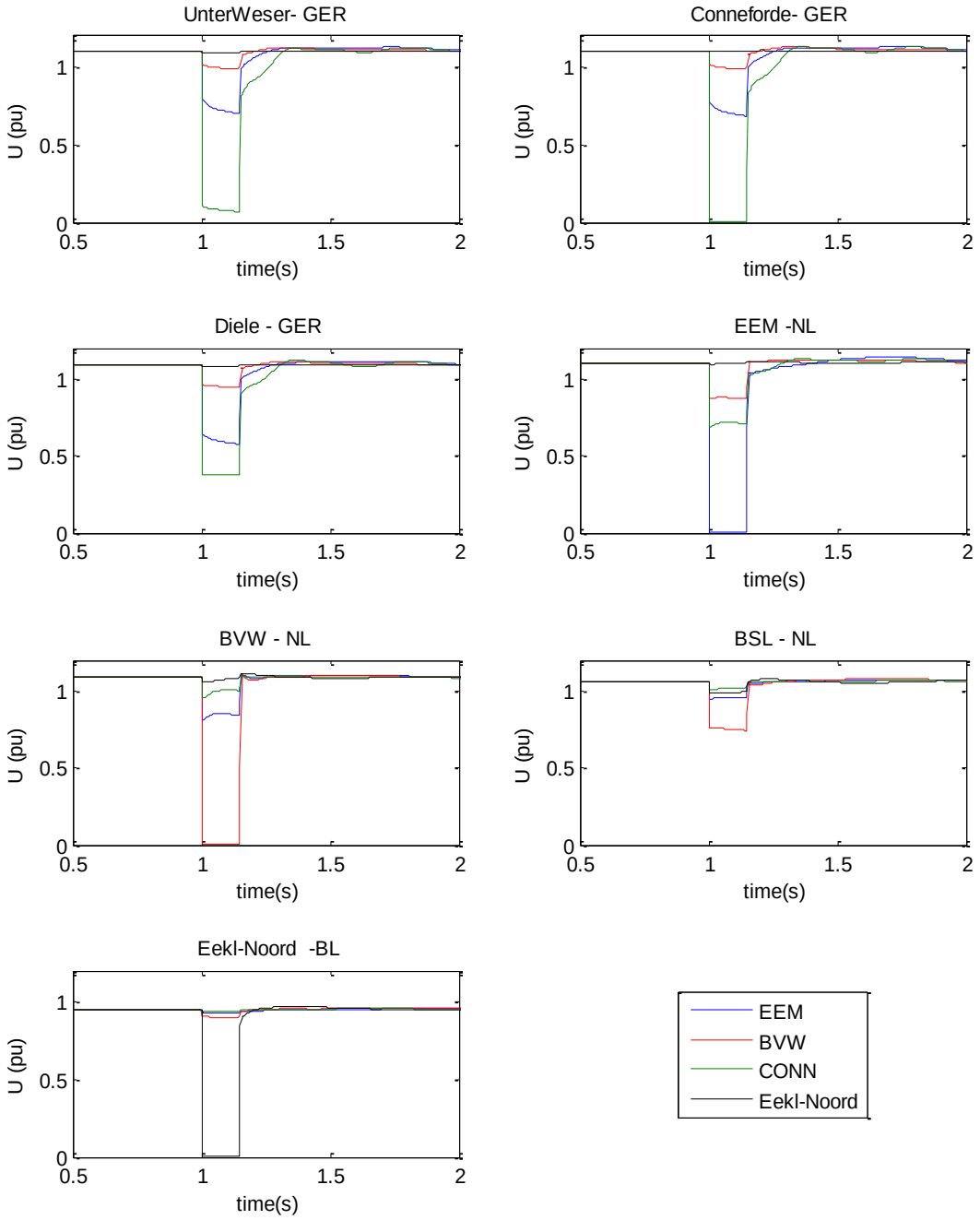

Figure D: AC voltage profiles for different fault locations

Appendix B: Map showing the location of the selected generators in the Dutch Power system

Map showing the location of selected generators into the Dutch Power system

Figure E: Selected generators of the Dutch Power system

Appendix C: Four terminal MTdc network example

A simple four terminal dc network configuration is considered in order to illustrate and better understand the method that has been adapted to model MTdc networks cables [**36**] [**21**] [**29**].

The differential equations that describe the dc network in figure1 can be written in the state space form, such as:

$$\frac{dx}{dt} = Ax + Bu \tag{1}$$

Where the state matrix is defined as:

$$x = \begin{bmatrix} U_{dc}^{1} & U_{dc}^{2} & U_{dc}^{3} & U_{dc}^{4} & I_{12} & I_{13} & I_{24} & I_{34} \end{bmatrix}^{T} \tag{2}$$

and the input vector is the dc current injections of the VSCs operating in the MTdc network:

$$u = \begin{bmatrix} I_{dc1} & I_{dc2} & I_{dc3} & I_{dc4} \end{bmatrix}^{T} \tag{3}$$

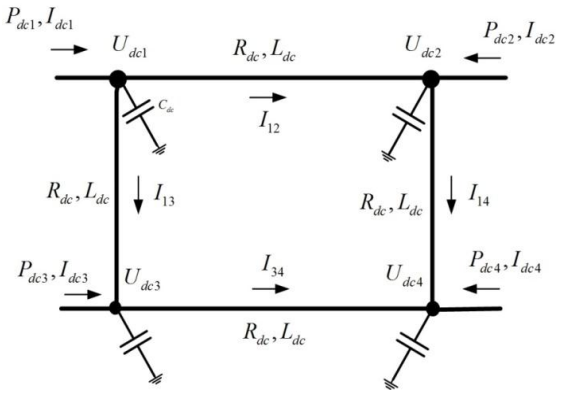

Figure F: Four-node MTDC network

Whereas the state space matrixes can be given as:

$$A = \begin{bmatrix} a_{11} & a_{12} \\ a_{21} & a_{22} \end{bmatrix}, \; B = \begin{bmatrix} b_{11} \\ b_{21} \end{bmatrix} \tag{4}$$

The sub-matrices that compose B matrix are defined as:

$$b_{11} = \frac{1}{C_{dc}}[\mathrm{I}]_{4\times4}\ ,\ b_{21} = 0 \tag{5}$$

And for the matrix A we have:

$$a_{11} = [0]_{4x4} \qquad a_{12} = \begin{bmatrix} -\frac{1}{C_{dc}} & -\frac{1}{C_{dc}} & 0 & 0 \\ \frac{1}{C_{dc}} & 0 & -\frac{1}{C_{dc}} & 0 \\ 0 & \frac{1}{C_{dc}} & 0 & -\frac{1}{C_{dc}} \\ 0 & 0 & \frac{1}{C_{dc}} & \frac{1}{C_{dc}} \end{bmatrix}_{4x4}$$

$$a_{21} = \begin{bmatrix} \frac{1}{L_{dc}} & -\frac{1}{L_{dc}} & 0 & 0 \\ \frac{1}{L_{dc}} & 0 & -\frac{1}{L_{dc}} & 0 \\ 0 & \frac{1}{L_{dc}} & 0 & -\frac{1}{L_{dc}} \\ 0 & 0 & \frac{1}{L_{dc}} & -\frac{1}{L_{dc}} \end{bmatrix}_{4x4} \qquad a_{22} = \begin{bmatrix} -\frac{R}{L_{dc}} & 0 & 0 & 0 \\ 0 & -\frac{R}{L_{dc}} & 0 & 0 \\ 0 & 0 & -\frac{R}{L_{dc}} & 0 \\ 0 & 0 & 0 & -\frac{R}{L_{dc}} \end{bmatrix}_{4x4} \tag{6}$$

At this point it is important to introduce the concept of incident matrix that is going to be used in the generic model of the dc network. In the incident matrix every row is related to the relevant branch of the dc network. Thus, for the network of figure1 there are four branches and thus four rows. Moreover, each element of each column is related to a specific node of the dc network. Hence, in every row, an element with value 1 means that the current is flowing out of the node while -1, in the node.

In every single row of the incidence matrix, only two elements are non-zero elements. With all the above taken into account the incident matrix that corresponds to the dc network configuration of figure 1is given as:

$$M = \begin{bmatrix} 1 & -1 & 0 & 0 \\ 1 & 0 & -1 & 0 \\ 0 & 1 & 0 & -1 \\ 0 & 0 & 1 & -1 \end{bmatrix} \tag{7}$$

With careful observation of the incident matrix and the sub-matrixes, it is possible to rewrite the state space form of the four terminal MTdc network such as:

$$a_{12}=\begin{bmatrix} -\frac{1}{C_{dc}} & -\frac{1}{C_{dc}} & 0 & 0 \\ \frac{1}{C_{dc}} & 0 & -\frac{1}{C_{dc}} & 0 \\ 0 & \frac{1}{C_{dc}} & 0 & -\frac{1}{C_{dc}} \\ 0 & 0 & \frac{1}{C_{dc}} & \frac{1}{C_{dc}} \end{bmatrix}_{4x4}=\begin{bmatrix} \frac{1}{C_{dc}} & 0 & 0 & 0 \\ 0 & \frac{1}{C_{dc}} & 0 & 0 \\ 0 & 0 & \frac{1}{C_{dc}} & 0 \\ 0 & 0 & & \frac{1}{C_{dc}} \end{bmatrix}\begin{bmatrix} -1 & -1 & 0 & 0 \\ 1 & 0 & -1 & 0 \\ 0 & 1 & 0 & -1 \\ 0 & 0 & 1 & 1 \end{bmatrix}_{4x4} \quad (8)$$

$$a_{12}=-\frac{1}{C_{dc}}[I]\begin{bmatrix} 1 & 1 & 0 & 0 \\ -1 & 0 & 1 & 0 \\ 0 & -1 & 0 & 1 \\ 0 & 0 & -1 & -1 \end{bmatrix}_{4x4}=-\frac{1}{C_{dc}}[I]\begin{bmatrix} 1 & -1 & 0 & 0 \\ 1 & 0 & -1 & 0 \\ 0 & 1 & 0 & -1 \\ 0 & 0 & 1 & -1 \end{bmatrix}_{4x4}^{T}=-\frac{1}{C_{dc}}[I]_{4x4}[M]^{T}$$

From above it is possible to calculate the sub-matrix a_{12} of dc network at figure 1 provided the number of nodes, the incident matrix and the parameters of the dc cables. The last characteristic is very important for developing generic models of MTdc networks where can easily be extended to any possible layout. By utilizing the same concept we get for the sub-matrix a_{21} and a_{22}:

$$a_{21}=\begin{bmatrix} \frac{1}{L_{dc}} & -\frac{1}{L_{dc}} & 0 & 0 \\ \frac{1}{L_{dc}} & 0 & -\frac{1}{L_{dc}} & 0 \\ 0 & \frac{1}{L_{dc}} & 0 & -\frac{1}{L_{dc}} \\ 0 & 0 & \frac{1}{L_{dc}} & -\frac{1}{L_{dc}} \end{bmatrix}_{4x4}=\frac{1}{L_{dc}}\begin{bmatrix} 1 & -1 & 0 & 0 \\ 1 & 0 & -1 & 0 \\ 0 & 1 & 0 & -1 \\ 0 & 0 & 1 & -1 \end{bmatrix}_{4x4}=\frac{1}{L_{dc}}[M] \quad (9)$$

$$a_{22}=\begin{bmatrix} -\frac{R}{L_{dc}} & 0 & 0 & 0 \\ 0 & -\frac{R}{L_{dc}} & 0 & 0 \\ 0 & 0 & -\frac{R}{L_{dc}} & 0 \\ 0 & 0 & 0 & -\frac{R}{L_{dc}} \end{bmatrix}_{4x4}=-\frac{R}{L_{dc}}[I]_{4x4} \quad (10)$$

To sum up, it has been proved that for the four-terminal network only the incident matrix and the parameters of the cables are required in order to build the state space model that describes the dynamic behavior of the dc network cables. This is a very important advantage for the modeling of multi-terminal VSC-HVDC configurations. This concept can be generalized in any configuration and number of nodes.

Appendix D: Assumptions made for chapter 6

The main assumptions taken in chapter 6 are concentrated below:

- The 2010 dynamic model of TenneT is taken as reference
- The main grid reinforcements for 2025-2030 in the Dutch Part of the model are introduced as given by TenneT TSO B.V
- Only present generators which will still be in operation by 2025-2030 are considered in the unit commitment
- Asynchronous interconnectors are modeled by static loads with negative value.
- 4700MW onshore wind power is modeled by standard dynamic models connected at different locations of the Dutch power system
- 5200MW offshore wind power is considered in the Dutch part of the TenneT dynamic model
- 7500MW offshore wind power is considered in the German part of the model
- Certain grid reinforcements have been introduced between substations Diele-Unterweser and Conneforder in the German part of the onshore grid
- The GSVSCs in MTdc network performs proportional power sharing facilitating droop controllers
- Aggregate wind turbine dynamic models have been used

Appendix E: Parameters of test system in chapter 4

Generators model parameters of the 6th order model in PSSE: GENROU

GENROU	G1	G2	G3
T'do	6	6	6
T"do	0,05	0,05	0,05
T'qo	1	1	1
T"qo	0,05	0,05	0,05
Inertia H	3	3	3
Speed Damping D	0	0	0
Xd	1,4	1,4	1,4
Xq	1,35	1,35	1,35
X'd	0,3	0,3	0,3
X'q	0,6	0,6	0,6
X"d = X"q	0,2	0,2	0,2
Xl	0,1	0,1	0,1
S(1.0)	0,03	0,03	0,03
S(1.2)	0,4	0,4	0,4

Excitation system model: SEXS

SEXS	G1	G2	G3
TA/TB	0,1	0,1	0,1
TB (> 0)	10	10	10
K	100	100	100
TE	0,1	0,1	0,1
EMIN	0	0	0
EMAX	3	3	3

Governor Model: TGOV1

TGOV 1			
R	0,05	0,05	0,05
T1 (>0)(sec)	0,5	0,5	0,5
V MAX	1	1	1
V MIN	0	0	0
T2 (sec)	1,5	1,5	1,5
T3 (>0)(sec)	5	5	5
Dt	0	0	0

Grid side VSC model: GSVSC

GSVSC	GSVSC1	GSVSC2	GSVSC3
Ki_P - integral gain of the active power controller	20	20	20
Kp_P - proportional gain of the active power controller	0,001	0,001	0,001
Ki_Q - integral gain of the reactive power controller	20	20	20
Kp_Q - proportional gain of the reactive power controller	0,001	0,001	0,001
Ki_AC - integral gain of the AC Voltage controller	0,01	0,01	0,01
Kp_AC - proportional gain of the AC Voltage controller	1	1	1
Ki_DC - integral gain of the DC Voltage controller	50	50	50
Kp_DC - proportional gain of the DC Voltage controller	11	14	16
Imax - maximum value of I accepted in the current limiter before the con	1,15	1,15	1,15
Udc - Initial Value of the DC voltage	250000	250000	250000
Plower1: In two stage VMM	0	0	0
Pupper1: : In two stage VMM	0,4	0,5	0,2
Plower2: : In two stage VMM	0,4	0,5	0,2
Pupper2: : In two stage VMM	1	1	1
Udc_ref_H (V): : In two stage VMM	252000	255000	260000
Id_max: in one stage VMM	0,6	0,7	0,86
Direct Voltage control strategy: 1 for VMM , 2 droop	1	1	1

Wind park side VSC model: WPVSC

WPVSC	WPVSC1	WPVSC2
Ki_Vpcc - integral gain of the amplitude voltage controler	10	10
Kp_Vpcc - proportional gain of the amplitude voltage controler	0,1	0,1
Kp,angle – proportional gain of angle controller	10	10
Ki,angle – integral gain of angle controller	0,1	0,1
Imax - maximum value of I accepted in the current limiter before the con	1,15	1,15
Udc - Initial Value of the DC voltage	250000	250000

Direct drive wind turbine model

WT4G1	WP1	WP2
TIQCmd, Converter time constant for IQcmd, second	0,02	0,02
TIpCmd, Converter time constant for IPcmd, second	0,02	0,02
VLVPL1 - Low Voltage power Logic (LVPL), voltage 1 (pu)	0,4	0,4
VLVPL2 - LVPL voltage 2 (pu)	0,9	0,9
GLVPL - LVPL gain	1,11	1,11
High Voltage reactive Current (HVRC) logic,voltage (pu)	1,2	1,2
CURHVRCR - HVRC logic, current (pu)	2	2
RIp_LVPL, Rate of active current change	2	2
T_LVPL, Voltage sensor for LVPL, second	0,02	0,02

WT4E1	WP1	WP2
Tfv - V-regulator filter	0,15	0,15
Kpv - V-regulator proportional gain	20	20
Kiv - V-regulator integrator gain	100	100
Kpp - T-regulator proportional gain	0,0005	0,0005
Kip - T-regulator integrator gain	0	0
Kf - Rate feedback gain	0	0
Tf - Rate feedback time constant	80	80
QMX - V-regulator max limit	0,47	0,47
QMN - V-regulator min limit	-0,47	-0,47
IPMAX - Max active current limit	1,1	1,1
TRV - V-sensor	0	0
dPMX - Max limit in power PI controller (pu)	0,5	0,5
dPMN - Min limit in power PI controller (pu)	-0,5	-0,5
T_POWER - Power filter time constant	0	0
KQi - MVAR/Volt gain	0,1	0,1
VMINCL	0,9	0,9
VMAXCL	1,1	1,1
KVi - Volt/MVAR gain	120	120
Tv - Lag time constant in WindVar controller	0,05	0,05
Tp - Pelec filter in fast PF controller	0,05	0,05
ImaxTD - Converter current limit	1,7	1,7
Iphl - Hard active current limit	1,11	1,11
Iqhl - Hard reactive current limit	1,11	1,11